HEAT AND ENERGY EXCHANGE ABOVE DIFFERENT SURFACES USING SURFACE RENEWAL

by

MICHAEL GHEBREKIDAN MENGISTU

Thesis submitted in partial fulfilment of the requirement for the award of degree of

PhD

in Agrometeorology,
Soil-Plant-Atmosphere Continuum Research Unit
School of Environmental Sciences
Faculty of Science and Agriculture
University of KwaZulu-Natal
Pietermaritzburg
South Africa

March 2008

DECLARATION

I hereby declare that the research work reported in this thesis is the result of my own original investigations except where acknowledged.

Signed …….
Michael G. Mengistu

Signed ……..
Supervisor: Michael J. Savage
Professor of Agrometeorology

ACKNOWLEDGEMENTS

I would like to express my most sincere gratitude to my supervisor Professor Michael J Savage, Head of the School of Environmental Sciences, Agrometeorology Discipline, at the University of KwaZulu-Natal (UKZN) for his excellent supervision, invaluable advice, patience, criticisms and encouragement throughout the course of the study. I would also like to sincerely thank Dr CS Everson of the Council for Scientific and Industrial Research (CSIR) for his assistance during the setting of the field trials.

Special thanks to staff members and students of the Agrometeorology Discipline, UKZN, specifically to Mrs Jothimala Manickum, Mr Peter Dovey, Mr Nile Eltayeb, and Dr George Odhiambo for the diversified help during field, laboratory, and administrative work. Their contribution facilitated an excellent working environment.

Funding from the UKZN, CSIR, and Water Research Commission (South Africa) for this study, on which this thesis is based, is gratefully acknowledged.

I am also grateful to Dr C Jarmain, Dr PJ Dye, Mr A Clulow, Mr M Gush, Mr E Prinsloo (CSIR) for the technical support and assistance during the setting of the experiments.

My thanks also go to Mr SJ Hilcove the owner of the Bellevue farm (Pietermaritzburg), the farm manager Mr H Ovenstone, and the workers of the farm for allowing the use of the facilities and for providing their grassland field available for this work; the Komatiland Plantations for allowing the use of their facilities and for providing the Outeniqua Yellow wood plot; the research staff of the Hluhluwe Game reserve for providing the *Chromolaena odorata* site and their facilities available for this work.

Last but not least, I would like to express my special thanks to my parents and friends for their continuous encouragement and moral support during my study period. Praise, honour, and glory be to the Lord of heaven and earth!

ABSTRACT

The demand for the world's increasingly scarce water supply is rising rapidly, challenging its availability for agriculture and other environmental uses, especially in water scarce countries, such as South Africa, with mean annual rainfall is well below the world's average. The implementation of effective and sustainable water resources management strategies is then imperative, to meet these increasingly growing demands for water. Accurate assessment of evaporation is therefore crucial in agriculture and water resources management. Evaporation may be estimated using different micrometeorological methods, such as eddy covariance (*EC*), Bowen ratio energy balance (*BR*), surface renewal (*SR*), flux variance (*FV*), and surface layer scintillometry (*SLS*) methods. Despite the availability of different methods for estimating evaporation, each method has advantages and disadvantages, in terms of accuracy, simplicity, spatial representation, robustness, fetch, and cost. Invoking the shortened surface energy balance equation for which advection and stored canopy heat fluxes are neglected, the measurement of net irradiance, soil heat flux, and sensible heat flux allows the latent energy flux and hence the total evaporation amount to be estimated.

The *SR* method for estimating sensible heat, latent energy, and other scalars has the advantage over other micrometeorological methods since it requires only measurement of the scalar of interest at one point. The *SR* analysis for estimating sensible heat flux from canopies involves high frequency air temperature measurements (typically 2 to 10 Hz) using 25 to 75 μm diameter fine-wire thermocouples. The *SR* method is based on the idea that parcel of air near a surface is renewed by an air parcel from above. The *SR* method uses the square, cube, and fifth order of two consecutive air temperature differences from different time lags to determine sensible heat flux. Currently, there are three *SR* analysis approaches: an ideal *SR* analysis model based on structure function analysis; an *SR* analysis model with finite micro-front period; and an empirical *SR* analysis model based on similarity theory. The *SR* method based on structure function analysis must be calibrated against another standard method, such as the eddy covariance method to determine a weighting factor α which accounts for unequal heating of air parcels

below the air temperature sensor height. The SR analysis model based on the finite micro-front time and the empirical SR analysis model based on similarity theory need the additional measurement of wind speed to estimate friction velocity.

The weighting factor α depends on measurement height, canopy structure, thermocouple size, and the structure function air temperature lag. For this study, α for various canopy surfaces is determined by plotting the SR sensible heat flux H_{SR} against eddy covariance H_{EC} estimates with a linear fit forced through the origin.

This study presents the use of the SR method, previously untested in South Africa, to estimate sensible heat flux density over a variety of surfaces: grassland; Triffid weed (*Chromolaena odorata*); Outeniqua Yellow wood (*Podocarpus Falcatus*) forest; heterogeneous surface (*Jatropha curcas*); and open water surface. The sensible heat flux estimates from the SR method are compared with measurements of sensible heat flux obtained using eddy covariance, Bowen ratio, flux variance, and surface layer scintillometer methods, to investigate the accuracy of the estimates. For all methods used except the Bowen ratio method, evaporation is estimated as a residual using the shortened energy balance from the measured sensible heat and from the additional measurements of net irradiance and soil heat flux density.

Sensible heat flux H_{SR} estimated using the SR analysis method based on air temperature structure functions at a height of 0.5 m above a grass canopy with a time lag r = 0.5 s, and $\alpha = 1$ showed very good agreement with the eddy covariance H_{EC}, surface layer scintillometer H_{SLS}, and Bowen ratio H_{BR} estimates. The half-hourly latent energy flux estimates obtained using the SR method λE_{SR} at 0.5 m above the grass canopy for a time lag r = 0.5 s also showed very good agreement with λE_{EC} and λE_{SLS}. The 20-minute averages of λE_{SR} compared well with Bowen ratio λE_{BR} estimates.

Sensible heat and latent energy fluxes over an alien invasive plant, Triffid weed (*C. odorata*) were estimated using SR, EC, FV and SLS methods. The performance of the three SR analysis approaches were evaluated for unstable

conditions using four time lags r = 0.1, 0.4, 0.5, and 1.0 s. The best results were obtained using the empirical SR method with regression slopes of 0.89 and root mean square error (RMSE) values less than 30 W m^{-2} at measurement height z = 2.85 and 3.60 m above the soil surface for time lag r = 1.0 s. Half-hourly H_{SR} estimates using r = 1.0 s showed very good agreement with the FV and SLS estimates. The SR latent energy flux, estimated as a residual of the energy balance λE_{SR}, using time lag r = 1.0 s provided good estimates of λE_{EC}, λE_{FV}, and λE_{SLS} for z = 2.85 and 3.60 m.

The performance of the three SR analysis approaches for estimating sensible heat flux above an Outeniqua Yellow wood stand, were evaluated for stable and unstable conditions. Under stable conditions, the SR analysis approach using the micro-front time produced more accurate estimates of H_{SR} than the other two SR analysis approaches. For unstable conditions, the SR analysis approach based on structure functions, corrected for α using EC comparisons produced superior estimates of H_{SR}. An average value of 0.60 is found for α for this study for measurements made in the roughness sublayer. The SR latent energy flux density estimates λE_{SR} using H_{SR} based on structure function analysis gave very good estimates compared with eddy covariance (λE_{EC}) estimates, with slopes near 1.0 and RMSE values in the range of 30 W m^{-2}. The λE_{SR} estimates computed using the SR analysis approach using the micro-front time also gave good estimates comparable to λE_{EC}.

The SR and EC methods were used to estimate long-term sensible heat and latent energy flux over a fetch-limited heterogeneous surface (*J. curcas*). The results show that it is possible to estimate long-term sensible heat and latent energy fluxes using the SR and EC methods over *J. curcas*. Continuous measurements of canopy height and leaf area index measurements are needed to determine α. The weighting factor α was approximately 1 for placement heights between 0.2 and 0.6 m above the Jatropha tree canopy. The daily sensible heat and latent energy flux estimates using the SR analysis gave excellent estimates of daily EC sensible heat and latent energy fluxes.

Measurements of sensible heat and estimates of the latent energy fluxes were made for a small reservoir, using the *SR* and *EC* methods. The *SR* sensible heat flux H_{SR} estimates were evaluated using two air temperature time lags r = 0.4 and 0.8 s at 1.0, 1.3, 1.9, 2.5 m above the water surface. An average α value of 0.175 for time lag r = 0.4 s and 0.188 for r = 0.8 s was obtained. The H_{SR} and H_{EC} estimates were small (-40 to 40 W m^{-2}). The heat stored in water was larger in magnitude (-200 to 200 W m^{-2}) compared to the sensible heat flux. The *SR* and *EC* latent energy fluxes were almost the same in magnitude as the available energy, due to the small values of the sensible heat fluxes. The daily evaporation rate ranged between 2.0 and 3.5 mm during the measurement period.

The *SR* method can be used for routine estimation of sensible heat and latent energy fluxes with a reliable accuracy, over a variety of surfaces: short canopies, tall canopies, heterogeneous surface, and open water surface, if the weighting factor α is determined. Alternatively, the *SR* method can be used to estimate sensible heat flux which is exempt from calibration using the other two *SR* analysis approaches, with additional measurement of wind speed for estimating friction velocity iteratively. The advantages of the *SR* method over other micrometeorological methods are the relatively low cost, easy installation and maintenance, relatively low cost for replicate measurements. These investigations may pave the way for the creation of evaporation stations from which real-time and sub-hourly estimates of total evaporation may be obtained relatively inexpensively.

TABLE OF CONTENTS

LIST OF TABLES

LIST OF FIGURES

Chapter 1: Introduction

1.1 Motivation and objectives

The world's available water resources are limited and water is increasingly becoming scarce, especially in countries, such as South Africa, with mean annual rainfall well below the world's average. The demand for water is growing rapidly due to a fast growing population, increase in irrigated agricultural lands, growing economy resulting in increased usage of water by industries, and other environmental uses. Moreover, the challenges of increasing water scarcity are exacerbated by the rising costs of developing new water supplies, degradation of soil in irrigated areas, groundwater depletion, water pollution, evaporative losses, and inefficient use of water. The implementation of effective and sustainable water resources management strategies is then imperative, to meet these increasingly growing demands for water. Accurate assessment of the hydrological cycle components, in particular evaporation is therefore crucial in agriculture and water resources management (Savage *et al.*, 2004).

The South African National Water Act (National Amendment Water Act, 1998) states that scarce water resources should be conserved and equitable allocation of water must be implemented to promote the efficient use of water. The Act requires all major water use sectors be registered and must develop a water use, conservation and protection policy. In addition, the Act also refers to a possible prescription of methods for making a volumetric determination of water for purposes of water allocation, and charges for water use, in case of activities that result in stream flow reduction, such as infrastructure development and catchment management activities. In light of the above-mentioned demand on water resources and given this scenario, it is therefore very important to measure or estimate evaporation continuously and with a reliable accuracy.

The estimation of evaporation is most often difficult and expensive. Practically therefore, the estimation of evaporation over large scales and over long time periods is prohibitively expensive. Many studies have used automatic weather station data to estimate grass reference evaporation or tall crop reference evaporation (Allen *et al.*,

2006), and then use a crop factor approach to obtain the estimates of evaporation. Savage (2007) suggested that high frequency temperature based method pave the way for evaporation stations from which real-time and sub-hourly estimates may be obtained relatively inexpensively.

Evaporation may be estimated using a variety of techniques, including soil water monitoring, lysimetry, and micrometeorological methods. Soil water monitoring is labour intensive and is often inaccurate unless averaged over a long period of time. Lysimeters are expensive, and they are not suitable for widespread evaporation measurements. Micrometeorological methods, such as eddy covariance, Bowen ratio energy balance, surface renewal, flux variance, and optical scintillation provide a proper means of measuring or estimating evaporation, as they do not disturb the microenvironment and they minimize sampling problems by integrating fluxes over a large area. The eddy covariance is a direct method, which uses high frequency measurements of air temperature, wind speed, and water vapour pressure fluctuations. This method is limited by its complexity, high cost and sensitivity of the instruments to damage, and requires distortion corrections, favourable wind directions, careful sensor positioning and alignment. The Bowen ratio method is limited by constraints imposed by extensive fetch requirements. The flux variance method is based on Monin-Obukhov similarity theory (MOST), which refers to the surface layer over an extensive flat and homogeneous surface. Several studies have revealed that the scintillation method is an attractive alternative to measure path-averaged sensible heat flux. Nevertheless the cost of the scintillometer is still high, and the method is based on MOST. Thus, the search for affordable, simple, and accurate methods for determining evaporation is vital for water resources management. Despite the availability of different methods for estimating evaporation, each method has advantages and disadvantages, in terms of accuracy, simplicity, spatial representation, robustness, fetch, and cost.

The surface renewal (*SR*) method is a relatively new, low cost, attractive and simple method. Surface renewal analysis for estimating sensible heat and latent energy flux (evaporation) from canopies involves high frequency air temperature measurements using unshielded and unventilated fine-wire thermocouples. The *SR* method is based on the idea that an air parcel near a surface is renewed by an air

parcel from above. Several studies were reported on the use of the *SR* analysis for estimating sensible heat flux above different canopy surfaces in the past decade. However, the *SR* method must be calibrated against another standard method, such as the eddy covariance method to account for unequal heating of air parcels below the air temperature sensor height. Currently, there are three *SR* analysis approaches: an ideal *SR* analysis model based on structure function analysis; *SR* analysis model with finite micro-front period; and combined *SR* analysis model and similarity theory.

The main aim of this research is to use the *SR* method above various canopies and water, previously untested in South Africa apart from WRC scintillometer report (Savage *et al*., 2004), to estimate sensible heat flux density and compare with eddy covariance, Bowen ratio, flux variance, and surface layer scintillometry estimates, and also to estimate evaporation from additional measurements of net irradiance and soil heat flux density using the shortened energy balance equation.

Essentially the purpose of this study is to estimate sensible heat and latent energy fluxes using the *SR* method over a variety of surfaces, including open water, grassland, Chromolaena, Yellow wood forest, and heterogeneous surface (*Jatropha curcas* trees planted in rows). The following are the specific objectives of this study:

- to estimate and compare sensible heat and latent energy flux density over an open and mixed grassland using *SR* analysis at various heights using two time lags, and compare the *SR* method with eddy covariance, Bowen ratio, and displaced-beam optical scintillometry methods;

- to evaluate the performance of the *SR* method for estimating the sensible heat and latent energy flux (total evaporation) above Triffid weed (*Chromolaena odorata*) and compare the *SR* method with eddy covariance, flux variance, and displaced-beam optical scintillometry methods;

- to estimate and compare sensible heat and latent energy fluxes above Outeniqua Yellow wood forest using the three *SR* analysis approaches: (1) idealized *SR* analysis based on structure function analysis proposed by Paw U *et al*. (1995); (2) *SR* analysis model with finite micro-front time proposed by Chen *et al*. (1997b);

and (3) empirical *SR* analysis model based on similarity theory proposed by Castellvi *et al*. (2002);

- to investigate the applicability of the *SR* method in estimating long-term sensible heat and latent energy fluxes over heterogeneous surfaces such as *J. curcas*;

- to calibrate the sensible heat flux estimates from the *SR* method using measurements obtained from the eddy covariance method and to evaluate the performance of the *SR* method for estimating sensible heat and latent energy fluxes above open water surface.

1.2 Thesis structure

This thesis consists of eight chapters with Chapter 1 as the introductory part of the study and Chapter 2 mainly focusing on the literature review, especially on the theoretical background of the methods used in this study. Chapters 3 to 7 are experimental chapters, focusing on the use of the *SR* method over a variety of selected surfaces.

The first experimental chapter (Chapter 3), discusses the use of the *SR* analysis to estimate sensible heat and latent energy flux at four different measurement heights using two time lags above an open and mixed grassland. Also presented in this chapter is the comparison of the sensible heat and latent energy flux estimates from the *SR* analysis with eddy covariance, Bowen ratio, and optical scintillometry estimates for unstable atmospheric conditions.

In Chapter 4, the performances of the three *SR* analysis approaches in estimating sensible heat and latent energy fluxes over alien invasive Chromolaena were evaluated for unstable conditions using four time lags. Comparisons of the *SR* sensible heat and latent energy flux estimates with eddy covariance, flux variance, and optical scintillation estimates are also presented.

In Chapter 5, the performances of the three *SR* analysis approaches, in estimating sensible heat and latent energy fluxes above an Outeniqua Yellow wood

forest are evaluated for unstable and stable atmospheric conditions using four air temperature time lags at different measurement heights. The sensible heat and latent energy fluxes from the *SR* analysis are compared with eddy covariance measurements for different seasons.

The *SR* and eddy covariance methods are used over a heterogeneous surface, *J. curcas*, to estimate long-term sensible heat and latent energy fluxes (Chapter 6). Comparison of the seasonal estimates of evapotranspiration using the eddy covariance and *SR* methods are presented, spanning a period of almost two years.

Chapter 7 presents the use of the *SR* method for estimating sensible heat flux and open water evaporation from a shallow reservoir. The *SR* method, to the author's knowledge, has not been tested over open water surfaces. The aim of this study is therefore to calibrate the sensible heat flux measurements obtained with the *SR* method against measurements obtained using the eddy covariance method. The performance of the *SR* and eddy covariance methods for estimating sensible heat and latent energy fluxes above open water surface is evaluated.

Chapter 8 presents the overall summary and conclusions as well as recommendations for further studies.

Chapter 2: Literature review

2.1 Introduction to the atmospheric boundary layer

The atmospheric boundary layer (ABL) is the lowest part of the atmosphere which is formed as a result of the interactions between the atmosphere and the surface of the earth. The thickness or height of the ABL varies over time scales of a few hours to about a day and ranges from several tens of meters to several kilometres (Arya, 2001). The atmospheric boundary layer and its characteristics are discussed in detail by Panofsky and Dutton (1984), Stull (1988), Garratt (1992), and Kaimal and Finnigan (1994). The ABL is turbulent and well mixed, and roughly consists of an inner region and outer region (Ekman layer). The structure of an idealized atmospheric boundary layer is schematically shown in Fig. 2.1. In the diagram, h_b is the boundary layer depth, z is the height, and z_o is the roughness length. In the outer region, the flow shows little dependence on surface characteristics, but the Coriolis force due to the earth's rotation is important. However, in the inner region, flow is mainly dependent on the surface characteristics and is little affected by earth's rotation (Kaimal and Finnigan, 1994).

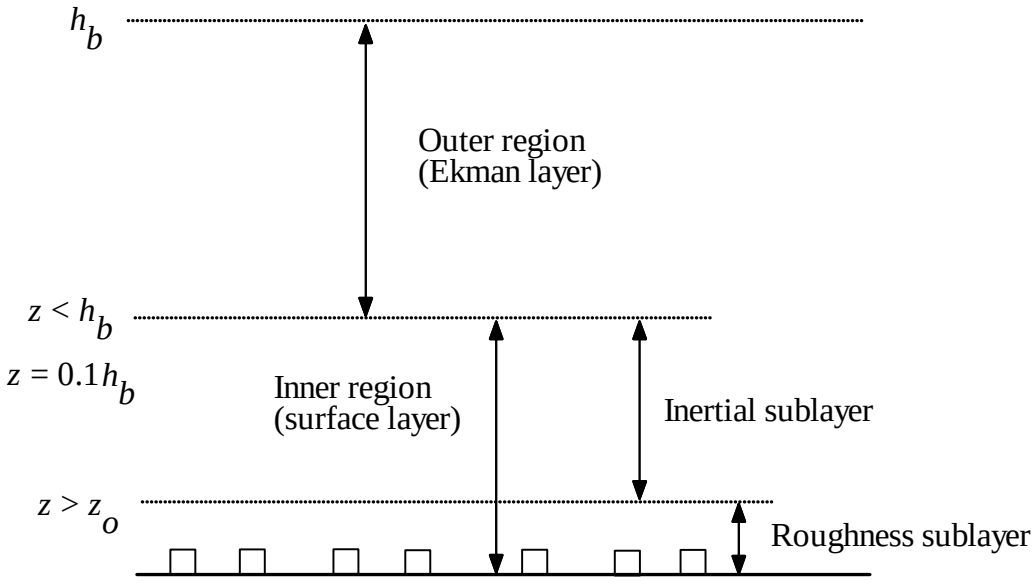

Fig. 2.1 Schematic of the regions of the atmospheric boundary layer (Garratt, 1992).

2.1.1 The atmospheric surface layer

The atmospheric surface layer is the lower part of the atmospheric boundary layer where most of the surface flux measurements are performed (Fig. 2.1). The surface layer is mainly dependent on the surface characteristics, and within this layer the interaction between the Earth's surface and the atmosphere is mainly accomplished by turbulent motions (Garratt, 1992). The surface layer is divided in two sublayers: the roughness (interfacial) sublayer; and inertial sublayer (constant flux layer).

The roughness sublayer is the layer of air within and just above the roughness elements comprising the land or sea surface (Garratt, 1992). The roughness sublayer normally extends from the ground to a distance of 2 to 3 times the canopy height. Within this layer, the turbulence and mean profiles are strongly affected by the structure of the roughness elements such as, the uneven height of plants and the spacing of plants (Mahrt, 2000). The inertial sublayer is the layer above the roughness sublayer and represents the top portion of the surface layer (Fig. 2.1), and is the layer where the scalar flux is approximately constant. Within this sublayer, the horizontal wind speed profile in neutrally buoyant conditions is logarithmic (Garratt, 1992).

In general, Monin-Obukhov similarity theory (MOST) successfully predicts mean and turbulent statistics in the inertial sublayer, but is not applicable within the roughness sub-layer as turbulence and local circulations are strongly affected by individual roughness elements. The thickness of the roughness sublayer is proportional to the degree of roughness and heterogeneity at the canopy surface. The roughness sublayer depth z^* may be estimated as:

$$z^* = h + 2(h - d) \approx 5h/3 \tag{2.1}$$

where h is the canopy height and d is the zero plane displacement height (Sellers *et al.*, 1986). Measurements of fluxes are proportional to measurement height z in the roughness sublayer while in the inertial sublayer it is proportional to $z - d$ (Chen *et al.*, 1997b).

2.1.2 Turbulence

Turbulence is the chaotic, strongly rotational motion of many flows, which is manifested in the form of irregular, almost random fluctuations in velocity, air temperature, and scalar concentrations around their mean values in time and space (Arya, 2001). Turbulence separates air parcels and mixes air properties, and has eddy structures arranged in a continuous spectrum of sizes and intensities (Panofsky and Dutton, 1984). An eddy is an abstract concept used to describe turbulence which may be considered “akin to a vortex or a whirl in common terminology” (Arya, 2001). Eddies are complex three-dimensional structures that also change in shape and size with time.

The motions in the atmospheric boundary layer are almost always turbulent, and in the surface layer, turbulent flows are diffusive and intermittent. Turbulence mixes air with different properties and creates fluxes of momentum, heat, and latent energy in the atmospheric boundary layer (Panofsky and Dutton, 1984). The turbulent fluxes of momentum, heat, and latent energy have a strong effect on conditions near the surface of the earth, and are responsible for the weather and climate in which agricultural crops grow. Many studies have been done in the past century on atmospheric turbulence, with the pioneering work of Osborne Reynolds before 1900 (Panofsky and Dutton, 1984, and references therein). However, of paramount interest to the field of micrometeorology is the study reported by Monin and Obukhov (1954), which developed a method for combining theories of mechanical and convective turbulence to determine sensible heat and momentum fluxes. This method is commonly referred to as the Monin-Obukhov similarity theory (MOST).

2.1.3 Monin-Obukhov similarity theory

The atmospheric surface layer is also known as the constant flux layer because fluxes are nearly constant with height, with variations of less than 10 % (Panofsky and Dutton, 1984) under steady-state and horizontal homogeneous conditions. MOST relates mean profiles of scalars and wind speed to turbulent fluxes of heat, latent energy, and momentum in a horizontally homogeneous atmospheric surface layer (Brutsaert, 1982).

Monin and Obukhov (1954) introduced two scaling parameters, which are independent of height in the surface layer for the structure of turbulence. The friction velocity u_* (Garratt, 1992):

$$u_* = [(\overline{u'w'})^2 + (\overline{v'w'})^2]^{1/4} \tag{2.2}$$

where u, v, and w are the three dimensional orthogonal wind speeds, and u', v', and w' are the fluctuations from the mean of u, v, and w respectively. The u and v components represent the stream-wise and lateral directions of the wind speed, and w is the vertical wind speed. The second scaling parameter introduced, which is a function of momentum and sensible heat fluxes, is the Obukhov length, L_o:

$$L_o = -\frac{\rho c_p T_a u_*^3}{kgH} \tag{2.3}$$

where ρ is the density of air, c_p the specific heat capacity of air at constant pressure, T_a the absolute air temperature, u_* the friction velocity, k the von Karman constant, g the acceleration due to gravity, and H the sensible heat flux density. The negative sign is the sign of the sensible heat flux corresponding to the vertical air temperature difference between two heights. The Obukhov length can be interpreted as the height, above $d + z_o$, for which free convection dominates (Arya, 2001; Savage *et al*., 2004).

Other similar key scaling parameters which determine the structure of turbulence, are the turbulent temperature scale T_*:

$$T_* = \frac{H}{\rho c_p u_*} \tag{2.4}$$

and the turbulent humidity scale q_*:

$$q_* = \frac{E}{\rho u_*} \tag{2.5}$$

where E is the water vapour mass flux density (kg s^{-1} m^{-2}).

Monin and Obukhov (1954) stated that in a horizontally homogeneous surface layer the mean flow and turbulent characteristics can depend only on friction velocity u_*, the height above the surface z, the surface kinematic heat flux $H/\rho c_p$, and the buoyancy variable g/T_a (Garratt, 1992; Arya, 2001). That is, turbulent characteristics depend upon a dimensionless stability parameter ζ:

$$\zeta = z/L = (z-d)/L_o \tag{2.6}$$

where z is the height above the surface and d is the zero plane displacement height.

MOST can be used to normalize various atmospheric parameters and statistics by using the scaling parameters u_* and L_o, which has become a universal function of ζ. The dimensionless stability parameter ζ is a theoretical indicator of the atmospheric stability. In Table 2.1, general properties of $(z-d)/L_o$, and stability classes are described.

2.1.4 Footprint of surface layer flux measurements

Understanding the turbulent transport of surface layer fluxes from natural and vegetated surfaces is very important in land-atmosphere interaction studies in the ABL. Turbulent flux sensors are deployed to measure signals that reflect the influence of the underlying surface on the turbulent exchange (Schmid, 2002). Surface layer flux measurements are influenced by diffused fluxes upwind of the surface under study, which may include large areas with different types of sources and sinks (Gash, 1986).

Table 2.1 Summary of the stability classes using the dimensionless stability parameter $\zeta = (z-d)/L_o$ (Deardorf, 1978; Panofsky and Dutton, 1984).

Class	Range in $\zeta = (z-d)/L_o$	Description
Convective	ζ < -0.05	Heat convection dominant
Unstable	-0.05 ≤ ζ < -0.02	Mechanical turbulence dominant
Neutral	-0.02 ≤ ζ < 0.02	Purely mechanical turbulence (wind shear dominates)
Slightly stable	0.02 ≤ ζ < 0.2	Mechanical turbulence slightly damped by temperature stratification
Strongly stable	ζ > 0.2	Mechanical turbulence severely reduced by temperature stratification

This spatial context of the measurement of surface layer fluxes is commonly referred to as the footprint of a measurement (Schmid, 2002), or the effective fetch (Pasquill, 1972, cited by Schmid, 2002). The footprint of a turbulent flux measurement defines the spatial context of the measurement or the 'field of view' of the measurement of the surface-atmosphere exchange (Schmid, 2002). The footprint function $F(x, z_m - d)$ for a turbulent flux at a distance x from the source and at a measurement height z_m, for a surface with a zero displacement height d is defined as (Horst and Weil, 1992):

$$F(x, z_m - d) = \int_{-\infty}^{x} S(x) f(x, z_m - d)\, dx \qquad (2.7)$$

where $F(x, z_m - d)$ is the flux measured at height $z_m - d$, $S(x)$ the source strength at a distance x, f the footprint at a distance x (with distance x taken as the downwind fetch).

Flux footprint analysis is commonly used to quantify the contributing source areas to scalar flux measurement or to examine adequate fetch requirements (Hsieh *et al.*, 2000). As a 'rule of thumb' the fetch-to-height ratio is 100 to 1. However, Leclerc and Thurtell (1990) reported that 100 to 1 fetch-to-height ratio underestimates fetch requirements for a smooth surface in stable conditions. Over a homogeneous surface, the exact location of a sensor is not an issue, because the fluxes from all parts of the

surface are assumed equal (Schmid, 2002). However, for a heterogeneous surface, the measured signal depends on which part of the surface has the strongest influence on the sensor, and thus on the location and size of its footprint (Schmid, 2002). Therefore, turbulent flux sensors must be located sufficiently high so that the footprint of the flux measurement covers a representative sample of the surface being studied throughout the range of atmospheric conditions encountered at the site (Finnigan, 2004).

2.1.5 Radiation and energy balance in the atmospheric boundary layer

Solar radiation is the only significant source of energy available at the earth's surface used for heating the air and soil, evaporating water, and driving photosynthesis within the earth-atmosphere system (Campbell and Diak, 2005). Net irradiance is the sum of all incoming and outgoing irradiances at the earth's surface (Arya, 2001). For a smooth, horizontal, homogeneous, and extensive surface, net irradiance R_n is the sum of the incoming short wave I_s and long wave L_d irradiances, less the reflected short wave $r.I_s$ and emitted long wave L_u irradiances:

$$R_n = I_s - r.I_s + L_d - L_u \tag{2.8}$$

and commonly referred to as the radiation balance equation. Net irradiance is the major source of energy for heating and cooling at the surface of the earth and is one of the major components of the energy balance equation.

Micrometeorological methods (eddy covariance, surface renewal, Bowen ratio, scintillometry, and flux variance) used to estimate total evaporation are ultimately based on the energy balance equation, which accounts for all losses of energy that are available for vapourizing water. The shortened energy balance equation is expressed as:

$$R_n = G + H + \lambda E \tag{2.9}$$

where R_n is the net irradiance, G is the soil heat flux density, H is the sensible heat flux density, and λE is the latent energy flux density where advection is assumed to

be negligible. For a short and flat surface, the shortened energy balance equation also neglects the energy associated with photosynthesis and respiration, and energy stored in plant canopies as they are usually small compared with the other terms (Thom, 1975). Therefore, the four essential energy fluxes for a short and flat surface are the net irradiance, sensible heat, latent energy, and soil heat flux density if advection is negligible (Savage *et al*., 2004).

The sign convention is that during the day net irradiance is positive with terms on the right hand side of Eq. (2.9) leaving the earth's surface regarded as positive. The available energy flux density A at the canopy surface (W m^{-2}) is therefore, the difference between the net irradiance and the soil heat flux density:

$$A = R_n - G = H + \lambda E \tag{2.10}$$

The available energy, $R_n - G$, is equal to the right hand term of Eq. (2.10), $H + \lambda E$ the turbulent fluxes.

Soil heat flux density, G, is the amount of thermal energy through unit area of soil per unit of time (Sauer and Horton, 2005), and is a function of the change in soil temperature with time and the thermal and physical properties of the soil. The soil heat flux G is estimated as the sum of the flux measured using the soil heat flux plates G_{plate} at a depth of 80 mm and the energy flux stored in soil above the plates G_{stored}:

$$G = G_{plate} + G_{stored} \tag{2.11}$$

The stored heat flux density G_{stored} is estimated from measurements of the temporal change in soil temperature and the specific heat capacity of the soil above the soil heat flux plate. The stored flux G_{stored} is calculated as (Savage *et al*., 1997):

$$G_{stored} = \rho_{soil} c_{soil} \Delta z \overline{\Delta T_{soil}} / \Delta t \tag{2.12}$$

where ρ_{soil} is the bulk density of the soil (kg m^{-3}), c_{soil} is the specific heat capacity of the soil (J kg^{-1} ^{o}C^{-1}), Δz is the soil depth, $\overline{\Delta T_{soil}}$ is the average soil temperature difference (between 20 and 60 mm) during a measurement interval Δt. The volumetric heat capacity of the soil is calculated as:

$$\rho_{soil}\, c_{soil} = \rho_{soil}\, c_{dsoil} + \rho_w\, \theta_v\, c_w \tag{2.13}$$

where c_{dsoil} is the dry soil specific heat capacity ($\approx$800 J kg^{-1} ^{o}C^{-1}), ρ_w is the density of water (1000 kg m^{-3}), θ_v the volumetric soil water content (m^3 m^{-3}), and c_w is the specific heat capacity of water (= 4190 J kg^{-1} ^{o}C^{-1}).

The latent energy flux λE (W m^{-2}) is the result of total evaporation, and condensation at the surface and is the product of the specific latent heat of vapourization, λ (in J kg^{-1}) and the water vapour flux density E (kg s^{-1} m^{-2}). Latent energy flux density λE may be estimated indirectly as a residual of the shortened energy balance Eq. (2.9) using sensible heat flux density H, measured net irradiance R_n, and soil heat flux density G as:

$$\lambda E = R_n - G - H \tag{2.14}$$

Sensible heat flux H (W m^{-2}) is the heat flux which heats the air above the soil and plant canopy surfaces, and arises as a result of difference in temperatures between the surface and the air above. Sensible heat flux may be estimated using different micrometeorological methods, such as eddy covariance, surface renewal, Bowen ratio energy balance, flux variance, and optical scintillation. The different micrometeorological methods used in this study for estimating H are discussed in the subsequent sections.

Since the latent energy flux is estimated as the residual of the shortened energy balance equation, the errors and uncertainties in soil heat flux and net irradiance measurements need to be considered. These errors are due to calibration errors and errors associated with field measurements, including spatial variation differences. The errors associated with field measurements of soil heat flux are

dependent on the measurement errors due to change in soil temperature from one measurement period to another, errors in placement depth of the soil heat flux plates, and the error in the measurement of soil water content (Savage et al., 2004).

2.2 Surface renewal method

The concept of surface renewal (*SR*) was originally developed in the field of chemical engineering by Higbie (1935) to investigate interfacial heat transfer between a liquid and a gas (Paw U *et al*., 2005). The SR analysis as used for plant canopies was originally conceived as a simple 'transilient' theory (Stull, 1984), which arises from the concept that turbulent exchange can be described as the exchange of parcels from one known height to another, with weighting factors assigned to the fraction of exchange to one height from each of many other heights (Paw U *et al*., 2005).

Paw U and Brunet (1991) pioneered the SR method for estimating H, which is based on the idea that an air parcel near a surface is renewed by an air parcel from above. This method is relatively new, attractive and quite simple (Paw U *et al*., 1995; Snyder *et al*., 1996; Spano *et al*., 1997a, b, 2000; Drexler *et al*., 2004). The SR method for estimating fluxes from canopies involves high frequency air temperature measurements (typically 2 to 10 Hz) using fine wire thermocouples. The high frequency air temperature fluctuations exhibit organized coherent structures which resemble ramp events (Bergström and Högström, 1989; Gao *et al*., 1989; Shaw *et al*., 1989; Paw U *et al*., 1992). These coherent structures (Fig. 2.2) are responsible for transport of momentum, heat and other scalar quantities (Raupach *et al*., 1989; Qui *et al*., 1995; Raupach *et al*., 1996).

Sensible heat flux density H is estimated based on the high frequency air temperature fluctuations and latent energy flux density λE is obtained as the residual of the shortened energy balance equation (Eq. 2.9). There are three different approaches or models for estimating the sensible heat flux density using the SR analysis: an ideal SR method based on structure function analysis from Van Atta (1977); SR analysis model with finite microfront period (Chen *et al*., 1997b); and empirical SR analysis method based on Monin-Obukhov similarity theory (MOST) (Castellvi *et al*., 2002).

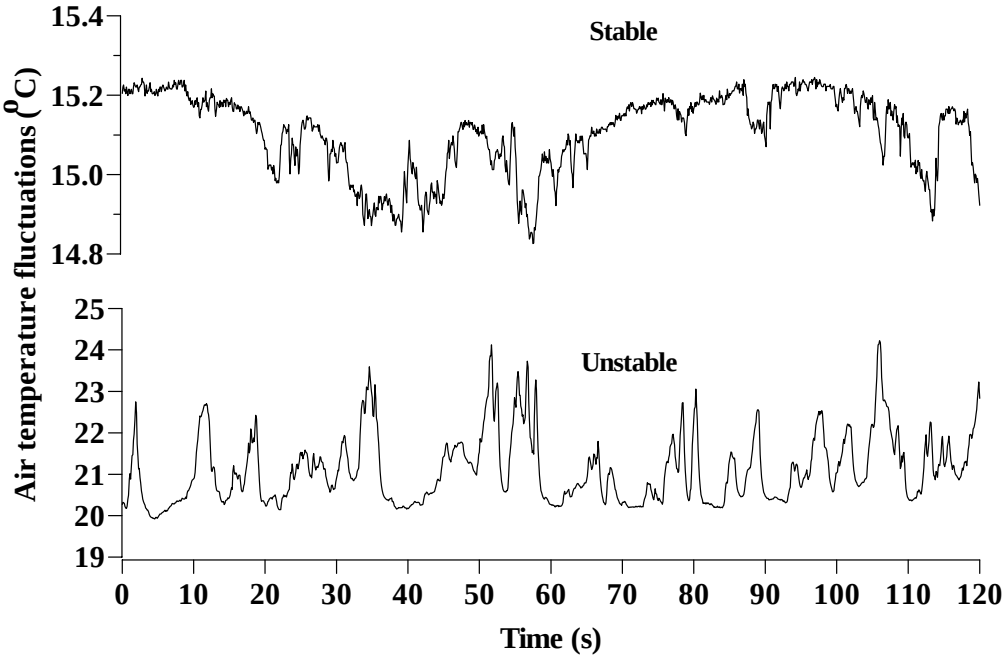

Fig. 2.2 Air temperature ramps observed in a sample of 120 s of 10 Hz air temperature traces. The measurements were taken at 0.5 m above grass (0.3 m tall) for unstable (10h00) and stable conditions (01h00), in the Hay Paddock area neighbouring Ashburton and close to Pietermaritzburg, South Africa for day of year 321 (2003).

2.2.1 Ideal surface renewal analysis model based on structure function analysis

The *SR* analysis model assumes that the turbulent exchange of air temperature is caused by instantaneous replacement of an air parcel that is in contact with a surface. The parcel heats or cools while it is at the surface because of energy exchange between the air and the canopy elements, then the parcel ejects from the surface and a new air parcel sweeps in to renew the ejected air (Paw *et al.*, 1995; Katul *et al.*, 1996; Snyder *et al.*, 1996; Spano *et al.*, 1997a).

Paw U and Brunet (1991) proposed this model by assuming that under unstable atmospheric conditions when the canopy is warmer than the air, any air temperature increase represents air being heated by the canopy. Under stable conditions, when the canopy is cooler than the air, any air temperature decrease

represents air being cooled by the canopy. For a given measurement period, the sensible heat flux density H at any height z is the net exchange of heat associated with all ramps during this period. Paw U *et al.* (1995) expressed H as the change in heat energy content of air with time:

$$H = \alpha \rho c_p \frac{dT}{dt} \frac{V}{A}, \tag{2.15}$$

where α is a correction factor (regression coefficient fit to the above equation when H is measured independently using other methods such as eddy covariance), dT/dt is the rate of change in air temperature (^{o}C s^{-1}) and V/A is the volume of air per unit horizontal area of air. If the air temperature measurement is taken at canopy height, then V/A (which is the vertical distance) will be the canopy height (z_c). High frequency air temperature data are measured at a fixed point and hence the use of Eq. (2.15) assumes that dT/dt is approximately equal to $\partial T/\partial t$ and internal advection is negligible (Paw U and Brunet, 1991; Paw U *et al*., 1995). This assumed linear proportionality between the advective term $\partial T/\partial t$ and the total derivative dT/dt has been discussed in detail by Paw U *et al*. (1995). However, this assumption may not be correct under all conditions. For example the assumption may be invalid when there is strong local advection and under high wind shear close to the canopy top of low vegetation and soil surface (Snyder *et al*., 1996). Low pass filtering techniques were used by Paw U *et al*. (1995) to smooth the high frequency air temperature data to remove the internal advection and to determine H. However, the filtering technique is cumbersome, due to the necessity of choosing filtering functions and use of numerical methods to identify scalar increases or decreases (Paw U *et al*., 2005).

When high frequency air temperature measurements are taken at a point at or above the canopy top, ramps are observed (Fig. 2.2) in the air temperature traces. These air temperature ramps are characterized by an amplitude a (^{o}C), a ramping period L_r (s) where the change in air temperature with time occurs, and a quiescent period L_q (s) for which there is no change in air temperature with time (Snyder *et al*., 1996; Snyder *et al*., 1997), as shown in Fig. 2.3.

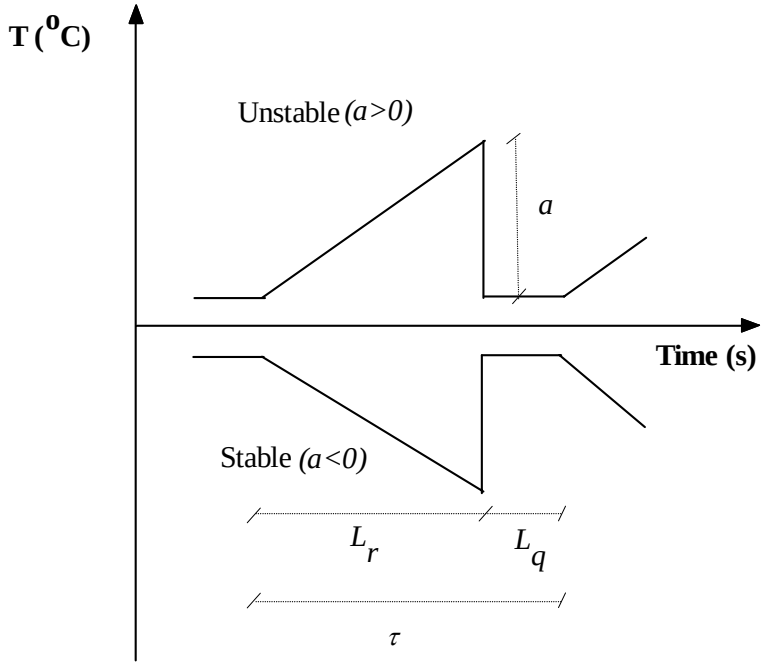

Fig. 2.3 An ideal surface renewal analysis ramp model, assuming a sharp instantaneous drop in air temperature with amplitude $a > 0$ for unstable and $a < 0$ for stable atmospheric conditions. The ramping period is L_r and L_q the quiescent time period with $\tau = L_r + L_q$ the total ramping period (inverse ramp frequency).

The total ramp duration τ or in other words the inverse ramp frequency is the sum of ramping period L_r and quiescent period L_q. The amplitude a is positive when the atmosphere is unstable and (the sign of H is positive) and a is negative for stable atmospheres (H is negative).

For estimating H, Snyder *et al*. (1996) simplified and modified the *SR* analysis by substituting dT/dt in Eq. (2.15) by a/τ (^{o}C s^{-1}) for the average rate of change in air temperature for the total ramping period:

$$H = \alpha \rho c_p \frac{a}{L_r + L_q} z, \tag{2.16}$$

where α is a weighting factor accounting for the spatially averaged (vertical) air temperature derivative from the bottom to the top of the air parcel (a correction factor for unequal heating or cooling below the sensor). The weighting factor α, depends on z (which is the measurement height), canopy structure, thermocouple size, and the time lag used in the air temperature structure function (Snyder *et al*., 1996; Duce *et al*., 1998; Spano *et al*., 1997a, b, 2000; Paw U *et al*., 2005). Generally, α = 0.5 for coniferous forest, orchards, and maize canopies for measurements taken at canopy height (Paw U *et al*., 1995). For short turf grass (0.1 m tall), excellent estimates of H were obtained using α = 1, when the measurements are taken at 0.35 m and 0.70 m above the turf grass (Snyder *et al*., 1996).

Snyder *et al*. (1996) used structure functions of air temperature and the analysis technique from Van Atta (1977) to estimate the amplitude a and inverse ramp frequency $\tau = L_r + L_q$. The structure function value $S^n(r)$ is calculated using the relation,

$$S^n(r) = \frac{1}{m-j}\sum_{i=1+j}^{m}(T_i - T_{i-j})^n, \tag{2.17}$$

where m is the number of data points in the time interval measured at frequency f (Hz), n is the power of the function, j is the time lag between data points corresponding to a time lag $r = j/f$ and T_i is the ith temperature sample. Van Atta suggested that, the time lag r must be much less than τ.

An estimate of the mean value for amplitude (a) during the time interval is determined by solving the equation for the real roots.

$$a^3 + pa + q = 0 \tag{2.18}$$

where

$$p = 10S^2(r) - \frac{S^5(r)}{S^3(r)} \tag{2.19}$$

and

$$q = 10S^3(r) \tag{2.20}$$

The ramping period τ is calculated using

$$\tau = -\frac{a^3 r}{S^3(r)} \tag{2.21}$$

The main advantage of this *SR* analysis model is that only high frequency air temperature data at a measurement height is required to obtain sensible heat flux density. In addition, it is relatively simple and measurements can be easily replicated at a lower cost. The disadvantage of this model is that it must be calibrated using sonic anemometer estimates of sensible heat flux to account for α. The weighting factor α, depends on structure function time lag (Snyder *et al*., 1996), air temperature sensor size (Duce *et al.*, 1998, cited by Paw U *et al*., 2005), and the measurement height (Paw U *et al*., 1995; Snyder *et al*., 1996). The size of the air temperature sensor affects the amplitude a and the ramping period τ, and hence α. The time constant represents the time it takes for the sensor to respond to 63.2 % of a step change in temperature. For a 75-μm diameter sensor for example, the time constant is 50 ms for low air flow (Medtherm, 2007). However, if the correction factor α is used, H values will be comparable regardless of the thermocouple diameter used (Duce *et al.*, 1998). Duce *et al*. (1998) found lower RMSE sensible heat flux values for a thermocouple diameter of 75-μm compared to 50, 25, and 12.5-μm diameters. Therefore, the use of 75-μm diameter sensors is adequate for air temperature measurements for the *SR* method. The α values for various surfaces using different time lags and sensor sizes are shown in Table 2.2, for unstable atmospheric conditions. For measurements made at the canopy top, the measurement height above the canopy z is zero.

Once the calibration factor α is determined it is quite stable and does not change from site to site regardless of the weather conditions unless there are considerable changes in vegetation canopy structure (Paw U *et al*., 1995; Snyder *et al*., 1996; Spano, 2000). The parameter α increases to some extent with temperature sensor size and this can cause a problem related to sensitivity of the *SR* model to slower response scalar sensors (Paw U *et al*., 2005) particularly near the canopy surface.

Table 2.2 The weighting factor α for a range of surfaces using different time lags and sensor sizes during unstable conditions. The slope of the regression of H estimated using the SR method *versus* H obtained using a standard method (eddy covariance) yields α for linear fits forced through the origin.

Surface	Canopy height (m)	Height above canopy (m)	Sensor size (μm)	Sampling frequency (Hz)	Time lag r (s)	α	Authors
Bare-soil	0.00	-	12.7	8	0.25	0.90	Duce *et al.* (1998)
Bare-soil	0.00	-	25.4	8	0.25	1.04	Duce *et al.* (1998)
Bare-soil	0.00	-	76.2	8	0.25	1.88	Duce *et al.* (1998)
Bare-soil	0.00	0.03	25.0	10	0.10	0.69	Chen *et al.* (1997b)
Endorreic salty lagoon	0.00	0.90	76.2	8	0.75	1.00	Zapta and Martinez-Cob (2001)
Mulch	0.05	0.09	25.0	10	0.10	0.51	Chen *et al.* (1997b)
Grass (alta fescue)	0.10	0.35	76.2	8	0.75	1.00	Snyder *et al.* (1996)
Grass (alta fescue)	0.10	0.30	76.2	8	0.25	0.97	Duce *et al.* (1997)
Wheat	0.70	0.30	76.2	8	0.50	1.00	Duce *et al.* (1997)
Sorghum	0.70	0.30	76.2	8	0.75	1.02	Duce *et al.* (1997)
Wheat	0.90	0.50	25.4	16	0.30	1.00	Anandakumar (1999)
Maize	2.60	0.00	12.5	10	0.10	0.50	Paw U *et al.* (1995)
Walnut orchard	6.00	0.00	12.5	10	0.10	0.50	Paw U *et al.* (1995)
Avocado	5.20	0.00	76.2	8	0.50	0.59	Spano *et al.* (1997b)
Sparse grape vine	2.20	0.00	76.2	8	0.50	0.87	Spano *et al.* (1997b)
Douglas-fir forest	16.70	6.30	25.0	2	0.50	0.52	Chen *et al.* (1997b)
Mixed deciduous forest	18.00	0.00	12.5	10	0.10	0.50	Paw U *et al.* (1995)

2.2.2 Surface renewal analysis model with finite microfront period

Chen *et al*. (1997a) proposed another scheme, which takes into consideration a finite microfront period L_f instead of a sharp decrease in air temperature (Fig. 2.4), and assumes an insignificant quiescent period L_q to avoid numerical complexity. The quiescent period exists, but when the model takes into account the quiescent period between the microfront and formation of the next ramp, there were no significant changes in the sensible heat flux estimates.

The SR model estimates the amplitude a and total ramp duration $\tau = L_r + L_f$, from fluctuations of high frequency air temperature measurements using a cubic temperature structure function as:

$$\frac{a}{\tau^{1/3}} = -\gamma \left[\frac{S^3_{(r_m)}}{r_m} \right]^{1/3}, \qquad (2.22)$$

where $S^3_{(r_m)}$ is the third order of the structure function for temperature, r_m is the sampling time interval (time lag) at which $-(S^3_{(r)}/r)^{1/3}$ is maximum, and γ is a coefficient which corrects for the difference between $a/\tau^{1/3}$ and the maximum value of $-(S^3_{(r)}/r)^{1/3}$.

Raupach *et al*. (1989) predicted that for canopies $1/\tau$ should scale with maximum wind shear (du/dz at $z = h$, where u is mean wind speed and h is canopy height). In the canopy and roughness sublayer, transport of momentum and scalar fluxes are dominated by eddies of length scale comparable to h, while in the inertial sublayer, dominant eddies scale with $z - d$, where d is zero-plane displacement height (Raupach *et al*., 1996; Chen *et al*., 1997b).

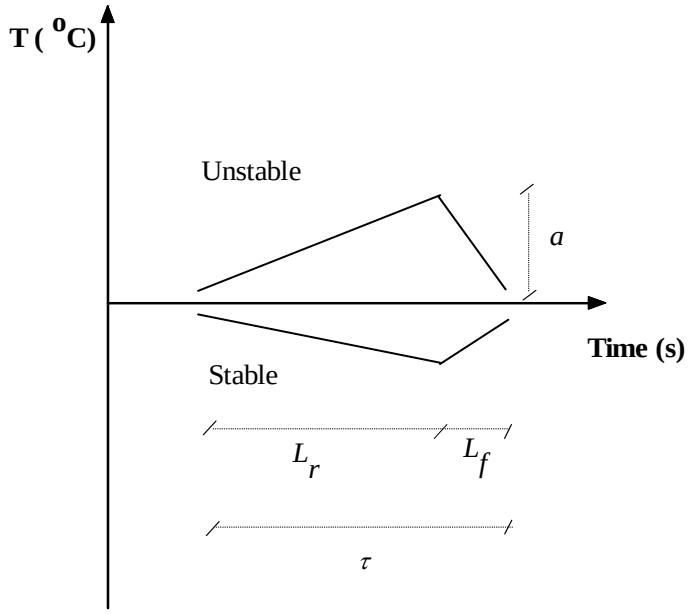

Fig. 2.4 Surface renewal analysis ramp model which assumes a finite microfront time, where a is the air temperature amplitude, L_r is the ramping period, L_f is the microfront period, and τ is the total ramp period.

Chen *et al*. (1997b) scaled $1/\tau$ as follows,

$$\frac{1}{\tau} = \begin{cases} \beta \dfrac{u_*}{h}, \;\; 0.2h < z \le h + 2(h-d), \\ \beta \dfrac{u_*}{z-d}, \; z > h + 2(h-d), \; z \le 0.2h, \end{cases} \tag{2.23}$$

where β is an empirical coefficient and u_* is the friction velocity. Following Sellers *et al*. (1986), the roughness sublayer is assumed to be between $z = h$ and $z = h + 2(h-d)$. The layer adjacent to the soil within canopies ($z \le 0.2h$) is treated the same as the inertial sublayer, with appropriate u_* and d for the soil or canopy understory (Lee and Black, 1993).

Chen *et al*. (1997b) recommended that for routine application of the model, only the maximum of $-(S^3_{(r)}/r)^{1/3}$ is required from high frequency air temperature data. According to the model, H is proportional to $z/h^{2/3}$ in the roughness sublayer and proportional to $z/(z-d)^{2/3}$ in the inertial sublayer. Substituting expressions for a and τ from Eqs (2.22) and (2.23) into Eq. (2.16) to obtain H yields,

$$H = \begin{cases} -\alpha\beta^{2/3}\gamma\rho c_p \left[\dfrac{S^3_{(r_m)}}{r_m}\right]^{1/3} u_*^{2/3} \dfrac{z}{h^{2/3}}, \;\; 0.2h < z \le h + 2(h-d), \\ -\alpha\beta^{2/3}\gamma\rho c_p \left[\dfrac{S^3_{(r_m)}}{r_m}\right]^{1/3} u_*^{2/3} \dfrac{z}{(z-d)^{2/3}}, \; z > h + 2(h-d), \; z \le 0.2h, \end{cases} \tag{2.24}$$

The empirical combined coefficient $\alpha\beta^{2/3}\gamma$ is a common factor in both roughness and inertial sublayers. Chen et al. (1997b) found a roughly constant value of 0.4 (Table 2.3) for the combined coefficient $\alpha\beta^{2/3}\gamma$, in their experiment on Douglas-Fir forest, bare soil, and straw mulch.

Sensible heat flux density may be estimated from the average cubic temperature structure function (using high frequency air temperature data) and measured friction velocity within the canopy and roughness sublayers and inertial sublayer, using this model for stable and unstable conditions. The disadvantage of this model is that additional measurement of horizontal wind speed is needed to determine the friction velocity iteratively, which is used in Eq. (2.24) for estimating H. Another drawback of this model is that very high frequency (80 Hz) air temperature data is required to determine the coefficients β and γ, because of the short duration of the microfront (Castellvi, 2004).

Table 2.3 Average coefficients α, β, γ, and the combined coefficient $\alpha\beta^{2/3}\gamma$, for Douglas-fir forest, straw mulch, and bare soil (Chen *et al*., 1997b)

Canopy	α	β	γ	$\alpha\beta^{2/3}\gamma$
Douglas-fir forest	0.527	0.705	1.001	0.418
Straw mulch	0.511	0.538	1.175	0.397
Bare soil	0.691	0.398	1.104	0.413

2.2.3 Combined surface renewal analysis model and similarity theory

Castellvi *et al*. (2002) proposed an *SR* analysis model based on turbulent diffusion approach (K theory), to estimate sensible heat flux density H using high frequency air temperature data, friction velocity, and similarity formulae. The K theory describes the sensible heat flux density as:

$$H = \rho c_p K_h \frac{dT}{dz} \tag{2.25}$$

where T is average air temperature during the measurement time, K_h is the turbulent transfer coefficient or eddy diffusivity for heat, and z is the height above the surface. Invoking Eq. (2.16) from the ideal *SR* model (Paw U *et al*., 1995), the variable (αz) represents the "effective eddy size" responsible for the air parcel renewal (Castellvi *et al*., 2002: Castellvi, 2004). Since ramp-like structures (characterized by amplitude a and total ramp duration τ) contribute to vertical transport, Castellvi *et al*. (2002) proposed the following relationship:

$$\begin{aligned} &\frac{a}{\alpha z} \propto \frac{\partial T}{\partial z} = \beta \frac{a}{z}, && \text{for the roughness sublayer} \\ &\frac{a}{\alpha z} \propto \frac{\partial T}{\partial z} = \beta \frac{a}{z-d}, && \text{for the inertial sublayer} \end{aligned} \tag{2.26}$$

where T is mean air temperature, β is a scale or link parameter (not to be confused with β in Eq. 2.23), and d is the zero-plane displacement height. When

measurements are taken well above the canopy top (inertial sublayer), MOST can be used to express K_h as follows:

$$K_h = k\,u_*(z-d)\,\phi_h^{-1}(\zeta) \tag{2.27}$$

where $\phi_h(\zeta)$ is the stability function for heat. Following Businger *et al*. (1971), the stability function $\phi_h(\zeta)$ is

$$\begin{aligned} &\text{unstable} && \phi_h(\zeta) = 0.74/\sqrt{1-9\zeta} \\ &\text{neutral} && \phi_h(\zeta) = 0.74 \\ &\text{stable} && \phi_h(\zeta) = 0.74 + 4.7\zeta \end{aligned} \tag{2.28}$$

where ζ is a dimensionless buoyancy (stability) parameter (Eq. 2.6).

Castellvi *et al*. (2002) proposed the following relationship to estimate H in the inertial and roughness sublayers by combining Eqs (2.26), (2.27), and (2.28) to yield

$$\begin{aligned} &\text{roughness sublayer} && H = \rho c_p \beta_2 a\,u_* \\ &\text{inertial sublayer} && H = \rho c_p \beta_1 a\,u_* \phi_h^{-1}(\zeta) \end{aligned} \tag{2.29}$$

where the amplitude β_1 is a scale parameter for the inertial sublayer, β_2 scale parameter for the roughness sublayer, and a is determined using the Van Atta (1977) approach with u_* and ζ determined by iteration. They found β_1 values ranging from 0.10 to 0.15 and β_2 values ranging from 0.23 to 0.33 above grass, wheat, and grapevine canopies for measurements taken in both inertial and roughness sublayers.

Castellvi (2004) derived the following relationship for estimating the weighting factor α in Eq. (2.16) measurements above the canopy,

$$\alpha = \begin{cases} \left[\dfrac{k}{\pi} \dfrac{(z-d)}{z^2} \dfrac{\tau u_*}{\phi_h(\zeta)} \right]^{1/2}, & (z-d) > z^* \\ \left[\dfrac{k}{\pi} \dfrac{z^*}{z^2} \dfrac{\tau u_*}{\phi_h(\zeta)} \right]^{1/2}, & h \le (z-d) \le z^* \end{cases} \tag{2.30}$$

where z^* is the roughness sublayer depth, which may be estimated using Eq. (2.1) (Sellers *et al*., 1986).

Combining Eqs (2.16) and (2.30) Castellvi (2004) proposed the following expression for estimating sensible heat flux density:

$$H = \begin{cases} \rho c_p \left(\dfrac{a}{\tau^{1/2}} \right) \left(\dfrac{k(z-d)}{\pi} \right)^{1/2} \left(\dfrac{u_*}{\phi_h(\zeta)} \right)^{1/2}, & (z-d) > z^* \\ \rho c_p \left(\dfrac{a}{\tau^{1/2}} \right) \left(\dfrac{kz^*}{\pi} \right)^{1/2} \left(\dfrac{u_*}{\phi_h(\zeta)} \right)^{1/2}, & h \le (z-d) \le z^* \end{cases} \tag{2.31}$$

Equation (2.31) is valid when measurements are made over homogeneous canopies also stationary conditions should apply during the sampling period. However, the relationship is exempt from calibration regardless of the stability conditions (Castellvi, 2004). Also by combining Eqs (2.30), (2.31), and invoking the relationship between the ramp period and amplitude (Eq. 2.22) from the microfront model, Castellvi (2004)[†] derived the following relationship to estimate sensible heat flux density:

$$H = \begin{cases} \rho c_p \left(\dfrac{g}{T} \right)^{1/5} \dfrac{\left[k(z-d) \right]^{4/5}}{\pi^{3/5}} \left[-\gamma^3 \dfrac{S^3_{(r_m)}}{r_m} \right]^{3/5} \dfrac{1}{a^{3/5}} \left[\dfrac{1}{-\zeta \phi^3{}_h(\zeta)} \right]^{1/5}, & (z-d) > z^* \\ \rho c_p \left(\dfrac{g}{T} \right)^{1/5} k^{4/5} \left(\dfrac{z^*}{\pi} \right)^{3/5} z^{1/5} \left[-\gamma^3 \dfrac{S^3_{(r_m)}}{r_m} \right]^{3/5} \dfrac{1}{a^{3/5}} \left[\dfrac{1}{-\zeta \phi^3{}_h(\zeta)} \right]^{1/5}, & h \le (z-d) \le z^* \end{cases} \tag{2.32}$$

[†]There is a typographical error in Eqs (5) and (6) of Castellvi and Martinez-Cob (2005) that contains $k(z-d)^{4/5}$ instead of the correct term $[k(z-d)]^{4/5}$

Equation (2.32) depends on the stability parameter ζ, and hence wind speed measurements are required as an input. Also, the method is not totally exempt from calibration because of parameter γ (Castellvi, 2004; Castellvi and Martinez-Cob, 2005). Parameter γ varies by less than 25 % with respect to unity for different canopies (Chen *et al*., 1997b). Equation (2.32) performed well using γ = 1.1 (Table 2.3) for measurements taken at different heights above the canopy (Castellvi and Martinez-Cob, 2005). The function $\left[-\zeta \phi^3{}_h(\zeta)\right]^{-1/5}$ in Eq. (2.32) can be set to approximately 2.4 for the stability range $-3 \le \zeta \le -0.03$, with a relative error of less than 8.5 % and can be expressed as (Castellvi, 2004):

$$H = \begin{cases} 2.4\rho c_p \left(\frac{g}{T}\right)^{1/5} \frac{\left[k(z-d)\right]^{4/5}}{\pi^{3/5}} \left[-\gamma^3 \frac{S^3_{(r_m)}}{r_m}\right]^{3/5} \frac{1}{a^{3/5}}, & (z-d) > z^* \\ 2.4\rho c_p \left(\frac{g}{T}\right)^{1/5} k^{4/5} \left(\frac{z^*}{\pi}\right)^{3/5} z^{1/5} \left[-\gamma^3 \frac{S^3_{(r_m)}}{r_m}\right]^{3/5} \frac{1}{a^{3/5}}, & h \le (z-d) \le z^* \end{cases} \quad (2.33)$$

Equation (2.33) holds under slightly unstable conditions (is valid in both the roughness and inertial sublayers and only requires air temperature data as an input), and may be considered exempt from calibration (Castellvi, 2004).

The main advantage of this *SR* analysis approach is that it is not sensitive to measurement height, and is based on the fact that vertical velocity of the mean eddies responsible for the renewal process has been properly scaled for the corresponding amplitude of the air temperature of the mean ramp events (Castellvi *et al*., 2002). However, this method is not as attractive as the original ideal *SR* analysis model based on structure functions proposed by Paw U *et al*. (1995), and it requires the additional wind speed measurement to estimate the sensible heat flux density.

2.3 Eddy covariance method

In fully turbulent flow, the mean vertical fluxes of heat, water vapour, and momentum can be defined directly in terms of the turbulent (eddy) components of

vertical velocities and of the properties being transferred (Rosenberg *et al.*, 1983; Kaimal and Finnigan, 1994). Mean flux across any plane implies covariance between the wind component normal to that plane and the scalar entity of interest (Kaimal and Finnigan, 1994; Arya, 2001).

The eddy covariance (*EC*) method provides a direct measure of the vertical turbulent flux of a scalar entity of interest F_s across the mean horizontal stream lines (Swinbank, 1951) providing fast response sensors (≈ 10 Hz) for the wind vector and scalar entity of interest are available (Meyers and Baldocchi, 2005). For a sufficiently long averaging period of time over horizontally homogeneous surface, the flux is expressed as:

$$F_s = \rho_a \overline{w's'} \tag{2.34}$$

where ρ_a is the density of air, w is the vertical wind speed and s is the concentration of the scalar of interest. The primes in Eq. (2.34) indicate fluctuation from a temporal average (i.e., $w' = w - \overline{w}$; $s' = s - \overline{s}$) and the over bar represents a time average. The vertical wind component is responsible for the flux across a plane above a horizontal surface. Based on Eq. (2.34), the sensible heat flux H can be expressed as:

$$H = \rho_a c_p \overline{w'T_s'} \tag{2.35}$$

where c_p is the specific heat capacity of air, w' denotes the fluctuation from the mean of the vertical wind speed, and T_s' is the fluctuation of air temperature from the mean. The averaging period of the instantaneous fluctuations, of w' and s' should be long enough (30 to 60 minutes) to capture all of the eddy motions that contribute to the flux (Meyers and Baldocchi, 2005).

The *EC* technique, when properly applied, can be used routinely for direct measurements of surface layer fluxes of momentum, heat, water vapour, and carbon dioxide between a surface and turbulent atmosphere (Savage *et al.*, 1997; Massman, 2000; Massman and Lee, 2002; Finnigan *et al.*, 2003). Like other

micrometeorological methods, an adequate fetch is required for the *EC* method; a fetch to height ratio greater than 100 is usually considered adequate (Wieringa, 1993). The *EC* measurements of w' should ideally be at a height that allows small-sized eddies between the anemometer transducer to be sensed (Savage *et al*., 1995). If the sensor height is too close to the canopy small-sized eddies may not be sensed, resulting in a possible underestimation of the flux. Savage *et al*. (1995) suggested that measurements, under unstable conditions above short turf grass surface, at a height of 1 m above the plant canopy should be sufficient without need of corrections for spectral attenuation of the eddy structures from spatial averaging.

The *EC* method requires sensitive, expensive instruments to measure high frequency wind velocities and scalar quantities. Besides, eddy covariance data need rigorous quality control and filtering, such as anemometer tilt correction (coordinate rotation, planar fit), spike detection, and trend removal (Meyers and Baldocchi, 2005). Sensors must measure vertical wind speed, sonic temperature and atmospheric humidity with sufficient frequency response to record the most rapid fluctuations important to the diffusion process (Drexler *et al*., 2004).

2.4 Bowen ratio energy balance method

The Bowen ratio energy balance method (*BREB*) which was first introduced by Bowen (1926), is one of the widely used micrometeorological methods to measure sensible heat and latent energy fluxes. The Bowen ratio β_o is the ratio of heat loss by conduction to that loss by evaporation, and in recent years the use of β_o has been applied to fluxes of other gases (Fritschen and Fritschen, 2005). The Bowen ratio, β_o, is defined as the ratio of the sensible heat flux H to the latent energy flux λE and is defined as:

$$\beta_o = \frac{H}{\lambda E} = \frac{\rho_a c_p K_h \partial T / \partial z}{\frac{\rho_a c_p}{\gamma} K_v \partial e / \partial z} \tag{2.36}$$

where K_h the turbulent exchange coefficient for heat transport, K_v the exchange coefficient for water vapour, $\partial T/\partial z$ the gradient of air temperature, $\partial e/\partial z$ the gradient of water vapour pressure, and γ the psychrometric constant. Assuming $K_h = K_v$ and that $(\partial T/\partial z)/(\partial e/\partial z) \approx \Delta T/\Delta e$ (Rosenberg *et al*., 1983), Eq. (2.36) then can be expressed as:

$$\beta_o = \gamma \frac{\Delta T}{\Delta e} = \gamma \frac{T_2 - T_1}{e_2 - e_1} \tag{2.37}$$

where $T_2 - T_1$ is the air temperature difference between the upper and lower measurements within the fully adjusted boundary layer, and $e_2 - e_1$ the water vapour pressure difference between upper and lower measurements. Substituting Eq. (2.37) in the simplified energy balance equation (Eq. 2.9), and solving for λE yields

$$\lambda E = \frac{R_n - G}{1 + \beta_o} \tag{2.38}$$

where $\beta_o \neq -1$.

The *BREB* method relies on certain assumptions discussed in detail by Fristchen and Simpson (1989) and Fristchen and Fristchen (2005). The assumptions of the *BREB* are: (i) steady-state conditions, (ii) the transport is one-dimesional, and (iii) the surface is homogeneous (the exchange coefficients or eddy diffusivity for heat and water vapour transfer are assumed to be equal). For the assumption of vertical transport to be valid, profile measurements must be made within the internal boundary layer, which means there must be adequate fetch. A fetch to height ratio near 100:1 is recommended by Monteith and Unsworth (1990) for measurements over uniform vegetation. However, Heilman *et al*. (1989) reported low fetch to height ratio values when β_o is small.

Generally, the *BREB* method has certain advantages for field measurement of evaporation, as the method requires simple instruments, and provides continuous

measurements over large areas and time scales of less than an hour (Rosenberg *et al*., 1983). The *BREB* method is quite accurate when β_o is close to zero, and the relative error increases as the absolute magnitude of β_o increases (Angus and Watts, 1984). Measurements of *BREB* method were reported to be in good agreement with lysimeter measurements in non-advective conditions (Tanner, 1960; Asktorab *et al*., 1989; Prueger *et al*., 1997; Savage *et al*., 1997). Cellier and Olioso (1993) found good agreement between the *BREB* and eddy covariance methods. Several studies (Fuchs and Tanner, 1970; Sinclair *et al*., 1975; Nie *et al*., 1992) have reported the accuracy and error in measuring total evaporation using the *BREB* method.

The disadvantages of the *BREB* method include: sensitivity to the biases of the instruments used for measuring the gradients of air temperature and water vapour pressure (Rosenberg *et al*., 1983); it assumes that $K_h = K_v$, which is generally true during neutral and unstable conditions near the surface but may not be true during stable conditions (Drexler *et al*., 2004); large errors in latent energy flux can occur near sunrise and sunset as $\beta_o \approx -1.0$; and extensive fetch requirements (Savage *et al*., 1997).

2.5 Flux variance method

The flux variance (*FV*) method pioneered by Tillman (1972) is based on measurements of scalar fluxes and on Monin-Obukhov similarity theory (MOST). Many studies have been made to investigate the applicability of the *FV* method, though mainly under unstable conditions to estimate sensible heat flux density (see, e.g., Wesely, 1988; Weaver, 1990; Lloyd *et al*., 1991; de Bruin *et al*., 1993; Padro, 1993; Kustas *et al*., 1994; Albertson *et al*., 1995; Katul *et al*., 1995, 1996; Hsieh and Katul, 1996; Wesson *et al*., 2001; Sugita and Kawakubo, 2003; Prueger *et al*., 2004) for both homogeneous and heterogeneous surfaces.

On the basis of MOST for unstable atmospheric conditions over a homogeneous and flat surface, Tillman (1972) obtained a relation of the form

$$\sigma_T / T_* = C_1 (C_2 - z/L_o)^{-1/3}, \qquad z/L_o < 0 \tag{2.39}$$

where $z/L_o < 0$ corresponds to unstable conditions, σ_T is the standard deviation of air temperature over the measurement time period, T_* is a turbulent temperature scale (Eq. 2.4), C_1 and C_2 are similarity constants, z is the measurement height above the ground, and L_o is the Obukhov length. As z/L_o approaches zero (for neutral conditions), σ_T/T_* converges to a constant C_3,

$$C_3 = \sigma_T/T_* \tag{2.40}$$

then

$$C_2 = (C_1/C_3)^3 \tag{2.41}$$

Tillman (1972) found values of 0.95, -2.5, and 0.05 for C_1, C_3, and $C_2 = (C_1/C_3)^3$ respectively, based on temperature data presented by Wyngaard *et al*. (1971). For free convection ($z/L_o \leq -0.2$), Wyngaard *et al*. (1971) obtained the following relationship:

$$\sigma_T/T_* = C_1(-z/L_o)^{-1/3} \tag{2.42}$$

Hsieh *et al*. (1996) noted that the free convection limit is not well defined by Wyngaard *et al*. (1971) and Tillman (1972). For estimating sensible heat flux density, Tillman (1972) proposed the following equation for the forced and free convection range:

$$H = \rho c_p \left(\frac{\sigma_T}{C_1}\right)^{3/2} \left[\frac{kg(z-d)}{T_a}\right]^{1/2} \left(\frac{C_2 - \zeta}{-\zeta}\right)^{1/2}, \quad \zeta < 0 \tag{2.43}$$

where T_a is the mean absolute air temperature, and ζ is a stability parameter defined as $(z-d)/L_o$. The free convection form of Eq. (2.43) is obtained by considering the limit for $\zeta > C_2$ (Tillman, 1972),

$$H = \rho c_p \left(\frac{\sigma_T}{C_1}\right)^{3/2} \left[\frac{kg(z-d)}{T_a}\right]^{1/2}, \qquad \zeta \le -0.05 \tag{2.44}$$

Katul *et al*. (1995), Albertson *et al*. (1995), Lloyd *et al*. (1991), and Padro (1993) found accurate estimates of sensible heat flux density using Eq. (2.44) for a wide range of atmospheric stability.

Based on similarity theory, Tillman (1972) noted that non-dimensional functions such as the skewness of temperature are determined by z/L_o. Tillman (1972) defined the skewness of temperature as:

$$S_T = \frac{1}{\sigma_T^{\,3}}\left[\frac{1}{n}\sum_{i=1}^{n}(T_i - \overline{T})^3\right] \tag{2.45}$$

where T_i is air temperature at time i, $\overline{T}$ is the mean temperature, and σ_T is the standard deviation of T_i. The stability parameter z/L_o can be expressed by plotting z/L_o versus S_T in linear and semi-log form as:

$$z/L_o = -A\exp(B S_T) \qquad \text{for} \qquad -3 < z/L_o \le -0.01 \tag{2.46}$$

where A and B are positive constants obtained by taking the natural log of Eq. (2.46) and using a linear least square fit, assuming that errors occur in z/L_o and in S_T. By substituting Eq. (2.46) for z/L_o in Eq. (2.43), Tillman (1972) derived the following equation for sensible heat flux density for the forced and free convection range:

$$H = \rho c_p \left\{ \left(\frac{\sigma_T}{C_1} \right)^3 \left(\frac{kgz}{\overline{T_a}} \right) \frac{C_2 + A\exp(BS_T)}{A\exp(BS_T)} \right\}^{1/2} \tag{2.47}$$

High frequency air temperature data is only needed as input in Eq. (2.47), which makes the FV method attractive, however friction velocity is required in Eq. (2.43) to calculate the stability parameter z/L_o. Tillman (1972) proposed the following relationship for estimating friction velocity (u_*):

$$u_* = \left[\left(\frac{kgz}{\overline{T_a}} \right) \left(\frac{\sigma_T}{C_1} \right) \frac{(C_2 - z/L_o)^{1/3}}{(-z/L_o)} \right]^{1/2}, \quad -3.0 < z/L_o \leq -0.03 \tag{2.48}$$

Substituting Eq. (2.46) for z/L_o in Eq. (2.48) gives u_* as:

$$u_* = \left\{ \left(\frac{\sigma_T}{C_1} \right) \left(\frac{kgz}{\overline{T_a}} \right) \frac{\left[C_2 + A\exp(BS_T) \right]^{1/3}}{A\exp(BS_T)} \right\}^{1/2} \tag{2.49}$$

The FV method is attractive for long-term surface flux measurements since it does not require distortion corrections, favourable wind directions, careful sensor positioning and alignment necessary for eddy covariance (Lloyd *et al.*, 1991; Katul *et al.*, 1996). The disadvantage of the FV method is that it is based on MOST, which refers to a surface layer over an extensive flat and homogeneous surface and the absence of flux divergence (Wesson *et al.*, 2001).

2.6 Scintillometry method

A scintillometer is an optical device that consists of a radiation source (transmitter) and a receiver which consists of a highly sensitive detector and a data acquisition system which can measure the turbulent intensity of the refraction index of air (Hill, 1992; Thiermann and Grassl, 1992; de Bruin *et al.*, 1995). The scintillometer measurements are based on the intensity fluctuations of a beam of electromagnetic radiation after propagation over a horizontal path caused by inhomogeneities in the

refractive index of the air. The fluctuations of the refractive index are caused by turbulent fluctuations of temperature and humidity (Thiermann and Grassl, 1992). At the receiver end the fluctuation of the beam intensity is analyzed to give the variance of the natural logarithm of intensity related to a property called the refractive index structure parameter C_n^2 ($m^{-2/3}$) defined by Hill (1992) as:

$$C_n^2 = \frac{\overline{n(s_1)^2 - n(s_2)^2}}{s_{12}^{2/3}} \tag{2.50}$$

where $n(s)$ is the refractive index at location s and the distance s_{12} lies in between the so-called inner scale of turbulence (which is of the order of 5 to 10 mm) and the outer scale, which is of the order of the height of the beam above the surface (de Bruin *et al*., 1995).

The optically most active eddies have sizes of the order of the Fresnel zone radius Z_F defined as

$$Z_F = \sqrt{\lambda R} \tag{2.51}$$

where λ is the optical wave length and R is the beam path length. The distance between the transmitter and the receiver can range from tens to thousands of meters depending on the type of scintillometer (Thiermann and Grassl, 1992). Depending on the aperture size compared to the Fresnel zone, scintillometers are classified into two major types. If the aperture size is less than the Fresnel zone, the scintillometer is classified as a small aperture scintillometer and the ones with large aperture sizes than the Fresnel zone are referred to as large aperture scintillometers. Different types of radiation source can be used with different beam wavelength. The beam wavelength for the different scintillometer types is also different, with large aperture scintillometer types having beam wavelength of 930 nm $\pm$ 5 nm.

In this study, a displaced-beam surface layer scintillometer (SLS40-A) is used. The transmitter emits a beam of one source which splits into two parallel displaced beams with orthogonal polarizations (Thiermann and Grassl, 1992). The SLS40-A

uses a class 3a type laser at a wavelength of 670 nm, a beam displacement distance of 2.7 mm and a detector diameter of 2.5 mm (Thiermann and Grassl, 1992). From the variance of the logarithm of the amplitude of the signals from the two beams, and the covariance of the two beams, inner scale length l_o (mm) which is the smallest diameter of the occurring eddies and C_n^2 can be determined (Hartogensis *et al*., 2002). The path length of the SLS40-A (that is the separation distance between the transmitter and receiver units) is 50 to 250 meters (Scintec, 2006).

The refractive index structure parameter C_n^2 ($m^{-2/3}$) depends mainly on air temperature fluctuations in the atmosphere and slightly on humidity (Thiermann, 1992). Using the Kolomogrov (1941) cascade process of turbulent flow in the atmosphere, and neglecting the contribution by water vapour, the structure constant of temperature C_T^2 ($K^2\ m^{-2/3}$)can be calculated from C_n^2 (Green *et al*., 1994) as:

$$C_T^2 = C_n^2 \left(\frac{T_a^{\,2}}{7.89 \times 10^{-4} P} \right)^2 \tag{2.52}$$

where T_a is the absolute air temperature (K), and P is the atmospheric pressure (kPa), where the dependence on water vapour pressure has been ignored. The inner scale length l_o is related to the dissipation rate of the kinetic energy of turbulence ε ($m^2\ s^{-3}$) (Hill and Clifford, 1978) as:

$$l_o = 7.4 \left(\frac{\nu^3}{\varepsilon} \right)^{1/4} \tag{2.53}$$

where ν is the kinematic viscosity of air ($1.46 \times 10^{-5}\ m^2\ s^{-1}$ at standard temperature and atmospheric pressure).

The scintillometry method is dependent on algorithms based on MOST, for determining atmospheric surface-layer fluxes. The inner scale length l_o, structure constant of temperature C_T^2, and empirical algorithms based on MOST functions are used to determine the friction velocity u_* and the turbulent temperature scale T_*

(Hartogensis *et al*., 2002). A detailed theory of these algorithms is described in Thiermann and Grassl (1992) and Hill (1997). Sensible heat flux H and momentum flux τ_o are then obtained from u_* and T_* as (Thiermann and Grassl, 1992):

$$H = \rho c_p u_* T_* \tag{2.54}$$

and

$$\tau_o = \rho u_*^2 \tag{2.55}$$

Several studies (Hill, 1992; Hill *et al*., 1992; Thiermann and Grassl, 1992; Green *et al*., 1994; de Bruin *et al*., 1995; McAneney *et al*., 1995; Andreas, 2000; Green *et al*., 2001; de Bruin and Meijninger, 2002; Savage *et al*., 2004; Savage *et al*., 2005) have indicated that scintillometer measurements can be used for reliable and routine measurements of momentum and sensible heat flux. Green *et al*. (2000) and Meijninger and de Bruin (2000) used a large aperture scintillometer to determine sensible heat flux over irrigated areas. Meijninger *et al*. (2002) showed that the large aperture scintillometer can be applied over heterogeneous terrain provided the beam of the scintillometer is in the surface layer. Kohsiek *et al*. (2002) used an extra large aperture scintillometer with a 9.8 km path length. Large aperture scintillometer has also been used to validate satellite-derived estimates of the surface fluxes (Watts *et al.*, 2000).

The advantage of the displaced-beam surface layer scintillometer (*SLS*) used in this study over large aperture scintillometers is that it does not need the additional wind speed measurement to estimate friction velocity. Other advantages of *SLS* over the eddy covariance and other conventional point measurement methods is that flow distortion effects are minimized due to intensity fluctuations being path averaged in a parabolic manner with maximum at mid-way and decreasing to zero at either ends of the optical path be used (Thiermann and Grassl, 1992).

The disadvantage of scintillometers is that they cannot distinguish between the upward and downward direction of the sensible heat flux density (Savage *et al*., 2004)

and the methods suffers from a saturation problem because the method is based on the theory of weak scattering which may not always apply (Wang *et al*., 1978; Thiermann, 1992). In addition, the cost of a scintillometer is high compared to the cost of the conventional point measurement sensors such as eddy covariance and the temperature based methods.

2.7 Energy balance closure

All weather and climate models are based on the fundamental fact that energy must be conserved at the earth's surface, namely conservation of energy and conservation of mass (Twine, *et al*., 2000; Oncley *et al*., 2007). If components of the energy balance are measured independently and accurately, then Eq. (2.9) should be satisfied, and closure is said to be satisfied. However, energy balance closure could still be achieved if two or more terms have incorrect values and that the terms in Eq. (2.9) still sum to zero (Savage *et al*., 2004). If the components of the shortened energy balance equation are measured independently then,

$$R_n - G - H - \lambda E = c \tag{2.56}$$

where c is termed the energy balance closure (W m^{-2}), and closure is satisfied if $c = 0$ W m^{-2}.

Several studies of the energy balance terms failed to achieve closure, and the lack of energy balance closure has been found over all types of surfaces from bare soil to forests and the vast majority have found higher energy input by radiation fluxes than loss by turbulent fluxes and ground heat flux (Oncley *et al*., 2007). Therefore, the measured fluxes should be corrected or adjusted or the uncertainties in the measured fluxes accepted (Twine *et al*., 2000). If closure is not achieved, then the available energy (Eq. 2.10), $R_n - G$, will not be equal to the turbulent fluxes $H + \lambda E$. Another measure of the lack of closure is the closure ratio or the energy balance closure discrepancy D given by (Twine *et al*., 2000):

$$D = \frac{H + \lambda E}{R_n - G} \tag{2.57}$$

for which a closure ratio of 1 yields energy balance closure. The closure ratio is a bias such that $0.7 < D < 1$, and this problem is serious if the cause for the discrepancies is not known (Twine *et al*., 2000).

Several reasons for lack of energy balance closure have been discussed by Twine *et al*. (2000), Wilson *et al*. (2002), and Cava *et al*. (2007) including: (1) sampling errors associated with different measurement source areas for the terms in Eq. (2.56), (2) a systematic bias in instrumentation, (3) neglected energy sinks, (4) the loss of low and/or high frequency contributions to the turbulent flux, (5) neglected advection of scalars, (6) measurement errors related to sensor separation, alignment problems, interference from tower or instrument-mounting structure, (7) errors in the measurement of R_n and/or G.

The two micrometeorological methods that use direct measurements of surface scalar fluxes are the Bowen ratio energy balance method (*BREB*) and the eddy covariance (*EC*) method used in conjunction with infrared gas analyzer. The $BREB$ method by definition is consistent with conservation of energy because it forces energy balance closure. A direct measure of water vapour concentrations using Infrared Gas Analyzer (IRGA) was not available. Therefore, all micrometeorological methods used in this study such as the EC, SR, FV, and SLS estimate the sensible heat flux H and calculate latent energy flux λE as a residual amount assuming a closure ratio of 1.

2.8 Brief overview of subsequent chapters

Applying the theory discussed in the previous sections, the applicability of the surface renewal method for estimating sensible heat and latent energy fluxes is investigated over different surfaces: grassland; Chromolaena; Yellow wood forest; heterogeneous surface (*Jatropha curcas*); and open water surface are discussed in the following chapters. The SR method must be calibrated against a standard method, such as the eddy covariance method to determine the weighting factor α. The weighting factor α is determined for the different surfaces. Sensible heat and latent energy fluxes from the SR method are then compared with the EC, BR, FV, and

SLS methods. Chapter 3 mainly deals with sensible heat and latent energy comparisons for unstable atmospheric conditions, of the *SR* analysis with the *EC*, *BR*, and *SLS* methods. The effect of measurement height on the weighting factor α is also investigated. The performances of the three *SR* analysis approaches are assessed over Triffid weed (*Chromolaena odorata*) and Outeniqua Yellow wood forest, in Chapters 4 and 5 respectively. Chapter 6 deals with the long-term estimation of sensible heat and latent energy fluxes over fetch-limited *J. curcas* using the *SR* and *EC* methods. Comparison of the seasonal estimates of total evaporation using the *SR* and *EC* methods are presented for a period of almost two years. The surface renewal method has not been tested over open water surfaces. Chapter 7 is therefore mainly concerned with the use of the *SR* method for estimating sensible heat flux and open water evaporation from a shallow reservoir.

Chapter 3: Sensible heat and latent energy flux for an open and mixed grassland using surface renewal analysis for unstable conditions

3.1 Introduction

Accurate and routine measurement of total evaporation is crucial in micrometeorology, agriculture and water resources management. Total evaporation may be estimated directly and indirectly using different micrometeorological methods, such as eddy covariance, Bowen ratio energy balance and optical scintillation. The eddy covariance is a direct method, which uses high frequency measurements of sonic temperature, wind speed, and water vapour pressure fluctuations. This method is limited by its complexity, high cost and sensitivity of the instruments to damage (Drexler *et al*., 2004). The Bowen ratio method is limited by constraints imposed by extensive fetch requirements and is a point measurement. Several studies carried out in the past few decades and in recent years have revealed that the scintillation method is an attractive alternative that yields path-averaged estimates of sensible heat flux density and momentum flux density (see e.g. Hill, 1992; Hill *et al*., 1992; Thiermann and Grassl, 1992; Green *et al*., 1994; de Bruin *et al*., 1995; Anandakumar, 1999; Meijninger and de Bruin, 2000; Savage *et al*., 2004). A scintillometer is a device that optically measures the intensity fluctuations of visible or infrared radiation, caused by interference after the radiation has been scattered by inhomogenities of the refractive index of the air along the path of propagation. A detailed review of the theory, which invokes the Monin-Obukhov similarity theory for measuring surface-layer fluxes of sensible heat and momentum using optical scintillation, is described by Hill (1992). In contrast to point measurements displaced-beam scintillometers provide path-averaged measurements of sensible heat and momentum fluxes over distances between 50 and 250 m (Thiermann and Grassl, 1992). Nevertheless, the cost of the scintillometer is high.

Paw U and Brunnet (1991) introduced a simple and low cost method, called surface renewal (*SR*) to estimate the sensible heat flux density over natural surfaces. This method uses high frequency air temperature data, typically between 2 and 10 Hz, and is based on the idea that an air parcel from above sweeps to the surface and replaces a parcel that ejects from the canopy. Traces of high frequency air temperature data are known to be coherent and exhibit ramp-like patterns that have been described by Gao *et al*. (1989), Shaw *et al*. (1989) and Paw U *et al*. (1992). These ramp traces can be used to estimate sensible heat flux density using *SR* analysis over different plant and forest canopies (Paw U *et al*., 1995; Katul *et al*., 1996; Snyder *et al*., 1996; Spano *et al*., 1997; Spano *et al*., 2000). Snyder *et al*. (1996) used air temperature structure functions using time lags r as suggested by Van Atta (1977), instead of the low pass filtering techniques used to smooth air temperature data applied by Paw U *et al*. (1995), to extract the ramp characteristics. Chen *et al*. (1997a) proposed a model in which the relatively rapid change in air temperature at the end of each ramp is not instantaneous, but occurs in a finite micro-front time and the ramps are assumed to follow each other without any delay. Chen *et al*. (1997b) presented a new air renewal model that calculates sensible heat flux density at different heights within and above a canopy from the average cubic temperature structure function and measured average friction velocity. Castellvi *et al*. (2002) proposed a new method for estimating sensible heat flux density that combined surface renewal analysis and similarity theory at any height above the canopy. Castellvi (2004) modified the companion method presented by Castellvi *et al*. (2002) and suggested a new method of calculating sensible heat flux density that is exempt from calibration regardless of the stability conditions. The detailed theory and derivation of the equations used to calculate sensible heat flux density using this method is available in Castellvi (2004). However, the methods proposed by Chen *et al*. (1997a) and Castellvi (2004) are not as attractive as the original *SR* method used by Paw U *et al*. (1995), since they require the additional measurement of friction velocity and a stability parameter as an input. In this study, the procedure proposed by Snyder *et al*. (1996) is used to estimate sensible heat flux density to avoid the additional requirement of the friction velocity.

The objectives of this study are to estimate and compare sensible heat and latent energy flux density for a grassland surface using *SR* analysis at four different heights using two time lags (r = 0.25 s and r = 0.50 s), and make a comparison of the *SR* method with eddy covariance, displaced-beam optical scintillometry, and Bowen ratio methods.

3.2 Theory

In *SR* analysis, it is assumed that turbulent coherent structures exchange scalars (air temperature and water vapour pressure) between the surface and the atmosphere (Paw U *et al*., 2005). The *SR* analysis assumes that the sensible heat flux density H at measurement height z is determined as:

$$H_{SR} = \alpha z \rho c_p \frac{a}{\tau} \tag{3.1}$$

where α is a correction or weighting factor, ρ the air density (kg m^{-3}), c_p the specific heat capacity of dry air at constant pressure (J kg^{-1} K^{-1}), a the amplitude (^{o}C), and τ (s) the total ramping period (equal to the inverse ramp frequency) of air temperature ramps. The amplitude and inverse ramp frequency can be determined from the second, third, and fifth order of the structure function for air temperature (Van Atta, 1977). The structure function is defined as:

$$S^n(r) = \frac{1}{m-j} \sum_{i=1+j}^{m} (T_i - T_{i-j})^n \tag{3.2}$$

where m is the number of data points in the time interval measured at frequency (f) in Hz, n is the order of the structure function, j is the time lag between data points corresponding to a time lag $r = j/f$ and T_i is the ith temperature sample.

For the *SR*, *EC*, and *SLS* methods, latent energy flux density λE was estimated using a shortened energy balance equation from measurements of sensible heat flux density H, net irradiance R_n and soil heat flux density G:

$$\lambda E = R_n - G - H \tag{3.3}$$

For the *BR* technique, by definition $\beta = H/\lambda E$ and invoking the energy balance yields the latent energy flux density as

$$\lambda E = (R_n - G)/(1+\beta),\ 1+\beta \neq 0. \tag{3.4}$$

3.3 Materials and methods

The experiment, part of a larger experiment (Savage *et al.*, 2004), was conducted from 2 November 2003 to 22 January 2004 above an open and mixed grassland in the Hay Paddock area neighbouring Ashburton and close to Pietermaritzburg, South Africa (29.63^o S, 30.43^o E) with an altitude of 671.32 m above MSL. The average slope of the study site is 1^o 15’ to the SE. The fetch distance was 135 m from the prevailing S-E winds for the eddy covariance system (*EC*) and 90 and 138 m for the displaced-beam surface layer scintillometer (*SLS*) transmitter and receiver respectively. The fetch for the next-most dominant winds from the N-W was 117 m for the EC system and 146 and 114 m for the *SLS* transmitter and *SLS* receiver.

For the surface renewal (*SR*) method, four unshielded type-E fine-wire thermocouples (75 μm diameter) were used to measure air temperature, placed at heights of 0.5, 0.8, 1.0, 1.5 m above the grassland canopy surface. The canopy height varied from 0.3 m to 0.5 m during the experimental period. Two of the thermocouples were connected to a CR10X datalogger (Campbell Scientific, Logan, Utah, USA) with a reference thermistor for thermocouple measurements. The remaining thermocouples were connected to a CR23X datalogger. The thermocouples were pointed into the predominant wind direction which occurred during day light hours. Air temperature data were sampled at a frequency of 8 Hz and then lagged by 0.25 s and 0.50 s before forming the second, third and fifth structure function as required by the Van Atta (1977) approach for surface renewal analysis. The data were then averaged and stored every two minutes in the dataloggers. Structure functions using the time lags and the analysis technique from Van Atta (1977) were used to determine the amplitude a (^{o}C) and the inverse ramp frequency τ (s) characterizing

temperature fluctuations as presented by Snyder *et al*. (1996). The two-minute SR sensible heat flux density H_{SR} (W m^{-2}) was calculated using Quick Basic 4.0 software, under MS-DOS and the data then averaged to 20 minutes and 30 minutes.

Adjacent to the SR system, a three-dimensional sonic anemometer (SWS-211/3V, Applied Technologies, Boulder, Colorado, USA), was used as an EC system to measure the sensible heat flux density H_{EC} at a height of 2.12 m. This sonic anemometer, with a path length of 100 mm, was connected to a digital to analogue converter that then connected to a CR23X datalogger. Sampling frequency of the three components of wind velocity, u, v, w and sonic temperature T_s was 10 Hz and data were processed online using the CR23X datalogger. The two-minute and 30-minute averages of u, v, w, T_s, wind direction θ ($= \arctan v/u$), and the covariances between w and T_s were calculated and stored for further analysis. The sensible heat flux H_{EC} is usually described as: $H_{EC} = \rho c_p \overline{w'T_s'}$, where w' and T_s' are the fluctuations from the mean vertical wind speed w and sonic temperature T_s, respectively. A fast responding open path water vapour pressure and carbon dioxide concentration sensor (LI-7500, LI-COR Inc., Lincoln, USA) and a second Applied Technologies 3-D sonic anemometer (model SATI/3V) with a sonic path length of 150 mm were also used to calculate sensible heat, latent energy, momentum, and carbon dioxide flux using the *EC* technique.

A dual-beam surface layer scintillometer (model SLS40-A, Scintec Atmosphärenmessetechnik, Tübingen, Germany), was used to measure the sensible heat flux density H_{SLS} every two minutes. The beam path was adjacent to the SR and EC systems. The scintillometer was positioned at a height of 1.65 m above the soil surface and the path length between the receiver and transmitter units was 101 m. The SLS beam height was referenced to the height at which wind speed was estimated to be 0 m s^{-1}. The SLS40-A employs a diode laser source with a wavelength of 670 nm and 1 mW (2 mW peak) mean output power. A computer was connected to the signal processing unit (SPU) of the scintillometer through the computer serial port. The beam displacement and detector separation distances are 2.5 mm each, with a detector diameter of 2.7 mm. Software together with an instrument allows online scintillometer

beam measurements at a frequency of 1 kHz and subsequent calculation, every 2 min, of the structure parameter for refractive index C_n^2, structure parameter for temperature C_T^2, the inner scale of turbulence as indicated by the inner scale of refractive index fluctuations l_o, kinetic energy dissipation rate ε, sensible heat flux density H_{SLS}, momentum flux density τ and the Obukhov length L_o. Two-minute averages of all SLS-calculated parameters were stored on a computer hard drive for further analysis. For each two-minute period, only data for which the inner scale of refractive index fluctuations l_o was greater than 2 mm and the percentage of error free data was greater than 25 % were accepted for further analysis. The *SLS* method is dependent on algorithms which are based on MOST (Hill, 1997) with the sensible heat flux determined as $H = \rho c_p T_* u_*$, where T_* is temperature scale of turbulence and u_* is the friction velocity.

A modified Bowen ratio fixed arm system (*BR*), after the 023A system of Campbell Scientific Inc. and connected to a 21X datalogger, was used to measure air temperature and water vapour pressure profile differences between heights of 1.55 and 2.96 m (Savage *et al*., 2005). Air temperature was measured using 75-µm type-E thermocouples and water vapour pressure measured using a cooled mirror Dew-10 hygrometer (General Eastern Corp., Watertown, Massachusetts, USA). Measurements were performed every 1 s and averages calculated every 20 minutes. For measuring the remaining components of the energy balance, three Q*7 net radiometers (REBS, Seattle, Washington, USA) placed at 2 m above the soil surface and placed two meters apart were used to measure net irradiance. Seven soil heat flux plates (model HFT-S, REBS) placed one meter away from each other were used to measure soil heat flux density at a depth of 80 mm and a system of parallel-thermocouples at depths of 20 and 60 mm used to calculate the soil heat flux density stored above the plates (Tanner, 1960). Volumetric soil water content in the first 60 mm of the soil surface was measured using a frequency domain reflectometer (ThetaProbe, model ML2X, Delta-T Devices, Cambridge, UK). The sensors were connected to a CR23X datalogger and measurements were every one second and averages obtained every two minutes which were in turn used to calculate 20-minute averages for the *BR* calculations. The energy balance sensors, the *EC* system, the *SR* system and the *BR*

system were positioned mid-way between the transmitter and receiver units of the scintillometer.

The sign of the amplitude of the air temperature ramps was used to differentiate between unstable and stable conditions for each 30-minute period.

3.4 Results and discussion

3.4.1 Sensible heat flux density

Half-hourly sensible heat flux density values computed using the surface renewal analysis H_{SR} (using α =1) for a time lag r = 0.50 s, at four measurement heights: z_1 = 0.5 m, z_2 = 0.8 m, z_3 = 1.0 m, and z_4 = 1.5 m above the grass canopy surface are compared with EC sensible heat flux density H_{EC}, as shown in Figs 3.1a, b, c, and d. These comparisons are performed to observe the effect of measurement height on the sensible heat flux density estimates using surface renewal analysis H_{SR} and its agreement with eddy covariance H_{EC} estimates under unstable atmospheric conditions (amplitude of the air temperature ramps greater than zero). As shown clearly in Fig. 3.1, very good agreement is observed between half-hourly estimates of H_{SR} and H_{EC} with the former at z_1 = 0.5 m. The agreement between the other three heights of H_{SR} and H_{EC} are also good, but there was bias. The highest level measurement at 1.5 m overestimated the sensible heat the most. Snyder *et al*. (1996), in their experiment over 0.1-m alta fescue grass found a relatively poor agreement at the highest level (z = 1.2 m above the soil surface) and at the canopy top (z = 0.1 m). They attributed the lack of accuracy for estimating H_{SR} at the highest measurement level to the fact that the height is above the fully adjusted boundary layer. Surprisingly, a relatively better agreement is observed between H_{SR} at the second highest level at 1.0 m and H_{EC} in this experiment, compared to measurements at the heights 0.8 and 1.5 m.

In Table 3.1, the calibration of H_{SR} values using two time lags r = 0.25 s and r = 0.50 s against H_{EC} measurements are presented respectively. The slope of the regression through the origin is α and is determined by forcing the linear fits through the origin. The comparisons between H_{EC} and uncalibrated H_{SR} flux estimates (Table 3.1) indicate that α is different for all the measurement heights and time lags. For both time lags, α and the coefficient of determination are close to 1 for the 0.5 m height, and best estimates of H_{SR} were obtained for this height as shown in Fig. 3.1a.

(a) 0.5 m

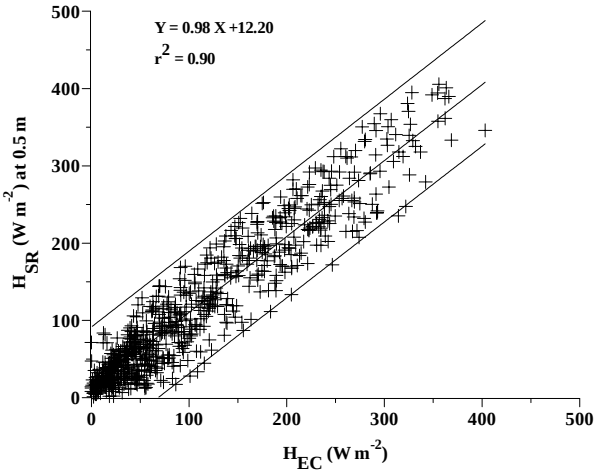

(b) 0.8 m

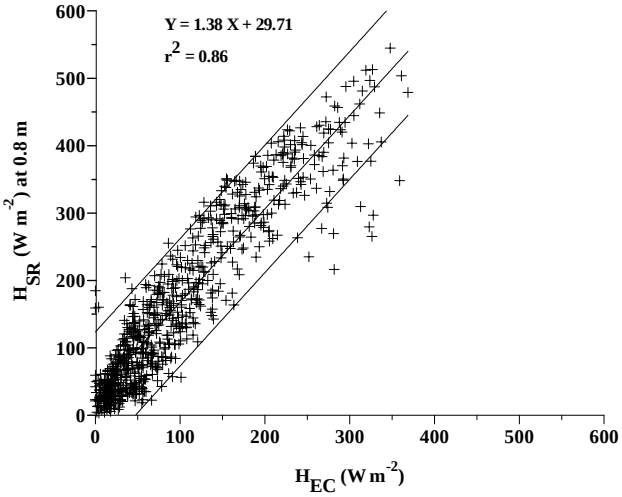

(c) 1.0 m

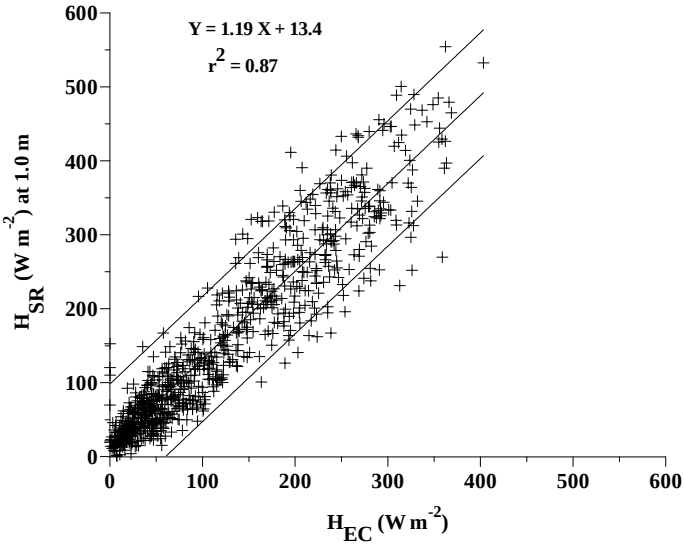

(d) 1.5 m

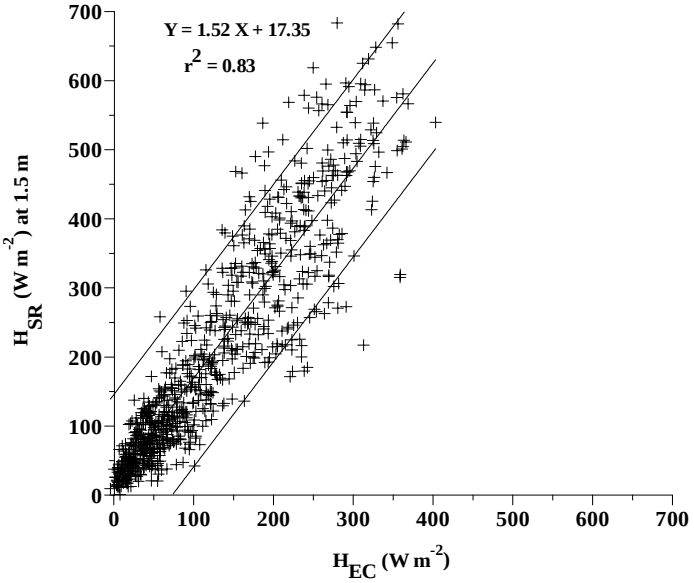

Fig. 3.1 Half-hourly surface renewal H_{SR} estimates *vs* eddy covariance H_{EC} estimates of sensible heat flux density for unstable conditions only using a time lag r of 0.5 s, for day of year 308 to 328 and 347 to 365 (2003), during the period 06h00 to 18h00: (a) H_{SR} at 0.5 m above the grass canopy *vs* H_{EC} at 2.12 m; (b) H_{SR} at 0.8 m above the grass canopy *vs* H_{EC}; (c) H_{SR} at 1.0 m above the grass canopy *vs* H_{EC}; (d) H_{SR} at 1.5 m above the grass canopy *vs* H_{EC}. The wide confidence bands represent the 95 % confidence level for a single predicted value.

Table 3.1 Regression statistics of half-hourly H_{SR} *vs* H_{EC} estimates for November and December 2003, from 06h00 to 18h00 for time lags r = 0.25 and 0.50 s. The weighting factor α is the slope of the linear fit forced through the origin and the root mean square error (RMSE) is relative to the 1:1 line.

Height above canopy (m)	n	Time lag r (s)	Intercept (W m^{-2})	Slope	RMSE (W m^{-2})	Coefficient of determination	Weighting factor α
0.5	758	0.25	16.34	1.07	34.01	0.89	0.82
	758	0.50	12.20	0.98	30.64	0.90	0.92
0.8	753	0.25	33.88	1.95	66.96	0.84	0.44
	753	0.50	29.71	1.38	49.20	0.86	0.61
1.0	786	0.25	19.45	1.29	56.52	0.83	0.67
	786	0.50	13.40	1.19	43.40	0.87	0.76
1.5	786	0.25	18.77	1.67	81.90	0.79	0.52
	786	0.50	17.35	1.52	64.90	0.83	0.58

Very good agreement between H_{SR} and H_{EC} is noticed for the 0.5 m height above the canopy for r = 0.5 s as shown in Table 3.1. The other heights over-predicted H_{EC}, and hence α is needed to correct for the uneven heating of the air parcels from the ground to the specific measurement height (Eq. (3.1)). For a 0.1-m tall alta fescue grass, Snyder *et al*. (1996) found very good agreement between H_{SR} and H_{EC} estimates using α = 1.0 for measurement heights of 0.3, 0.6, and 0.9 m, and time lags of r = 0.25, 0.50, 0.75, and 1.0 s. For this experiment, the α value for heights above canopy of 0.8, 1.0, and 1.5 m is greater than 1.0 for time lags of 0.25 and 0.50 s (Table 3.1).

The variations with time of ramp amplitude a, frequency $1/\tau$, wind speed from the sonic anemometer, and H_{SR} at 0.5 m above the canopy, for time lags r = 0.25 s and r = 0.50 s are presented in Fig. 3.2 for day of year 308 (2003) during unstable atmospheric conditions from 08h00 to 16h00. Diurnal variation of the sensible heat flux density depicted on the upper part of Fig. 3.2 followed the diurnal trend of the ramp amplitudes and frequencies for both time lags. However, H_{SR} seems to be more sensitive to changes in ramp frequency $1/\tau$ than to a. The H_{SR} estimates for r = 0.50 s agreed with H_{EC} whereas the H_{SR} for r = 0.25 s was overestimated

for high sensible heat conditions. As shown in Fig. 3.2, the ramp amplitude for the time lag 0.50 s is greater in magnitude than that for a time lag of 0.25 s. However, the inverse ramp frequency is greater for r = 0.25 s compared to 0.50 s and it could be one of the reasons for the over-prediction of H_{SR} when r = 0.25 s is used.

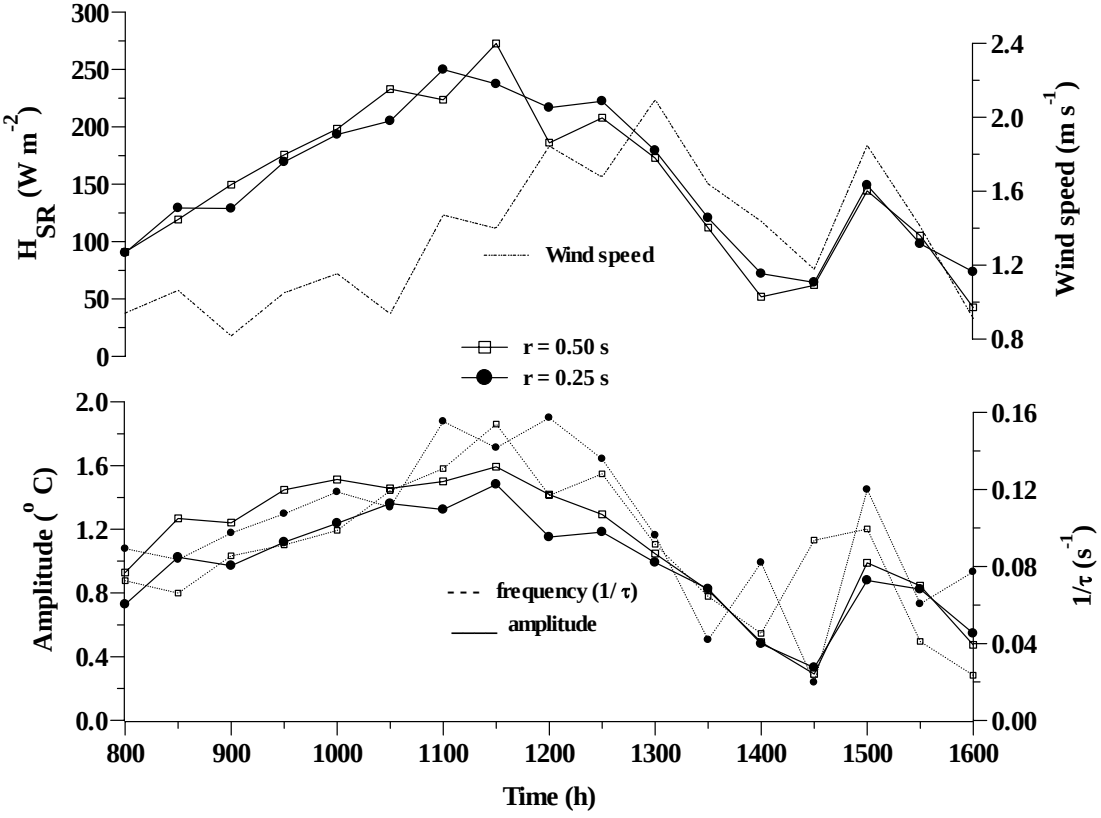

Fig. 3.2 The variation of surface renewal sensible heat flux H_{SR} estimates, ramp amplitude (^{o}C), ramp frequency (s^{-1}), and wind speed with time for a height of 0.5 m above the canopy using time lags r = 0.25 s and r = 0.50 s for day of year 308 (2003).

Diurnal variations of the half-hourly H_{SR} estimates from the four measurement heights, H_{EC} estimates, and net irradiance are presented in Fig. 3.3 for a partly cloudy and for a cloudless day. The sensible heat flux densities showed significant fluctuations with changes in net irradiance (Fig. 3.3a) between 11h00 and 14h00 due to clouds. It can be seen also from Fig. 3.3 that the variations in net irradiance are instantly reflected in all sensible heat flux densities.

Half-hourly H_{SR} estimates for 0.5 m above the grass canopy using a time lag r = 0.50 s are compared with the H_{SLS} estimates from the surface layer scintillometer for a ten-day period (12 to 22 January, 2004) from 06h00 to 18h00 as shown in Fig. 3.4. The correspondence between the two methods is very good (Fig. 3.4a and b) despite the fact that H_{SLS} is a path-averaged measurement and H_{SR} is a point measurement. The weighting factor α, the slope of the linear fit through the origin of the uncalibrated H_{SR} and H_{SLS} is 1.05. The agreements between the other heights of the uncalibrated surface renewal H_{SR} and H_{SLS} estimates are biased (data not presented).

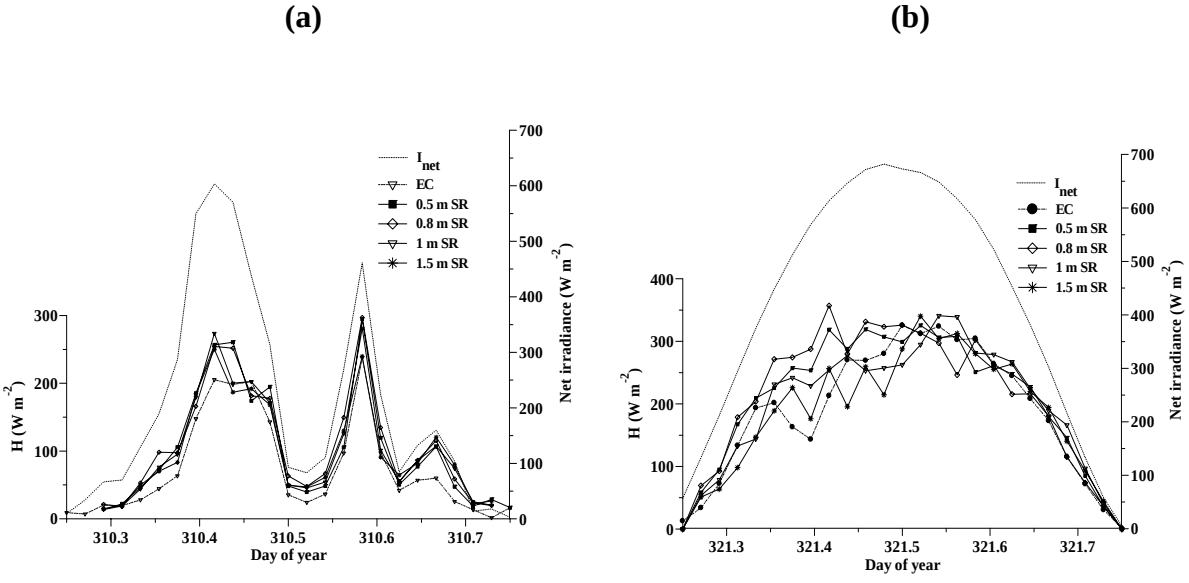

Fig. 3.3 Diurnal variations of half-hourly estimates of sensible heat flux densities (H_{SR} at four measurement heights and H_{EC}) and net irradiance (right-hand y-axis) from 06h00 to 18h00: (a) partly cloudy, day of year 310 (2003); (b) cloudless, day of year 321 (2003)

(a)

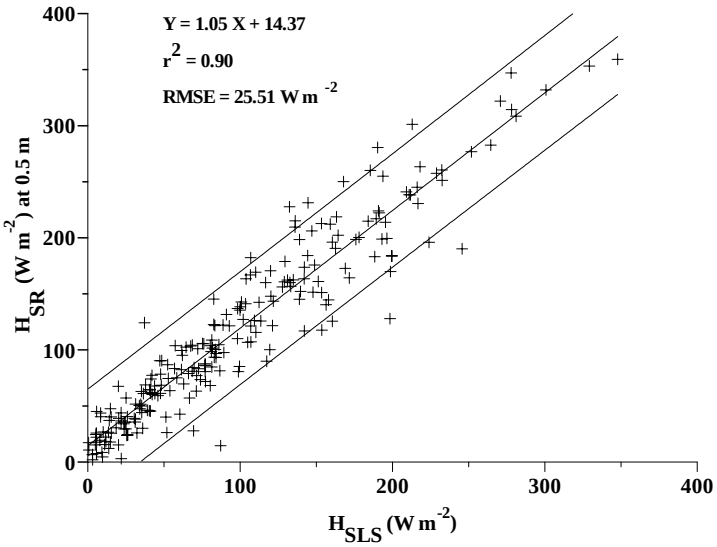

(b)

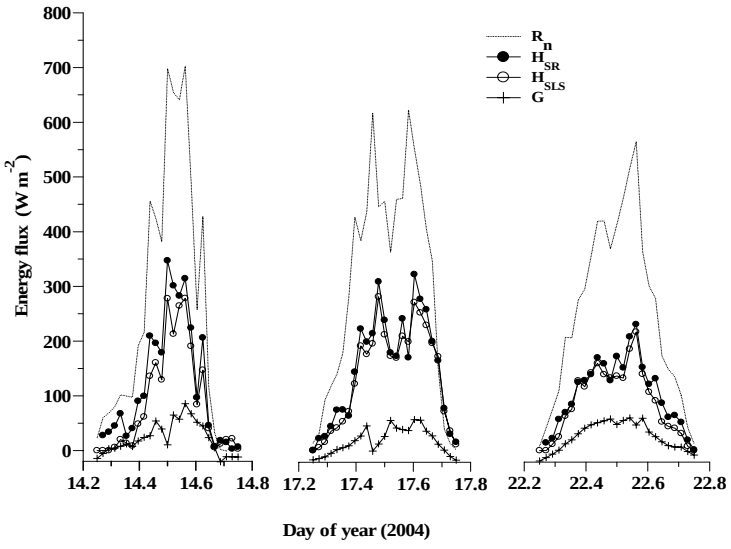

Fig. 3.4 Half-hourly H_{SR} and H_{SLS} estimates of sensible heat flux density using the time lag r = 0.50 s for unstable conditions from 06h00 to 18h00: (a) H_{SR} at 0.5 m above the grass canopy *vs* H_{SLS} (at 1.2 m above the canopy) for day of year 12 to 22 (2004); (b) diurnal comparisons between H_{SR} at 0.5 m above the grass canopy and H_{SLS} estimates for three days in January, 2004. Net irradiance (R_n) and soil heat flux (G) are also shown.

Comparisons of the sensible heat flux density estimates from the surface renewal H_{SR} and Bowen ratio H_{BR} methods are also made for a period of 16 days (day of year 6 to 22) in January 2004, the former method resulting in a point measurement and the latter a profile measurement. Presented in Fig. 3.5 is the comparison of 20-minute averages of the H_{SR} at 0.5 m above the canopy and H_{BR} estimates from 06h00 to 18h00. The agreement between the two systems is very good with a slope of 0.96 and coefficient of determination of 0.93. However, the root mean square error (RMSE = 30.63 W m^{-2}) is greater compared to the RMSE for the H_{SR} and H_{EC} comparisons presented in Table 3.1.

Diurnal comparisons of the H_{SR} and H_{BR} estimates along with net irradiance are also plotted in Fig. 3.6 for three contrasting days. Three different x-axes are used to separate the curves for days that are cloudless (day of year 9, 2004), widely-varying net irradiance conditions (day of year 10) and partly cloudy (day of year 11). The BR method appeared to underestimate the sensible heat flux in the early morning and late afternoon as shown in Fig. 3.6. The agreement for day of year 9 (2004), almost cloudless, does not appear as good compared to day of year 10 and 11 (2004). Generally, the two systems showed good agreement and tracked the diurnal variation in net irradiance very well.

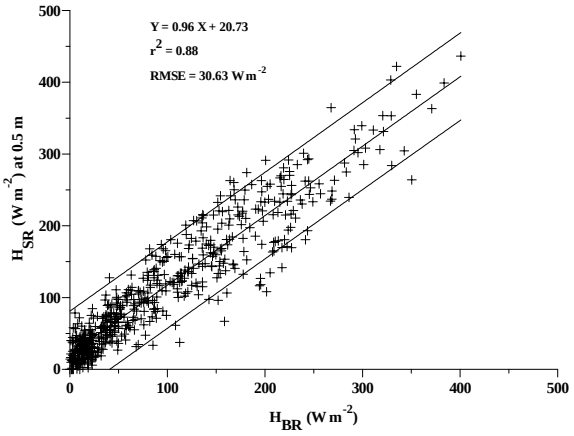

Fig. 3.5 Comparison between 20-minute averages of H_{SR} at 0.5 m above the canopy using r = 0.50 s and H_{BR} estimates of sensible heat flux density for day of year 6 to 22 (2004) from 06h00 to 18h00 during unstable conditions.

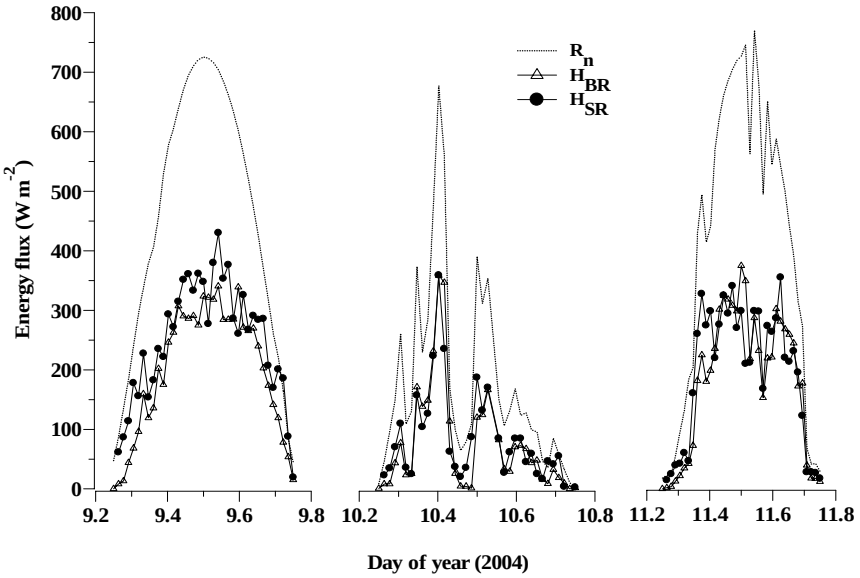

Fig. 3.6 Diurnal variation in 20-minute averages of H_{SR}, using a time lag r = 0.50 s, and H_{BR} estimates of sensible heat flux density along with net irradiance for day of year 9, 10, and 11 (2004) from 06h00 to 18h00. The *SR* measurement was at 0.5 m above the grass canopy and the *BR* arms were at 1.55 m and 2.96 m above the soil surface.

3.4.2 Latent energy flux density

An independent and direct *EC* measurement of λE was performed at this site using an open-path eddy covariance system over a period of 255 days in 2003, as reported by Savage *et al.* (2004). However, the comparisons of direct measurements of latent energy flux density using this open-path *EC* system, λE_{ECopen} with λE_{SLS} (residual), for example, was poor with an r^2 = 0.239 for the daily total λE comparisons of λE_{ECopen} and λE_{SLS} where λE_{SLS} was calculated as a residual (data not shown). Furthermore, for this period, the energy balance closure for the open path λE and H measurements was poor with λE_{ECopen} yielding a significantly lower measured value compared to that estimated from the residual estimate using H_{SLS}. Consequently, the open-path λE_{ECopen} data were not used and therefore λE estimates were obtained as a residual of the energy balance using all methods.

The latent energy flux density λE was estimated as a residual by using the energy balance Eqs (3.3) and (3.4). The regression statistics of the latent energy flux density from surface renewal analysis λE_{SR} using r = 0.5 s for the four measurement heights *vs* the latent energy flux density from the eddy covariance system λE_{EC} are shown in Table 3.2. The regression of λE_{SR} for z_1 = 0.5 m *vs* λE_{EC} is as well depicted in Fig. 3.7. The root mean square errors (RMSE) are relative to the 1:1 line and are a measure of accuracy of the estimates. The λE_{SR} estimates from the 0.5 m above canopy height gave excellent estimates of λE_{EC}. The other three heights underestimated the latent energy flux density and the agreements between λE_{SR} and λE_{EC} estimates are relatively biased.

Plots of half-hourly latent energy flux density from surface renewal analysis λE_{SR} above the grass canopy using r = 0.5 s versus surface layer scintillometer λE_{SLS} and 20-minute averages of λE_{SR} *vs* Bowen ratio λE_{BR} estimates are shown in Figs 3.8 and 3.9 respectively. The agreement between λE_{SR} and λE_{SLS} and λE_{BR} is very good, with slopes close to 1 and coefficient of determination greater than 0.90. The root mean square error of estimates (RMSE) is relatively higher for the λE_{SR} *vs* λE_{BR} comparison (Fig. 3.9) opposed to λE_{EC} and λE_{SLS}.

Table 3.2 Regression statistics of half-hourly λE_{SR} using r = 0.5 s *vs* λE_{EC} estimates of latent energy flux density for November and December 2003, from 06h00 to 18h00. The root mean square errors (RMSE) are relative to the 1:1 line.

Height above canopy (m)	Intercept (W m^{-2})	Slope	RMSE (W m^{-2})	Coefficient of determination	n
0.5	2.66	0.96	28.83	0.94	758
0.8	-0.66	0.93	31.08	0.93	753
1.0	-2.18	1.02	31.40	0.94	786
1.5	0.33	0.95	50.00	0.86	786

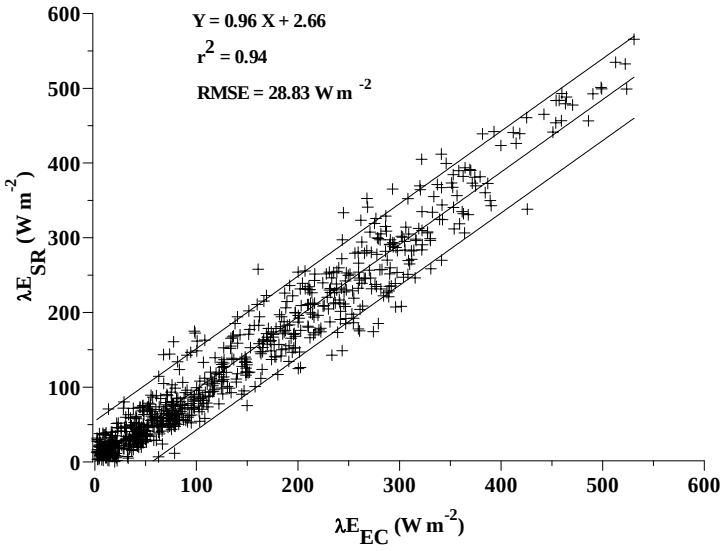

Fig. 3.7 Half-hourly latent energy flux density from surface renewal analysis, λE_{SR} at the 0.5 m above canopy height using r = 0.50 s plotted against the eddy covariance λE_{EC} estimate for unstable conditions in November and December, 2003.

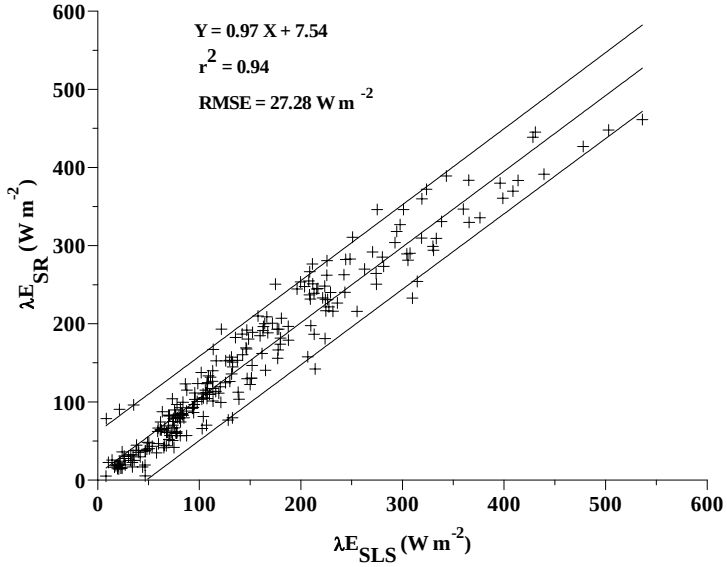

Fig. 3.8 Half-hourly latent energy flux density from surface renewal analysis, λE_{SR} at the 0.5 m above canopy height using r = 0.50 s plotted against surface layer scintillometer λE_{SLS} estimates (at 1.2 m above the canopy) for day of year 12 to 22 (2004).

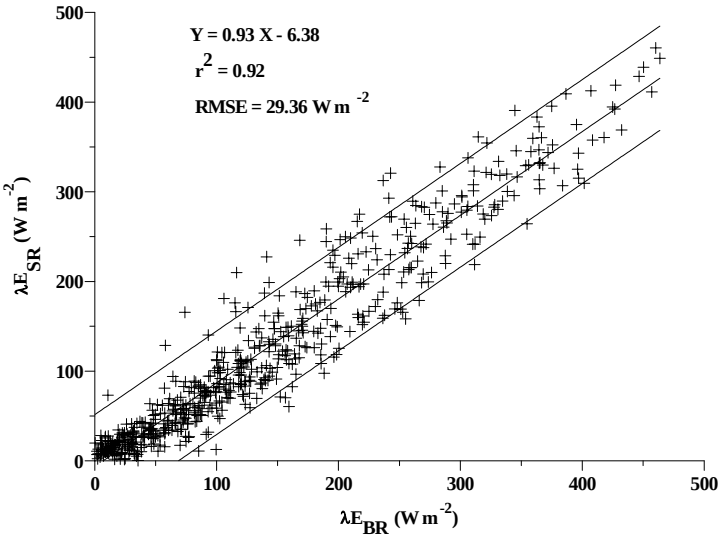

Fig. 3.9 Twenty-minute averages of latent energy flux density λE_{SR} from surface renewal analysis at 0.5 m above the grass canopy using r = 0.50 s plotted against Bowen ratio λE_{BR} estimates for day of year 6 to 22 (2004).

3.5 Summary and conclusions

High frequency air temperature data were collected at four measurement heights above an open and mixed grassland, to estimate sensible heat flux density using the surface renewal analysis method for time lags r = 0.25 s and r = 0.50 s, during daylight hours when the atmosphere is generally unstable. The time lag r = 0.50 s gave better H_{SR} estimates compared to r = 0.25 s. The measurements show very good agreement between the surface renewal sensible heat flux density H_{SR} estimates at 0.5 m above the canopy and the eddy covariance sensible heat flux density H_{EC} estimates. Good agreement for the other three heights (0.8, 1.0, 1.5 m) between H_{SR} and H_{EC} is also obtained with coefficient of determination greater than 0.8, but there was bias (the slopes are different from 1). The H_{SR} measurements at 0.5 m above the canopy also showed good agreement compared to the sensible heat flux density obtained using the Bowen ratio H_{BR} and surface layer scintillometer H_{SLS} methods, each with a different theoretical basis and varying from point to profile and

path-averaged measurements. The surface renewal method overestimated the sensible heat flux density for the measurements taken at the three highest level measurements.

The H_{SR} estimates at 0.5 m above the grass canopy provided accurate estimates of latent energy flux density (λE_{SR}) when used with measured net irradiance and soil heat flux density. Based on this study, the surface renewal method offers a simple, low cost, and accurate estimate of sensible heat and latent energy flux densities over grass when the weighting factor α is known.

Chapter 4: Sensible heat and latent energy flux estimation over Chromolaena using surface renewal analysis: comparison with eddy covariance, flux variance, and surface layer scintillometry

4.1 Introduction

Invasive alien plant species (IAPs) create a direct threat to South Africa's water resources, the ecological functioning of natural systems, and the productive use of land. Such species can waste a large amount of national water resources and lead to undesirable reduction of stream flow, approximately 7 % in South Africa (Versveld *et al*., 1998). IAPs often have much increased water usage compared with indigenous vegetation (Calder and Dye, 2000). Measurement of total evaporation is therefore an important aspect in determining the water use of IAPs, such as Triffid weed (*Chromolaena odorata*). Nevertheless, evaporation studies are limited due to the high cost of instrumentation, sensitivity of the instruments to damage, complexity, power requirements (Drexler *et al*., 2004), and the need for measurements over large area. Total evaporation may be estimated using micrometeorological methods such as eddy covariance, Bowen ratio energy balance, surface renewal, flux variance, and optical scintillation methods. However, most micrometeorological methods also require site homogeneity, extensive fetch, and application of the Monin-Obukhov similarity theory (MOST). Therefore, the search for affordable, simple, and accurate methods for determining surface fluxes over large areas has important implications for water resources management.

In this study, total evaporation from the alien invasive *C. odorata* plant is estimated using surface renewal (*SR*) analysis, eddy covariance (*EC*), flux variance (*FV*), and optical scintillation (*SLS*) methods. The *SR* method introduced by Paw U and Brunnet (1991), is a relatively low cost, and simple method (Paw U *et al*., 1995; Snyder *et al*., 1996; Spano *et al*., 1997a, b, 2000; Paw U *et al*., 2005). The *SR* analysis for estimating sensible heat and latent energy flux from canopies involves high frequency air temperature measurements using fine-wire thermocouples. Several studies were reported on the use of the *SR* analysis for estimating sensible heat flux above different canopy surfaces in the past decade (Paw U *et al*., 1995; Katul *et al*.,

1996; Snyder *et al*., 1996; Chen *et al*., 1997a, b; Spano *et al*., 1997a, b; Anandakumar, 1999; Spano *et al*., 2000; Zapata and Martinez-Cob, 2001; Castellvi *et al*., 2002; Castellvi, 2004; Castellvi and Martinez-Cob, 2005). The aim of this study is to evaluate the performance of the three *SR* approaches for estimating sensible heat and latent energy fluxes (total evaporation) above Triffid weed (*Chromolaena odorata*) and to make a comparison of the *SR* method with eddy covariance, flux variance, and optical scintillation methods.

4.2 Theory

4.2.1 Surface renewal

In *SR* analysis, it is assumed that turbulent coherent structures exchange scalars (sensible heat and latent energy) between surfaces and the atmosphere (Paw U *et al*., 2005). The full theory of the *SR* analysis is described in Paw U *et al*. (1995), Snyder *et al*. (1996), and Paw U *et al*. (2005). High frequency air temperature fluctuations exhibit organized coherent structures which look like ramp events (Bergström and Högström, 1989; Gao *et al*., 1989; Shaw *et al*., 1989; Paw U *et al*., 1992). These coherent structures are responsible for transport of momentum, heat and other scalar quantities (Raupach *et al*., 1989; Qui *et al*., 1995; Raupach *et al*., 1996). The *SR* analysis assumes that the sensible heat flux density (H) at measurement height z above the soil surface is determined as:

$$H = \alpha z \rho c_p \frac{a}{\tau} \tag{4.1}$$

where α is a correction or weighting factor, ρ is the air density, c_p is the specific heat capacity of dry air at constant pressure, a is the amplitude, and τ is the total ramping period (inverse ramp frequency) of air temperature ramps. The amplitude and inverse ramp frequency can be determined from the second, third, and fifth order of the structure function for air temperature (Van Atta, 1977).

Chen *et al*. (1997a, b) developed a *SR* analysis model based on a finite micro-front time during the formation of air temperature ramps, that estimates H from

fluctuations of high frequency air temperature measurements using cubic temperature structure function, and the additional measurement of friction velocity. According to the model, H is estimated using the following expression:

$$H = \begin{cases} -\alpha\beta^{2/3}\gamma\rho c_p \left[\dfrac{S^3_{(r_m)}}{r_m}\right]^{1/3} u_*^{2/3} \dfrac{z}{h^{2/3}}, & 0.2h < z \le h + 2(h-d), \\ -\alpha\beta^{2/3}\gamma\rho c_p \left[\dfrac{S^3_{(r_m)}}{r_m}\right]^{1/3} u_*^{2/3} \dfrac{z}{(z-d)^{2/3}}, & z > h + 2(h-d),\ z \le 0.2h, \end{cases} \tag{4.2}$$

where $\alpha\beta^{2/3}\gamma$ is an empirical combined coefficient (a roughly constant value of 0.4), $S^3_{(r_m)}$ is the third order of the structure function for air temperature, r_m is the time lag that maximizes $(S^3_{(r)}/r)^{1/3}$, u_* the friction velocity, h the canopy height, and d is the zero-plane displacement. Based on Sellers *et al*. (1986), the roughness sublayer is assumed to be between $z = h$ and $z = h + 2(h-d)$. Chen *et al*. (1997b) following Lee and Black (1993), have treated the layer adjacent to the soil within canopies ($z \le 0.2h$) the same as the inertial sublayer, with appropriate u_* and d for the soil or understory.

The variable (αz) in Eq. (4.1) is the volume of air per unit ground area exchanged on average for each ramp in the sample period for a height z (Paw U *et al*., 1995). Castellvi *et al*. (2002) interpreted αz as the mean eddy size responsible for the renewal process. Castellvi (2004), based on a one-dimensional diffusion equation, derived the following relationship for estimating the parameter α when measuring above the canopy:

$$\alpha = \begin{cases} \left[\dfrac{k}{\pi}\dfrac{z^*}{z^2}\dfrac{\tau u_*}{\phi_h(\zeta)}\right]^{1/2}, & h \le (z-d) \le z^* \\ \left[\dfrac{k}{\pi}\dfrac{(z-d)}{z^2}\dfrac{\tau u_*}{\phi_h(\zeta)}\right]^{1/2}, & (z-d) > z^* \end{cases} \tag{4.3}$$

where k is von Karman constant ($k \approx 0.35$), z^* the roughness sublayer depth, which may be estimated as $z^* = h + 2(h-d) \approx 5h/3$ (Sellers *et al*., 1986), ζ a stability

parameter defined as $(z-d)/L_o$, with L_o the Obukhov length, and $\phi_h(\zeta)$ the stability function for sensible heat transfer valid for the inertial sublayer.

Castellvi (2004), by combining Eqs (4.1), (4.3), and the definition of the Obukhov length (L_o), proposed the following empirical expression for estimating sensible heat flux density:

$$H=\begin{cases}\rho c_p\left(\dfrac{g}{T}\right)^{1/5}k^{4/5}\left(\dfrac{z^*}{\pi}\right)^{3/5}z^{1/5}\left[-\gamma^3\dfrac{S^3_{(r_m)}}{r_m}\right]^{3/5}\dfrac{1}{a^{3/5}}\left[\dfrac{1}{-\zeta\phi^3{}_h(\zeta)}\right]^{1/5}, & h\le(z-d)\le z^*\\ \rho c_p\left(\dfrac{g}{T}\right)^{1/5}\dfrac{[k(z-d)]^{4/5}}{\pi^{3/5}}\left[-\gamma^3\dfrac{S^3_{(r_m)}}{r_m}\right]^{3/5}\dfrac{1}{a^{3/5}}\left[\dfrac{1}{-\zeta\phi^3{}_h(\zeta)}\right]^{1/5}, & (z-d)>z^*\end{cases} \tag{4.4}$$

where g is the acceleration due to gravity, T the mean absolute air temperature, $S^3_{(r_m)}$ the third order of the structure function for air temperature, r_m the time lag that maximizes $(S^3_{(r)}/r)^{1/3}$, and γ is an empirical parameter which varies by less than 25 % from unity for different surfaces (Chen *et al*., 1997a). The free convection limit of Eq. (4.4) holds under slightly unstable conditions for $\zeta \le -0.03$ with a relative error of less than 8.5 % and can be expressed as (Castellvi, 2004):

$$H=\begin{cases}2.4\rho c_p\left(\dfrac{g}{T}\right)^{1/5}k^{4/5}\left(\dfrac{z^*}{\pi}\right)^{3/5}z^{1/5}\left[-\gamma^3\dfrac{S^3_{(r_m)}}{r_m}\right]^{3/5}\dfrac{1}{a^{3/5}}, & h\le(z-d)\le z^*\\ 2.4\rho c_p\left(\dfrac{g}{T}\right)^{1/5}\dfrac{[k(z-d)]^{4/5}}{\pi^{3/5}}\left[-\gamma^3\dfrac{S^3_{(r_m)}}{r_m}\right]^{3/5}\dfrac{1}{a^{3/5}}, & (z-d)>z^*\end{cases} \tag{4.5}$$

For a variety of short canopies, Castellvi (2004) found very good estimates of sensible heat flux density at different heights above the canopy, using $\gamma = 1.1$ in Eqs (4.4) and (4.5) compared to eddy covariance measurements.

4.2.2 Flux variance

The flux variance (*FV*) method (Tillman, 1972) is based on measurements of scalar fluxes and on Monin-Obukhov similarity theory (MOST). Many studies have investigated the applicability of the *FV* method, though mainly under unstable conditions to estimate sensible heat flux density (e.g., Wesely, 1988; Weaver, 1990; Lloyd *et al*., 1991; de Bruin *et al*., 1993; Padro, 1993; Kustas *et al*., 1994; Albertson *et al*., 1995; Katul *et al*., 1995, 1996; Hsieh and Katul, 1996; Wesson *et al*., 2001; Sugita and Kawakubo, 2003) for both homogeneous and heterogeneous surfaces. Tillman (1972) proposed the following for estimating the sensible heat flux:

$$H = \begin{cases} \rho c_p \left(\frac{\sigma_T}{C_1}\right)^{3/2} \left[\frac{kg(z-d)}{T}\right]^{1/2} \left(\frac{C_2 - \zeta}{-\zeta}\right)^{1/2}, & \zeta < 0 \\ -\rho c_p \left(\frac{\sigma_T}{C_3}\right)^{3/2} \left[\frac{kg(z-d)}{T}\right]^{1/2}, & \zeta \geq 0 \end{cases} \tag{4.6}$$

where σ_T is the standard deviation of high frequency air temperature over the measurement period, T is the mean absolute air temperature, C_1 and C_2 are similarity constants with values of 0.95 and 0.05 respectively, C_3 is an ill-defined constant which is -2.0 (Tillman, 1972), and ζ is a stability parameter defined as $(z-d)/L_o$. Several studies have shown that C_3 is a constant that ranges from -1.8 to -3.0, and site-specific calibration is required (Stull, 1991; Wesson *et al*., 2001). The free convection form of Eq. (4.6) is obtained by considering the limit for $\zeta > C_2$ (Tillman, 1972),

$$H = \rho c_p \left(\frac{\sigma_T}{C_1}\right)^{3/2} \left[\frac{kg(z-d)}{T}\right]^{1/2}, \qquad \zeta \leq -0.05 \tag{4.7}$$

4.2.3 Surface layer scintillometer

A scintillometer is a device that optically measures the intensity fluctuations of visible or infrared radiation, caused by interference after the radiation has been scattered by inhomogenities of the refractive index of the air along the path of

propagation. The scintillometry theory is based on structure functions and MOST (Hill, 1997), and pertinent to the theory is also the cascade theory of turbulence (Kolmogorov, 1941). A detailed review of the theory for measuring surface-layer fluxes of heat and momentum using optical scintillation is available in Hill (1992). A surface layer scintillometer (*SLS*) (Thiermann and Grassl, 1992) allows determination of micrometeorological parameters such as: the structure parameter for refractive index of air C_n^2; structure parameter for temperature C_T^2; the inner scale of turbulence as indicated by the inner scale of refractive index fluctuations l_o; kinetic energy dissipation rate ε; sensible heat flux density H; momentum flux density τ_o and the Obukhov length L_o. The *SLS* method, is dependent on algorithms which are based on MOST (Hill, 1997), and the sensible heat flux is determined as:

$$H = \rho c_p T_* u_* \tag{4.8}$$

where T_* is temperature scale of turbulence, and u_* is the friction velocity.

The *FV* and *SLS* methods, are based on MOST. Generally, MOST effectively predicts mean and turbulent statistics in the inertial sublayer where fluxes are approximately constant (Panofsky and Dutton, 1984). For this experiment, all measurements were made in the roughness sublayer where the applicability of MOST fails. Although attempts to correct flux-profile relationships for roughness sublayer effects have been semi-empirical, and tend to be surface specific (Garratt, 1980; Cellier and Brunet, 1992), the *FV* method is normalized by substituting z for $(z-d)$ in Eq. (4.6) for the roughness sublayer. The *SLS* method is also based on MOST and requires the beam height of the scintillometer to be significantly larger than the height of the roughness element ($z_o \approx 0.1h$) where h is the canopy height. In the inertial sublayer where MOST is applied the effective beam height z of the *SLS* is set to be the height above $d + z_o$, but for the roughness sublayer the effective beam height of the *SLS* has to be corrected and is set at the height above the soil surface, namely 3.0 m for this experiment.

Neglecting advection and the stored canopy heat, the shortened energy balance equation is used to estimate the latent energy flux λE using the surface renewal, eddy

covariance, flux variance, and surface layer scintillometry methods from the sensible heat flux density H, measured net irradiance R_n, and soil heat flux density G as:

$$\lambda E = R_n - G - H \tag{4.9}$$

4.3 Materials and methods

The study was carried out in the Hluhluwe Game Reserve, northern KwaZulu-Natal, South Africa (28°08' S, 32°17' E, altitude 91 m) over alien invasive plant, Triffid weed (*C. odorata*) from day of year 94 to 102 (5 to 13 April, 2006). The site is mainly dominated by the invasive Chromolaena plant with sparsely distributed Acacia trees. The vegetation height of the Chromolaena plant ranged from 2.0 to 2.4 m (average height of 2.2 m). The site has a moderate coastal climate (Whateley and Porter, 1983), with a long-term mean annual rainfall of 774.8 mm (Clemence *et al.*, 1987). Periodic fluctuations in above or below average annual rainfall occur, resulting in wet and dry spells of approximately nine years duration (Preston-Whyte and Tyson, 1988). The range in average monthly temperature is between 13 and 33 °C (Grobler, 1984). The fetch distance was 75 m from the prevailing N-E winds.

For the *SR* and *FV* methods, four unshielded type-E fine-wire thermocouples (75-µm diameter) were used to measure air temperature, placed at heights of 2.30, 2.85, 2.85, and 3.60 m above the soil surface. Thermocouple measurements were done differentially and air temperature data were sampled at a frequency of 10 Hz. Time lags of 0.25 s and 0.50 s (for day of year 94 to 98) and time lags of 0.1 and 0.4 (for day of year 98 to 101) were used for the surface renewal analysis before forming the second, third and fifth order of air temperature structure function values as required by the Van Atta (1977) approach. The data were then averaged and stored every two minutes in the datalogger. Structure functions using the time lags and the analysis technique from Van Atta (1977) were used to determine the amplitude a and the inverse ramp frequency τ characterizing temperature fluctuations as presented by Snyder *et al*. (1996). A constant value of 0.4 was used for the empirical combined coefficient $\alpha\beta^{2/3}\gamma$ (Chen *et al*., 1997b) in Eq. (4.2), and the value of $S^3_{(r)}/r$ was determined from the high frequency air temperature data in the

CR5000 datalogger (Campbell Scientific, Utah, USA) and constant values of $1/r_m$ = 1, 2, 2.5, and 10 Hz were used. The parameter γ in Eq. (4.4) was set to 1.0, a value obtained by Chen *et al*. (1997b) for their experiment in a Douglas-Fir forest. The roughness sub-layer depth z^* was estimated to be at 3.70 m from the ground surface, which is $5h/3$ (Sellers *et al*., 1986).

Two RM Young three-dimensional ultrasonic anemometers (Model 81000, Traverse city, Michigan, USA), were deployed to measure sensible heat flux density and friction velocity at 2.85 and 3.60 m above the soil surface. All sensors were mounted on a lattice mast, and were connected to a CR5000 datalogger. All eddy covariance data were also sampled at a frequency of 10 Hz and data were processed online in the datalogger and stored for further analysis. Friction velocity u_* was calculated as: $[(\overline{u'w'})^2 + (\overline{v'w'})^2]^{1/4}$ (Garratt, 1992), where u, v, and w are the three dimensional orthogonal wind speeds, and u', v', and w' are the fluctuations from the mean of u, v, and w respectively. Friction velocity was also estimated from the mean horizontal wind speed measured using a wind sentry wind speed and direction sensor (RM Young, Model 03001) at 3.0 m from the soil surface as follows (Kaimal and Finnigan, 1994):

$$u_* = bU_{SC} \tag{4.10}$$

where b is the slope of the linear fit of the actual friction velocity versus U_{SC} which is the mean horizontal scalar wind speed. The coefficient b is dependent on the height of the instrument and atmospheric stability (Weber, 1999). For this experiment, since the aim is to estimate total evaporation for unstable conditions, a value of b = 0.175 is used to estimate friction velocity from mean horizontal wind speed (Weber, 1999; Castellvi and Martinez-Cob, 2005). The stability function for heat transfer $\phi_h(\zeta)$ was calculated following Businger *et al*. (1971).

A dual-beam surface layer scintillometer (model SLS40-A, Scintec Atmosphärenmessetechnik, Tübingen, Germany), was used to measure the sensible heat flux density (H_{SLS}) every 1 minute. The scintillometer was positioned at a height of 3.0 m above the soil surface and the path length between the receiver and

transmitter units was 90 m. The SLS40-A employs a diode laser source with an output wavelength of 670 nm and 1 mW (2 mW peak) mean output power. A laptop computer was connected to the signal processing unit of the scintillometer through the serial port. The beam displacement and detector separation distances are 2.5 mm each with a detector diameter of 2.7 mm. Software together with an instrument allows online measurements at a frequency of 1 kHz and subsequent calculation of the structure parameter for refractive index, structure parameter for temperature, the inner scale of turbulence as indicated by the inner scale of refractive index fluctuations, kinetic energy dissipation rate, H_{SLS}, momentum flux density and the Obukhov length L_o. The one-minute estimates of all SLS-calculated parameters were stored on a computer hard drive for further analysis.

Net irradiance was measured using a NR-Lite net radiometer (Kipp & Zonen, Delft, The Netherlands) at 4.0 m above the soil surface. Two soil heat flux plates (model HFT-S, REBS, Seattle, USA) were used to measure soil heat flux density at a depth of 80 mm and a system of parallel thermocouples at depths of 20 and 60 mm were used to calculate the heat stored above the plates (Tanner, 1960). Volumetric soil water content in the first 60 mm of the soil surface was measured using a time domain reflectometer (CS616, Campbell Scientific). The sensors were connected to a CR23X datalogger and measurements were every 10 s and averages obtained every 10 minutes which were in turn used to calculate 30-minute averages for the latent energy flux estimates (Eq. 4.9).

The sign of the amplitude of the air temperature ramps was used to differentiate between the stable and unstable conditions for each 30-minute data. In addition, the sign of the available energy and the sensible heat flux measured with the sonic anemometer was also used to identify the data sets for unstable conditions.

4.4 Results and discussion

4.4.1 Sensible heat flux density for unstable conditions

The 30-minute averages of H_{SR} estimated using Eq. (4.1) for four different time lags r = 0.1, 0.4, 0.5, 1.0 s at heights above the soil surface of 2.30, 2.85, 2.85,

and 3.60 m are compared with EC sensible heat flux density at heights of 2.50 and 3.60 m for unstable atmospheric conditions. These comparisons are made to determine the effect of measurement height and time lags on the H_{SR} estimates and the weighting factor α. The half-hourly H_{SR} estimates computed using Eq. (4.1) are calibrated against the H_{EC} and are presented in Table 4.1. The slope of the linear fits through the origin is the weighting factor α. As shown in Table 4.1, α varied with measurement height and the time lag used. For z = 2.85 m, α is close to 1.0 when time lags, r = 0.5 and 1.0 s are used but different from unity for r = 0.1 and 0.4 s.

At the lowest measurement level (2.30 m above the soil surface), H_{SR} was underestimated and was in poor agreement compared to H_{EC} measurements for all time lags. The agreement between H_{SR} using r = 0.1 and 0.4 s and H_{EC} estimates is poor, and with bias (Table 4.2) for all measurement heights. The use of short time lags (r = 0.1 and 0.4 s) could be too fast for the air temperature ramps to form, and may be one of the reasons for the poor agreement observed between H_{SR} and H_{EC} estimates. The agreement between H_{SR} (Eq. 4.1) estimates using time lags r = 0.5 and 1.0 s and H_{EC} is very good, especially for the measurement height 2.85 m above the soil surface with α approximately 1. The highest measurement level, 3.60 m above the soil surface corrected using α (Table 4.1) also provided very good estimates of H_{EC} for time lags r = 0.5 and 1.0 s. As shown in Table 4.2, the H_{SR} (Eq. 4.1) estimates using time lag r = 1.0 s gave best estimates of H_{EC} for all measurement heights, with slopes close to 1 and lower RMSE values.

Table 4.1 Regression statistics of half-hourly H_{EC} versus H_{SR} estimates calculated using Eq. (4.1) for unstable conditions using time lags r = 0.1, 0.4, 0.5, 1.0 s. The weighting factor α is the slope of the linear fits through the origin.

Time lag	α (for z above the soil surface)				Coefficient of determination			
r (s)	2.30 m	2.85 m	2.85 m	3.60 m	2.30 m	2.85 m	2.85 m	3.60 m
0.1	0.79	0.60	0.56	0.50	0.03	0.65	0.69	0.51
0.4	0.66	0.43	0.84	0.36	0.62	0.74	0.76	0.67
0.5	1.70	1.00	1.03	0.87	0.89	0.85	0.85	0.88
1.0	1.78	1.08	1.10	0.95	0.85	0.90	0.84	0.88

Friction velocity in Eqs (4.2) and (4.4) is estimated using Eq. (4.10) and compared with the actual friction velocity from the sonic anemometer (Fig. 1). The estimated friction velocity u_* (Eq. 4.10) gave excellent estimates of the actual u_* measured using the sonic anemometer (Fig. 4.1), with slope and coefficient of determination very close to 1. Therefore Eq. (4.10) is used to estimate u_* in Eq (4.2) and for the data presented in Table 4.2, since a simple and inexpensive wind speed sensor can be used to estimate u_*.

Table 4.2 Linear regression of half-hourly H_{SR} (Eqs 4.1, 4.2, and 4.4) versus H_{EC} estimates using time lags r = 0.5 and 1.0 s. The root mean square error of estimates (RMSE) is relative to the 1:1 line. The sensible heat flux density H_{SR} (Eq. 4.1) is corrected using α presented in Table 4.1.

z (m)	Time lag	Slope			Intercept (W m^{-2})			Coefficient of determination			RMSE (W m^{-2})		
	r (s)	H_{SR} (1)	H_{SR} (2)	H_{SR} (4)	H_{SR} (1)	H_{SR} (2)	H_{SR} (4)	H_{SR} (1)	H_{SR} (2)	H_{SR} (4)	H_{SR} (1)	H_{SR} (2)	H_{SR} (4)
2.30	0.5	0.86	0.44	0.49	34.66	9.23	4.07	0.89	0.77	0.87	38.46	31.32	25.90
2.30	1.0	0.85	0.52	0.56	35.72	10.39	5.75	0.85	0.80	0.88	45.31	34.90	28.88
2.85	0.5	0.93	0.98	0.89	6.21	10.81	-0.87	0.88	0.91	0.92	45.12	37.44	32.54
2.85	1.0	0.99	0.99	0.89	-3.50	13.88	0.02	0.91	0.93	0.93	39.94	34.44	29.88
2.85	0.5	0.90	0.92	0.88	22.24	16.84	4.26	0.86	0.91	0.91	53.93	36.80	33.20
2.85	1.0	0.91	0.94	0.88	14.56	17.31	5.02	0.85	0.93	0.91	49.08	32.55	32.52
3.60	0.5	0.96	1.18	0.89	6.56	4.62	-6.71	0.89	0.90	0.95	40.32	45.86	24.89
3.60	1.0	0.96	1.19	0.89	4.40	3.31	-7.10	0.89	0.92	0.94	40.41	41.70	25.71

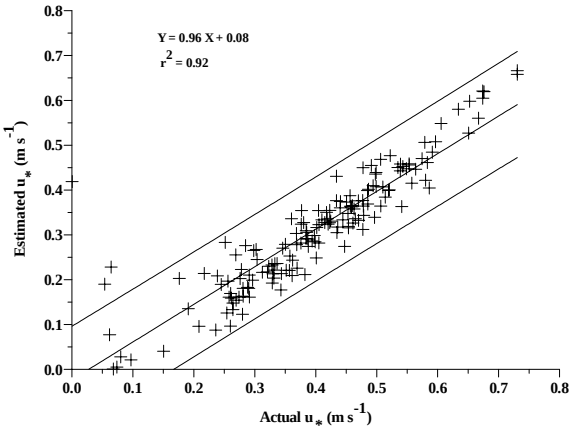

Fig. 4.1 Half-hourly estimated friction velocity u_* using Eq. (4.10) *vs* the actual u_* measured using the sonic anemometer. The middle solid line represents the regression line and the wide confidence bands represent 95 % confidence level for a single predicted value.

Chen *et al*. (1997b) showed that H_{SR} (Eq. 4.2) is proportional to the measurement height, z in the roughness sublayer for $z \le h + 2(h-d)$ and where H_{SR} is normalized with the term $z/h^{2/3}$. The sensible heat flux comparison of H_{SR} (Eq. 4.2) with H_{EC} measurements were more improved compared to the comparisons when using Eqs (4.1) and (4.4) at 2.85 m: the regression slopes are close to unity with coefficient of determinations greater than 0.90. However H_{SR} (Eq. 4.2) at 3.60 m yielded poor estimates of sensible heat flux with RMSE values greater than 40 W m^{-2} (Table 4.2). The *SR* sensible heat flux estimated using Eq. (4.2) at 3.60 m using time lag r = 1.0 s overestimated the H_{EC} measurements by 19 %. The lowest measurement height, closer to the canopy top (2.30 m) underestimated the H_{EC} measurements by almost 50 % (Table 4.2) for both time lags.

As shown in Table 4.2, Eq. (4.4) also provided good estimates of H_{SR} for the measurements taken at 2.85 and 3.60 m using r = 0.5 and 1.0 s. The H_{SR} (Eq. 4.4) gave superior estimates of H_{EC} compared to Eqs (4.1) and (4.2) at 3.60 m, with regression slopes of 0.89, coefficient of determination 0.94, and RMSE values less than 30 W m^{-2}. Although the additional measurement of wind speed is required in Eq. (4.2) to estimate friction velocity and to estimate ζ in Eq. (4.4), they are exempt from calibration unlike Eq. (4.1). Therefore Eq. (4.4) can be used to estimate H_{SR} with reasonable accuracy without calibration with additional measurement of wind speed data.

Measurements of sensible heat flux using two different thermocouples at the same height z = 2.85 m for the *SR* and *FV* were not statistically different, with regression slopes and coefficient of determination close to unity and RMSE values less than 25 W m^{-2} (data not shown). Therefore sensible heat flux measurements for the *SR* and *FV* at 2.85 m are averaged from two different thermocouple measurements. Simple linear regression of the half-hourly H_{SR} (Eqs 4.1, 4.2, and 4.4) using time lag r = 1.0 s *vs* the sensible heat flux estimates from the flux variance (H_{FV}) obtained using Eq. (4.6) are plotted in Fig. 4.2a, b, c, and d respectively. The

SR sensible heat flux estimates agreed well with the FV sensible heat flux estimates at 2.85 and 3.60 m. The performance of H_{SR} (Eq. 4.4) is superior to Eqs (4.1) and (4.2) at 2.85 and 3.60 m as shown in Fig. 4.2. At the highest measurement level, 3.60 m variability between H_{SR} and H_{FV} is observed (Fig. 4.2d). This height is the closest to the transition zone between the roughness and inertial sublayer.

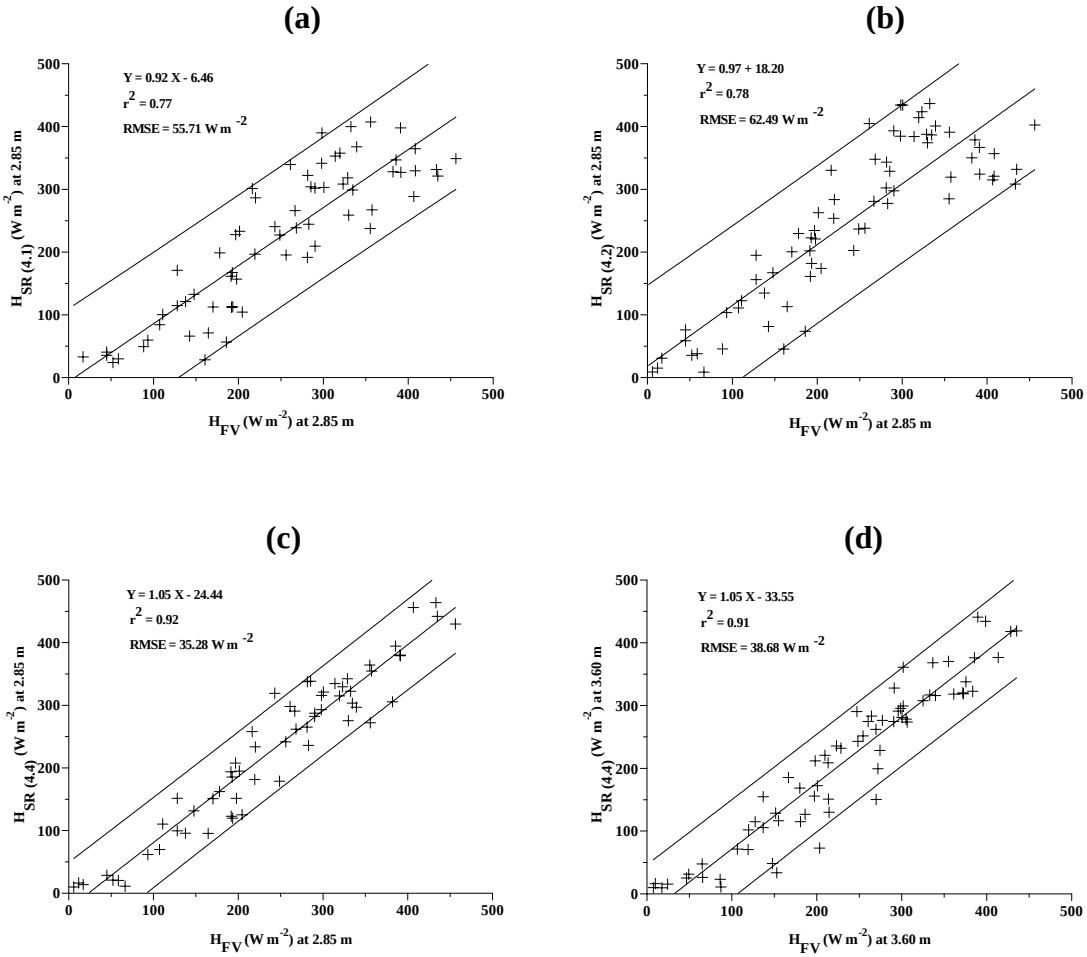

Fig. 4.2 Half-hourly H_{SR} estimates using a time lag r of 1.0 s versus flux variance H_{FV} estimates (Eq. 4.6) for unstable conditions: (a) H_{SR} (Eq. 4.1) *vs* H_{FV} at 2.85 m above the soil surface; (b) H_{SR} (Eq. 4.2) *vs* H_{FV} at 2.85 m above the soil surface; (c) H_{SR} (Eq. 4.4) *vs* H_{FV} at 2.85 m above the soil surface; (d) H_{SR} (Eq. 4.4) *vs* H_{FV} at 3.60 m above the soil surface.

Comparison of half-hourly H_{SR} (Eq. 4.4) estimates using a time lag, r = 1.0 s with H_{SLS} estimates from the surface layer scintillometer are also made for unstable conditions as shown in Fig. 4.3. The *SR* sensible heat flux estimates at 2.85 m underestimated H_{SLS} measurements by 11 %, and H_{SR} at 3.60 m underestimated by 10 %. For these comparisons, it is worth noting that H_{SLS} measurements are path-averaged over a beam distance of 90 m whereas H_{SR} estimates are point measurements. Furthermore, the *SLS* method is based on MOST and measurements should be made in the inertial sublayer. However for tall vegetation such as Chromolaena (average canopy height of 2.20 m), measurements are limited to the roughness sublayer due to fetch constraints and the need to have long tripods or mast to mount the *SLS* transmitter and receiver units. The correspondence between the two methods is in general good (Fig. 4.3a and b) taking into consideration the above limitations.

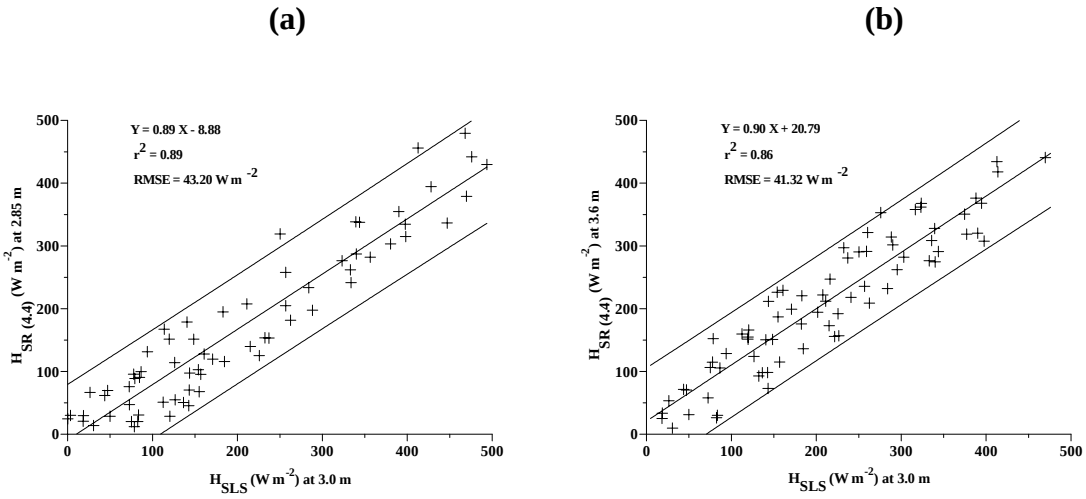

Fig. 4.3 Half-hourly H_{SR} estimates using a time lag r of 1.0 s *vs* surface layer scintillometer H_{SLS} estimates for unstable conditions for day of year 94 to 98 (2006): (a) H_{SR} (Eq. 4.4) at 2.85 m *vs* H_{SLS} at 3.0 m above the soil surface; (b) H_{SR} (Eq. 4.4) at 3.60 m *vs* H_{SLS} at 3.0 m above the soil surface.

4.4.2 Sensible heat flux density under free convection limit

The free convection limit of SR (Eq. 4.4) expressed in Eq. (4.5) holds for $\zeta \leq -0.03$ with a relative error of less than 8.5 % (Castellvi, 2004). The free convection limit for the flux variance (*FV*) method (Eq. 4.7) could be applied under slightly unstable conditions for $\zeta \leq -0.05$ (Tillman, 1972). The observed range of wind speed was 0.25 to 3.5 m s^{-1} (90 % of the measurement period < 2 m s^{-1}), and ζ varied between -10 and -0.1 based on the eddy covariance measurements during the period of 08h00 to 18h00. Atmospheric conditions were mostly convectively unstable during the experimental period for the day time. Hence the free convection limits of the SR (Eq. 4.5) and FV (Eq. 4.7) could be applied for this campaign. The free convection approach of SR analysis (Eq. 4.5) is attractive, since it only requires temperature data as input and is exempt from calibration. The linear regression analysis of estimated H_{SR} for the free convection limit (Eq. 4.5) versus that measured using eddy covariance H_{EC} and estimated using the free convection limit of the FV method (H_{FV}, Eq. 4.7) are listed in Table 4.3. The free convection form of the SR analysis (Eq. 4.5) showed very good performance at 2.85 m for both time lags r = 0.5 and 1.0 s compared with H_{EC} measurements with RMSE values less than 40 W m^{-2}, and relative error of 7 %. The H_{SR} (Eq. 4.5) at 3.60 m also performed well with a relative error of 5 % for r = 0.5 s and 6 % for r = 1.0 s. The free convection limit of the SR analysis (Eq. 4.5) showed very good agreement with the free convection limit of the FV method (Eq. 4.7), with regression slopes close to 1 and RMSE values less than 50 Wm^{-2}. These comparisons show that Eqs (4.5) and (4.7) can be used to estimate sensible heat flux with a relative error of less than 8 %.

Table 4.3 Linear regression of half-hourly H_{SR} (Eq. 4.5) for two measurement heights and two time lags (r = 0.5 and 1.0 s) *vs* measured H_{EC} and estimated using the FV method (Eq. 4.7) for the free convection limit.

z (m)	Time lag	Slope		Intercept (W m^{-2})		Coefficient of determination		RMSE (W m^{-2})	
	r (s)	SR *vs* EC	SR *vs* FV	SR *vs* EC	SR *vs* FV	SR *vs* EC	SR *vs* FV	SR *vs* EC	SR *vs* FV
2.85	0.5	0.96	1.03	-20.27	-20.49	0.91	0.87	37.11	46.10
2.85	1.0	0.96	1.00	-19.90	-14.12	0.92	0.88	34.53	42.34
3.60	0.5	0.93	0.96	-10.14	-6.11	0.94	0.85	25.86	39.80
3.60	1.0	0.91	0.93	-5.63	7.24	0.94	0.88	26.77	33.40

4.4.3 Latent energy flux density

The latent energy flux density λE was estimated using Eq. 4.9 as a residual of the simplified energy balance equation. The linear regression analysis of the latent energy flux from the *SR* analysis λE_{SR} using r = 0.5 and 1.0 s at 2.85 and 3.60 m versus the latent energy flux density from the eddy covariance system λE_{EC} at 2.50 and 3.60 m above the soil surface are presented in Table 4.4. The λE_{SR} estimates using the sensible heat flux equations (Eqs 4.1, 4.2, and 4.4) gave very good estimates of λE_{EC} as shown in Table 4.4. The latent energy flux computed as a residual of the energy balance using H_{SR} (Eq. 4.4) were in good agreement with estimates of λE_{EC} compared to Eqs (4.1) and (4.2). The surface renewal sensible heat flux H_{SR} (Eq. 4.2) produced λE_{SR} estimates with the highest RMSE values. The λE_{SR} estimates using the time lag r = 1.0 s provided very good estimates of λE_{EC} with lower RMSE values and regression slopes close to 1 compared to r = 0.5 s.

The half-hourly plots of λE_{SR} obtained using H_{SR} (Eq. 4.4) for r = 1.0 s versus flux variance λE_{FV} and surface layer scintillometer λE_{SLS} estimates are shown in Figs 4.4 and 4.5 respectively. The agreement between λE_{SR} and λE_{FV} is good, with slopes close to 1 and coefficient of determination greater than 0.80. The λE_{SR} at 2.85 m compared well with λE_{SLS}, but overestimated λE_{SLS} by 8 % (Fig. 4.5a). The λE_{SR} at 3.60 m gave very good estimates of λE_{SLS} (Fig. 4.5b), with slope of 0.99 and RMSE value of 32 W m^{-2}. Generally, λE_{SR} estimates are in good agreement with λE_{FV} and λE_{SLS} estimates.

Table 4.4 Regression statistics of half-hourly λE_{SR} using H_{SR} (Eqs 4.1, 4.2, and 4.4) *vs* λE_{EC} estimates of latent energy flux density for unstable conditions using time lags r = 0.5 and 1.0 s.

z (m)	Time lag	Slope			Intercept (W m^{-2})			Coefficient of determination			RMSE (W m^{-2})		
	r (s)	λE (1)	λE (2)	λE (4)	λE (1)	λE (2)	λE (4)	λE (1)	λE (2)	λE (4)	λE (1)	λE (2)	λE (4)
2.85	0.5	0.97	0.97	1.01	18.77	1.15	26.61	0.79	0.75	0.78	38.11	38.13	37.92
2.85	1.0	0.96	0.97	1.03	15.25	1.68	25.68	0.86	0.75	0.83	29.13	35.85	33.92
3.60	0.5	0.92	0.75	0.94	14.96	-8.43	31.90	0.80	0.50	0.84	32.83	52.07	27.17
3.60	1.0	0.94	0.75	1.00	8.43	-12.35	27.05	0.82	0.50	0.85	31.78	48.00	28.11

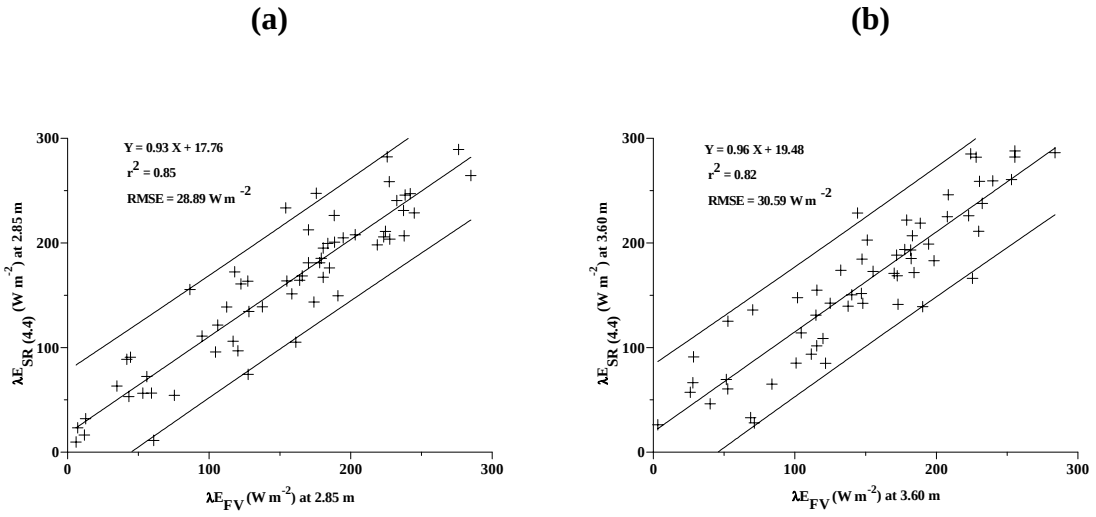

Fig. 4.4 Half-hourly latent energy flux density from the *SR* analysis λE_{SR} using H_{SR} (Eq. 4.4) for r = 1.0 s plotted against the flux variance λE_{FV} estimate for unstable conditions: (a) λE_{SR} *vs* λE_{FV} at 2.85 m above the soil surface; (b) λE_{SR} *vs* λE_{FV} at 3.60 m above the soil surface.

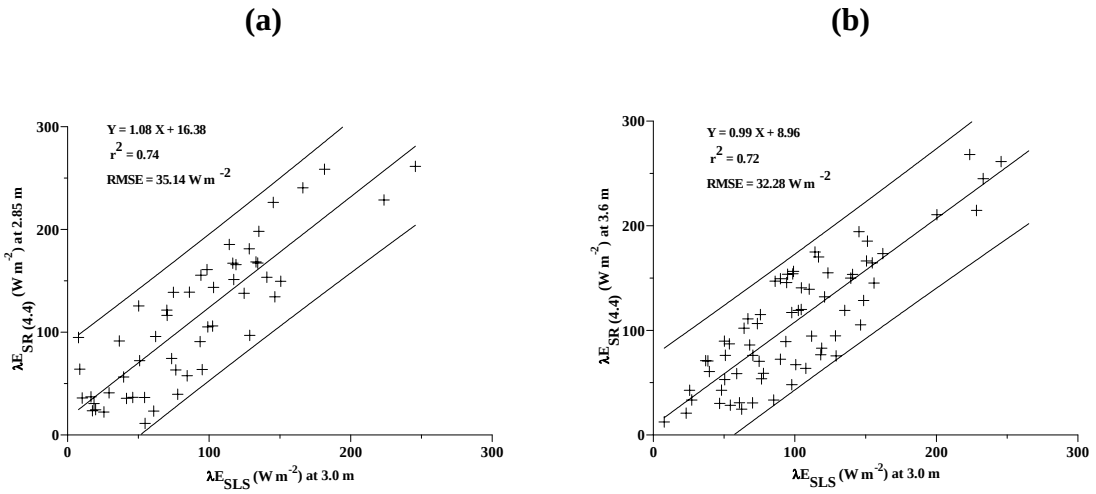

Fig. 4.5 Half-hourly λE_{SR} using H_{SR} (Eq. 4.4) for r = 1.0 s plotted against the surface layer scintillometer λE_{SLS} estimate for unstable conditions: (a) λE_{SR} at 2.85 m *vs* λE_{SLS} at 3.0 m above the soil surface; (b) λE_{SR} at 3.60 m *vs* λE_{SLS} at 3.0 m above the soil surface.

4.5 Summary and conclusions

Sensible heat and latent energy flux densities over 2.20 m tall alien invasive plant, Triffid weed (*C. odorata*) were estimated using SR, EC, FV and SLS methods in the roughness sublayer. The performance of the surface renewal analysis in estimating the sensible heat flux density is evaluated for unstable atmospheric conditions using four time lags r = 0.1, 0.4, 0.5, and 1.0 s. The use of MOST based methods, the *FV* and *SLS* methods for estimating sensible heat flux in the roughness sublayer under unstable conditions, is also evaluated.

The SR sensible heat flux closest to the canopy top, at 2.30 m above the soil surface underestimated the *EC, FV,* and *SLS* sensible heat flux estimates. The SR sensible heat flux, computed using time lags r = 0.1 and 0.4 s, provided poor estimates of sensible heat flux with bias compared to the H_{EC} measurements. Surface renewal analysis at 2.85 and 3.60 m using time lags r = 0.5 and 1.0 s gave comparative estimates of sensible heat and latent energy flux. The empirical SR estimates of sensible heat and latent energy fluxes were in good agreement with EC estimates compared to the SR methods based on the structure functions for air temperature and the finite micro-front time.

The free convection limit of the empirical SR analysis, performed very well in estimating the sensible heat flux. The use of the free convection limit of the empirical SR method under slightly unstable conditions has an advantage, since it only requires high frequency air temperature data. The FV and SLS measurements normalized for the roughness sublayer performed well in estimating the sensible heat and latent energy fluxes at 2.85 and 3.60 m above the soil surface. Comparisons of half-hourly SR sensible heat and latent energy fluxes using a time lag, r = 1.0 s also showed very good agreement with the flux variance and the surface layer scintillometry methods.

In conclusion, the empirical SR analysis method can provide accurate and reliable sensible heat and latent energy flux estimates exempt from calibration in the roughness sublayer if measurements of air temperature are taken well above the

Triffid weed canopy and measurement of wind speed using a simple and inexpensive instrument is available to estimate friction velocity. Alternatively, the free convection limit approach of the empirical SR analysis can be used to estimate sensible heat flux under slightly unstable conditions if wind speed data is not available.

Chapter 5: Estimation of sensible heat and latent energy flux density from an Outeniqua Yellow wood forest using surface renewal

5.1 Introduction

Evaporation monitoring from land, water, and vegetative surfaces is essential for water resources management and sustainable utilisation of water, in water scarce countries such as South Africa. In the past few decades, the accuracy of total evaporation (*ET*) estimates has improved due to development of new methods, and advances in methodology and instrumentation. Despite the availability of different methods for estimating *ET*, each method has advantages and disadvantages, in terms of its theoretical development, accuracy, simplicity, spatial representation, robustness, fetch, and cost of measurement equipment (Drexler *et al*., 2004). In recent years researchers are focussing on methods for estimating sensible heat H and latent energy λE fluxes using simple, low-cost, and robust instrumentation.

Surface renewal (*SR*) analysis for estimating sensible heat flux, latent energy flux, and other scalars has the advantage over other micrometeorological methods since it requires only measurement of the scalar of interest at one point. The *SR* analysis for estimating sensible heat flux from canopies involves high frequency air temperature measurements (typically 2 to 10 Hz) using fine-wire thermocouples. Therefore, the *SR* analysis is a relatively low cost, attractive and simple method (Paw U *et al*., 1995; Snyder *et al*., 1996; Spano *et al*., 1997a, b, 2000; Paw U *et al*., 2005). The *SR* analysis has been used for estimating H above different surfaces such as bare soil, short canopies and tall vegetation. Currently in South Africa, the search of methods for making a volumetric determination of water for purposes of water allocation and charges in the case of activities that result in stream flow reduction is a subject of interest (Savage *et al*., 2005). Besides, studies are being undertaken to determine the water use of grasses, different crops, and forests (Dye and Olbricht, 1993; Savage *et al*., 2004). The aim of this study is to estimate and compare sensible heat and latent energy fluxes above an Outeniqua Yellow wood forest using three *SR* analysis approaches: (1) ideal *SR* analysis method based on structure function proposed by Paw U *et al*. (1995); (2) *SR* analysis model using the so-called finite

micro-front time proposed by Chen *et al*. (1997b); and (3) empirical *SR* analysis model based on similarity theory proposed by Castellvi *et al*. (2002).

5.2 Theory

The full theory of the *SR* analysis is described in Paw U *et al*. (1995), Snyder *et al*. (1996), and Paw U *et al*. (2005). The *SR* analysis assumes that the sensible heat flux density (*H*) at measurement height above soil surface z is determined as:

$$H = \alpha z \rho c_p \frac{a}{\tau} \tag{5.1}$$

where α is a correction or weighting factor, ρ is the air density, c_p is the specific heat capacity of dry air at constant pressure, a is the amplitude of air temperature ramps, and τ is the total ramping period (inverse ramp frequency).

Chen *et al*. (1997a, b) developed a *SR* analysis model that estimates H from fluctuations of high frequency air temperature measurements using a cubic temperature structure function $S^3_{(r)}$, and from the additional measurement of friction velocity. The theory associated with the determination of the amplitude a and total ramp period τ is discussed in detail in Chen *et al*. (1997a). According to their model, H is estimated using the following expression:

$$H = \begin{cases} -\alpha\beta^{2/3}\gamma\rho c_p \left[\dfrac{S^3_{(r_m)}}{r_m}\right]^{1/3} u_*^{2/3} \dfrac{z}{h^{2/3}}, & 0.2h < z \le h + 2(h-d), \\ -\alpha\beta^{2/3}\gamma\rho c_p \left[\dfrac{S^3_{(r_m)}}{r_m}\right]^{1/3} u_*^{2/3} \dfrac{z}{(z-d)^{2/3}}, & z > h + 2(h-d),\ z \le 0.2h, \end{cases} \tag{5.2}$$

where $\alpha\beta^{2/3}\gamma$ is an empirical combined coefficient (a roughly constant value of 0.4), $S^3_{(r_m)}$ is the cube of the structure function for air temperature, r_m is the time lag that maximizes $(S^3_{(r)}/r)^{1/3}$, u_* the friction velocity, h the canopy height, and d is the zero-plane displacement. Based on Sellers *et al*. (1986), the roughness sublayer is assumed to be between $z = h$ and $z = h + 2(h-d)$. Chen *et al*. (1997b) following Lee

and Black (1993), have treated the layer adjacent to the soil within canopies ($z \le 0.2h$) the same as the inertial sublayer, with appropriate u_* and d for the soil or understory.

The variable (αz) in Eq. (5.1) is the volume of air per unit ground area exchanged on average for each ramp in the sample period for a height z (Paw U *et al*., 1995). Castellvi *et al*. (2002) interpreted αz as the mean eddy size responsible for the renewal process. Castellvi (2004), based on a one-dimensional diffusion equation, derived the following relationship for estimating the parameter α when measuring above the canopy:

$$\alpha = \begin{cases} \left[\frac{k}{\pi}\frac{(z-d)}{z^2}\frac{\tau u_*}{\phi_h(\zeta)}\right]^{1/2}, & (z-d) > z^* \\ \left[\frac{k}{\pi}\frac{z^*}{z^2}\frac{\tau u_*}{\phi_h(\zeta)}\right]^{1/2}, & h \le (z-d) \le z^* \end{cases} \tag{5.3}$$

where k is the von Karman constant ($k \approx 0.35$), z^* the roughness sublayer depth, which may be estimated as $z^* = h + 2(h-d) \approx 5/3 * h$ (Sellers *et al*., 1986), τ the total ramping period, ζ a stability parameter defined as $(z-d)/L_o$, with L_o the Obukhov length, and $\phi_h(\zeta)$ the stability function for sensible heat transfer valid for the inertial sublayer.

Castellvi (2004), by combining Eqs (5.1), (5.3), and the definition of the Obukhov length (L_o), proposed the following expression for estimating sensible heat flux density:

$$H = \begin{cases} \rho c_p \left(\frac{g}{T}\right)^{1/5} k^{4/5} \left(\frac{z^*}{\pi}\right)^{3/5} z^{1/5} \left[-\gamma^3 \frac{S^3_{(r_m)}}{r_m}\right]^{3/5} \frac{1}{a^{3/5}} \left[\frac{1}{-\zeta \phi^3{}_h(\zeta)}\right]^{1/5}, & h \le (z-d) \le z^* \\ \rho c_p \left(\frac{g}{T}\right)^{1/5} \frac{\left[k(z-d)\right]^{4/5}}{\pi^{3/5}} \left[-\gamma^3 \frac{S^3_{(r_m)}}{r_m}\right]^{3/5} \frac{1}{a^{3/5}} \left[\frac{1}{-\zeta \phi^3{}_h(\zeta)}\right]^{1/5}, & (z-d) > z^* \end{cases}$$

(5.4)

where g is the acceleration due to gravity, T the mean absolute air temperature, $S^3_{(r_m)}$ is the cubic of the structure function for air temperature, r_m the time lag that maximizes $(S^3_{(r)}/r)^{1/3}$, and γ is empirical parameter which varies by less than 25 % from unity (Chen *et al*., 1997a). The free convection limit for Eq. (5.4), for $\zeta \leq -0.03$ can be estimated using the following expression with a relative error of less than 8.5% (Castellvi, 2004):

$$H = \begin{cases} 2.4\rho c_p \left(\frac{g}{T}\right)^{1/5} k^{4/5} \left(\frac{z^*}{\pi}\right)^{3/5} z^{1/5} \left[-\gamma^3 \frac{S^3_{(r_m)}}{r_m}\right]^{3/5} \frac{1}{a^{3/5}}, & h \leq (z-d) \leq z^* \\ 2.4\rho c_p \left(\frac{g}{T}\right)^{1/5} \frac{\left[k(z-d)\right]^{4/5}}{\pi^{3/5}} \left[-\gamma^3 \frac{S^3_{(r_m)}}{r_m}\right]^{3/5} \frac{1}{a^{3/5}}, & (z-d) > z^* \end{cases} \quad (5.5)$$

For a variety of short canopies, Castellvi (2004) found very good estimates of sensible heat flux density at different heights above the canopy, using $\gamma = 1.1$ in Eqs (5.4) and (5.5) compared to eddy covariance measurements.

5.3 Materials and methods

The experiment was carried out at the Komatiland Plantations, about 12 km south-west of Tzaneen, South Africa (23°50' S, 30°03' E, elevation 853 m) over a 24-year old Outeniqua Yellow wood (*Podocarpus Falcatus*) stand. The study was conducted on day of year 263 to 272 (20 to 29 September, 2005), 39 to 47 (6 to 17 February, 2006), and 234 to 243 (22 to 31 August, 2006) in a 100 m by 250 m plot, in a north-south oriented riparian strip, surrounded by a stream and East Indian Mahogany forest on the west, and a Pine forest on the east. The average height of the trees was 10 m and the spacing between trees 3 m resulting in 1110 trees ha^{-1}. The average leaf area index (LAI) measured using LAI-2000 (LI-COR Inc, Lincoln, Nebraska, USA) and hemispherical photographs taken with a fish eye lens camera and Gap Light Analyzer software (GLA_V2, SFU, Burnaby, British Columbia, Canada) was 2.25 m^2 m^{-2}. The fetch distance was 105 m from the prevailing S-W winds and 50 m for the next-most dominant winds from the N-E.

Air temperature was measured using three unshielded type-E fine-wire thermocouples (75-μm diameter) placed at heights of 11.2, 14.2, and 18.0 m above the ground surface for day of year 263 to 272 (2005). For day of year 39 to 47 (2006), the heights were 11.2, 11.2, and 18.0 m, and were changed to 8.2, 12.0, 15.0 m for day of year 234 to 243 (2006). RM Young three-dimensional ultrasonic anemometer (Model 81000, R.M. Young, Traverse city, Michigan, USA), was set up to measure sensible heat flux density and friction velocity at 12.0 m. All sensors were mounted on a telescopic mast located in the middle of the plot, and were connected to a CR5000 datalogger (Campbell Scientific Inc., Logan, Utah, USA). Air temperature data were sampled at a frequency of 10 Hz and then lagged by 0.1 s and 0.4 s during 20 to 29 September, 2005 and 0.5 s and 1 s for the experiments conducted in 2006. The second, third and fifth air temperature structure function values required by the Van Atta (1977) approach were then formed after lagging the air temperature data by specified amounts - either by 0.1 and 0.4 s or 0.5 and 1.0 s. The data were then averaged and stored every two and thirty minutes in the datalogger. All eddy covariance data were also sampled at a frequency of 10 Hz and data were processed online in the datalogger. The high frequency data, the two-minute, and thirty-minute averages of the covariances between wind speed (u, v, and w), sonic temperature, T_s and wind direction were calculated and stored for further analysis. Friction velocity was calculated as $[(\overline{u'w'})^2 + (\overline{v'w'})^2]^{1/4}$ (Garratt, 1992) and eddy covariance sensible heat flux H_{EC} was calculated using $H_{EC} = \rho c_p \overline{w'T_s'}$.

For the *SR* analysis, Eqs (5.1), (5.2), and (5.4) were used to estimate sensible heat flux density H_{SR} for the different heights above the ground surface. In Eq. (5.1), the weighting factor α was determined by forcing the linear fits of H_{EC} *vs* H_{SR} estimates through the origin. The amplitude a and the inverse ramp frequency τ in Eq. (5.1) were determined from the air temperature structure functions using the time lags and the analysis technique from Van Atta (1977). A constant value of 0.4 (Chen *et al*., 1997b) was used for the empirical combined coefficient $\alpha\beta^{2/3}\gamma$ in Eq. (5.2), and the value of $S^3_{(r_m)}/r_m$ was determined from the high frequency air temperature data in the CR5000 datalogger. Constant values of $1/r_m$ = 2.5 and 10 Hz were used for

the first experiment, in 2005, and $1/r_m$ = 1 and 2 Hz were used for the experiments conducted in 2006, to see the effect of time lag on the sensible heat flux estimates. The parameter γ in Eq. (5.4) was set to 1.0, a value obtained by Chen *et al*. (1997b) for their experiment in a Douglas-Fir forest. The roughness sub-layer depth z^* was estimated to be at 16.7 m from the ground surface, which is $5h/3$ (Sellers *et al*., 1986).

Additional measurements included the remaining components of the energy balance. Net irradiance was measured using net radiometer (Model 240-110 NR-Lite, Kipp & Zonen, Delft, The Netherlands) at 18 m from the ground. Two soil heat flux plates (model HFT-S, REBS) were used to measure soil heat flux density at a depth of 80 mm and a system of parallel-thermocouples at depths of 20 and 60 mm were used to calculate the heat stored above the plates.

Latent energy flux density λE was estimated as a residual of the shortened energy balance using sensible heat flux density H, measured net irradiance R_n, and soil heat flux density G as $\lambda E = R_n - H - G$, where R_n is the net irradiance, H the sensible heat flux density, and G the soil heat flux density. Atmospheric stability was determined from the eddy covariance wind speed data and the sign of the ramp amplitude to distinguish between stable and unstable conditions.

5.4 Results and discussion

5.4.1 Sensible heat flux density

Half-hourly H_{SR} values computed using Eq. (5.1) for time lags r = 0.1 and 0.4 s, at three measurement heights: z_1 = 11.2 m, z_2 = 14.2 m, and z_3 = 18.0 m above the forest were plotted against H_{EC} estimates to determine the weighting factor α by forcing the linear regression through the origin (Table 5.1) for stable and unstable atmospheric conditions. The calculated mean α using Eq. (5.3) is also presented in Table 5.1 for stable and unstable conditions.

Table 5.1 Linear regression statistics of half-hourly H_{EC} (x-axis) *vs* H_{SR} (y-axis) (Eq. 5.1) estimates for day of year 263 to 272 (2005) using time lags r = 0.1 and 0.4 s. The weighting factor α is the slope of the linear fit forced through the origin and the root mean square error of estimates (RMSE) is relative to the 1:1 line. Canopy height h = 10 m.

Data set	Height (m)	Time lag r (s)	Regression α	Coefficient of determination	RMSE (W m^{-2})	n	α (Eq. 5.3)
Stable	11.2	0.1	0.326	0.16	19.18	197	0.005
Stable	11.2	0.4	0.260	0.23	18.32	198	0.005
Unstable	11.2	0.1	1.502	0.77	55.81	132	1.450
Unstable	11.2	0.4	1.071	0.84	49.02	140	1.430
Stable	14.2	0.1	0.311	0.18	18.99	194	0.004
Stable	14.2	0.4	0.245	0.24	18.20	199	0.005
Unstable	14.2	0.1	1.525	0.68	63.89	132	1.510
Unstable	14.2	0.4	1.113	0.75	59.80	138	1.404
Stable	18.0	0.1	0.251	0.06	19.98	186	0.004
Stable	18.0	0.4	0.200	0.18	18.70	196	0.004
Unstable	18.0	0.1	1.504	0.55	75.02	132	1.150
Unstable	18.0	0.4	1.089	0.68	66.78	138	1.110

All measurements were made in the roughness sublayer except for the top measurement height (18.0 m) which was in the inertial sublayer. The weighting factor (actual α) is the slope of the linear regression of the half-hourly H_{SR} *vs* H_{EC} estimates forced through the origin. The actual regression α is greater than the estimated α obtained using Eq. (5.3) for stable conditions for all the measurement heights and for both time lags as shown in Table 5.1. For unstable conditions, the actual regression α is almost the same in magnitude to the mean α obtained using Eq. (5.3) for r = 0.1 s at 11.2 and 14.2 m above the ground surface. However, it is less than the estimated α for r = 0.4 s. Half-hourly H_{SR} values at 11.2 m corrected using the actual α and estimated α using Eq. (5.3) are plotted against H_{EC} estimates at 12.0 m (Fig. 5.1) for day of year 263 to 272 (2005). The H_{SR} values corrected using the actual regression α for both stable and unstable conditions gave better estimates of H_{EC} (Fig. 5.1a) compared to the H_{SR} values (Fig. 5.1b) corrected using the estimated α (Eq. 5.3). The slope of the H_{SR} *vs* H_{EC} relationship is 0.95 using the actual regression α (Table 5.1) compared to 1.28 for the estimated α and the root mean square error (RMSE) is smaller for Fig. 5.1a.

(a)

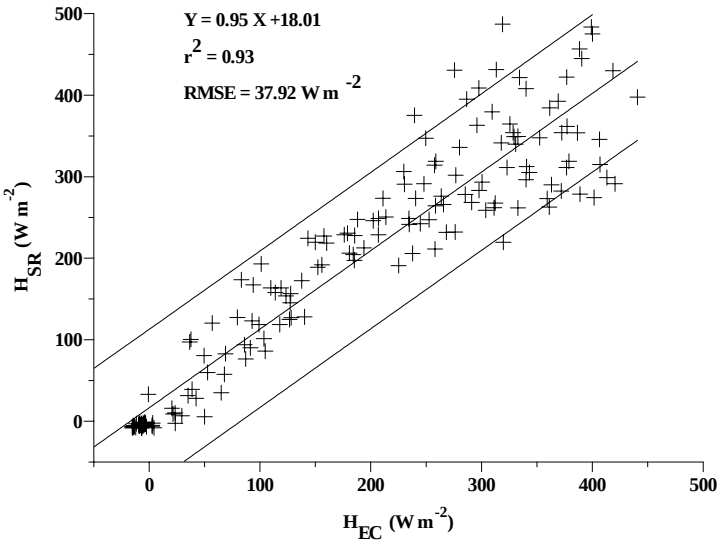

(b)

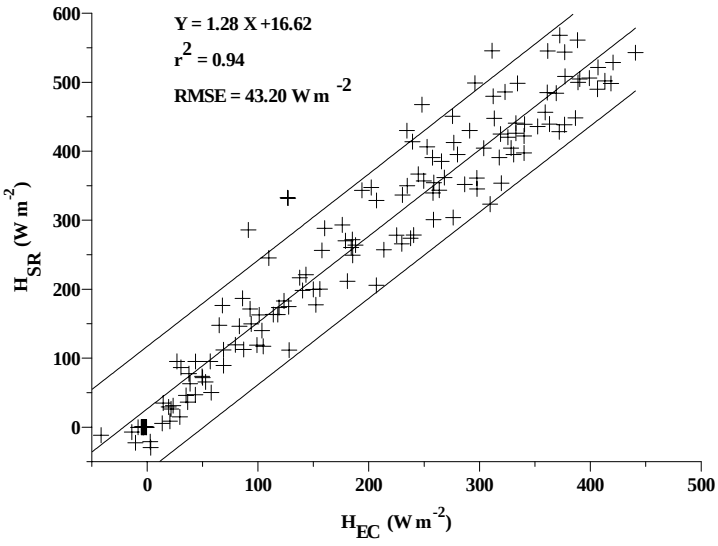

Fig. 5.1 Half-hourly surface renewal H_{SR} *vs* eddy covariance H_{EC} estimates of sensible heat flux density using a time lag r of 0.4 s, for day of year 263 to 272 (2005): (a) H_{SR} at 11.2 m above the ground surface corrected using the actual α *vs* H_{EC} at 12.0 m; (b) H_{SR} at 11.2 m above the ground surface corrected using estimated α (Eq. 5.3) *vs* H_{EC} at 12.0 m. The confidence bands represent 95 % confidence level for a single-predicted value.

Studies made under unstable conditions showed that the actual α was roughly 0.5 for measurements taken at the top of tall canopies (Paw U *et al*., 1995; Katul *et al*., 1996), but when measurements are taken well above the canopy (inertial sublayer), the value of α approached 1 (Snyder *et al*., 1996; Spano *et al*., 1997a; Zapata and Martinez-Cob, 2001). The results in Table 5.1 show that the parameter α is independent of measurement height and is close to unity (ranging from 1.07 to 1.11) for measurements made in the roughness and inertial sublayers when using a time lag r = 0.4 s. The use of a short time lag (r = 0.1 s) could be too fast for the temperature ramps to form, and may be one of the reasons for the actual α being different from unity, which is around 1.5 in the inertial sublayer for unstable conditions. Chen *et al*. (1997a) found an average time lag r_m = 0.83 s in their experiment in a Douglas-Fir forest. For this experiment, $-S^3_{(r)}/r$ is plotted against r from the high frequency air temperature data to determine the time lag which maximizes $(-S^3_{(r_m)}/r_m)^{1/3}$, and a value of r_m = 1.0 s is obtained as shown in Fig. 5.2.

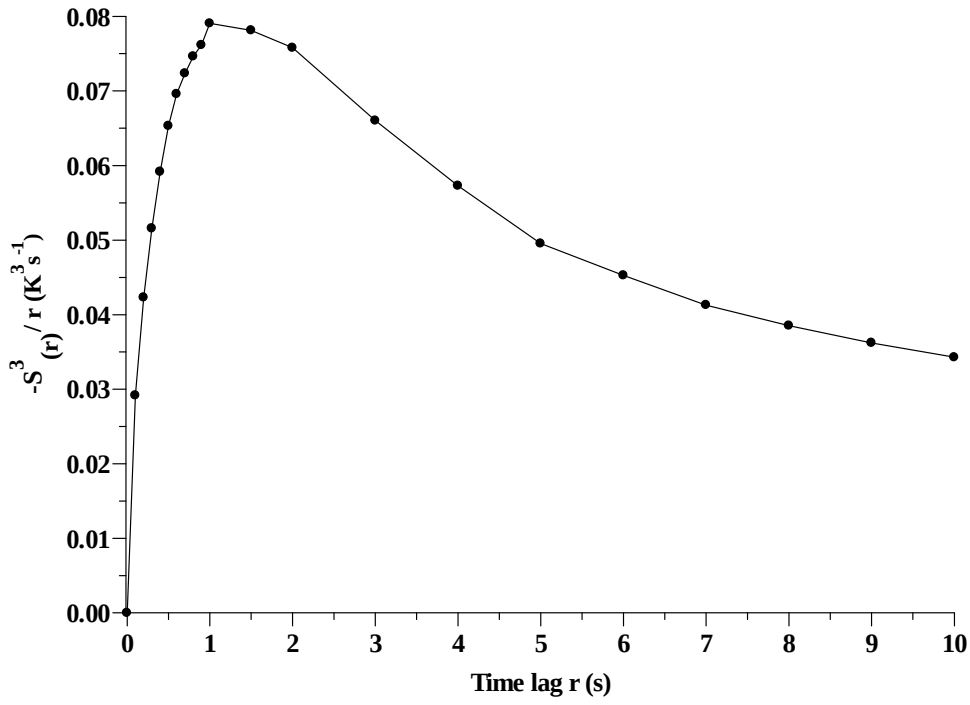

Fig. 5.2 Measured half-hourly averages of $-S^3_{(r)}/r$ *vs* time lag r at 11.2 m above ground surface for measurements taken on day of year 264 (2005) at 10h00.

The actual regression and estimated α using Eq. (5.3) for three measurement heights z = 8.2, 12.0, 15.0 m above the ground surface are presented in Table 5.2 for day of year 234 to 243 (2006). The time lags were changed to r = 0.5 and 1.0 s for the second and third set of experiments, to investigate the effect of time lag on the sensible heat flux estimates. The actual α is greater than the estimated α obtained using Eq. (5.3) for stable conditions as shown in Table 5.2. For unstable conditions, the actual α is smaller in magnitude than the mean α obtained using Eq. (5.3) for both time lags and all measurement heights. The actual α for r = 0.5 s is not that different in magnitude but it is relatively smaller when compared to r = 1.0 s for stable and unstable conditions. However, the actual and estimated α values are smaller in magnitude than the data presented in Table 5.1 for the time lags r = 0.1 and 0.4 s.

The surface renewal sensible heat flux density H_{SR} was estimated using Eqs (5.1), (5.2), and (5.4) and performance of each equation in estimating sensible heat flux was analyzed by a simple linear regression of H_{SR} *vs* H_{EC} estimates. The slope, intercept, coefficient of determination, and the RMSE were determined for Eqs (5.1), (5.2), and (5.4) and are presented in Tables 5.3, 5.4, and 5.5 for the three experiments.

Table 5.2 Linear regression analysis of half-hourly H_{SR} (Eq. 5.1) *vs* H_{EC} estimates for day of year 234 to 243 (2006) using time lags r = 0.5 and 1.0 s. The weighting factor α is the slope of the linear fit forced through the origin and the RMSE is relative to the 1:1 line.

Data set	Height (m)	Time lag r (s)	Regression α	Coefficient of determination	RMSE (W m^{-2})	n	α (Eq. 5.3)
Stable	8.2	0.5	0.220	0.33	30.65	160	0.014
Stable	8.2	1.0	0.250	0.33	12.37	167	0.014
Unstable	8.2	0.5	0.730	0.88	38.78	130	0.850
Unstable	8.2	1.0	0.770	0.91	34.90	134	0.920
Stable	12.0	0.5	0.120	0.37	11.85	171	0.024
Stable	12.0	1.0	0.140	0.48	10.80	172	0.026
Unstable	12.0	0.5	0.580	0.89	37.94	125	0.750
Unstable	12.0	1.0	0.600	0.90	36.11	130	0.810
Stable	15.0	0.5	0.096	0.50	11.09	151	0.012
Stable	15.0	1.0	0.110	0.57	9.76	171	0.014
Unstable	15.0	0.5	0.590	0.85	41.89	125	0.620
Unstable	15.0	1.0	0.610	0.87	39.81	125	0.670

In Table 5.3, for stable conditions, Eqs (5.2) and (5.4) performed better in estimating the sensible heat flux density compared to Eq. (5.1) for both time lags r = 0.1 and 0.4 s and all measurement heights, with slope and coefficient of determination close to unity and lower RMSE values. Under unstable conditions, for measurements taken at z = 11.2 m (roughness sublayer), Eq. (5.4) performed better for r = 0.1 s. However, Eqs (5.1) and (5.4) did well for r = 0.4 s. Sensible heat flux estimates obtained using Eq. (5.2) gave very good estimates of H_{SR} (Table 5.3) for the measurement taken at z = 14.2 m under unstable conditions. In the inertial sublayer (z = 18 m), Eq. (5.4) yielded very good estimates of H_{SR} using r = 0.1 s. However Eq. (5.1) performed best for r = 0.4 s under unstable conditions. In general, H_{SR} estimated using the time lag r = 0.4 s gave better estimates of H_{EC} compared to r = 0.1 s, with lower RMSE values and reduced bias. Overall, the sensible heat flux density estimated using Eq. (5.1) performed better than Eqs (5.2) and (5.4), although it needs correction using the actual α presented in Table 5.1.

The data presented for the second experiment (Table 5.4) was for the summer of 2006, with rain and overcast weather conditions and low sensible heat flux values. Although the weather was not conducive for such comparisons, the linear regression analyses are presented in Table 5.4 to assess the performance of the surface renewal method under this type of weather conditions. The time lags were changed to r = 0.5 and 1.0 s, and two thermocouples were placed at the same height z = 11.2 m above the ground surface to determine the difference in the sensible heat flux estimates using two sensors at the same height. The difference between the sensible heat flux estimates using two different sensors at the same measurement height z = 11.2 m is insignificant (Table 5.4). The sensible heat flux estimates using Eq. (5.2) yielded more accurate H_{EC} estimates under stable conditions for both time lags r = 0.5 and 1.0 s, and all measurement heights. For unstable conditions, Eq. (5.4) gave more accurate H_{SR} estimates for the measurements made at z = 11.2 m using both time lags r = 0.5 and 1.0 s, with slope and coefficient of determination close to 1, but with greater RMSE values than using Eqs (5.1) and (5.2). In the inertial sublayer, under unstable conditions, Eq. (5.1) produced better estimates of sensible heat flux density.

Table 5.3 Linear regression of half-hourly H_{SR} (Eqs 5.1, 5.2, and 5.4) *vs* H_{EC} estimates for day of year 263 to 272 (2005) using time lags r = 0.1 and 0.4 s. The RMSE is relative to the 1:1 line. The sensible heat flux density H_{SR} (Eq. 5.1) is corrected using the actual (regression) α presented in Table 5.1. Canopy height h = 10 m.

Data set	Height (m)	Time lag r (s)	Slope			Intercept (W m^{-2})			Coefficient of determination			RMSE (W m^{-2})		
			H_{SR}(5.1)	H_{SR}(5.2)	H_{SR}(5.4)	H_{SR}(5.1)	H_{SR}(5.2)	H_{SR}(5.4)	H_{SR}(5.1)	H_{SR}(5.2)	H_{SR}(5.4)	H_{SR}(5.1)	H_{SR}(5.2)	H_{SR}(5.4)
All data	11.2	0.1	0.63	0.68	1.26	-2.28	-7.57	26.80	0.88	0.94	0.96	34.32	25.22	40.62
All data	11.2	0.4	0.95	0.77	1.11	3.06	-7.58	31.98	0.94	0.94	0.88	33.36	27.86	52.08
Stable	11.2	0.1	0.18	1.30	0.59	-19.01	7.43	9.37	0.16	0.81	0.54	8.39	13.20	11.59
Stable	11.2	0.4	0.22	1.48	0.53	-17.53	8.82	8.09	0.23	0.86	0.53	8.44	12.38	10.41
Unstable	11.2	0.1	0.47	0.68	1.25	43.90	-7.98	32.96	0.57	0.83	0.85	47.20	34.25	60.29
Unstable	11.2	0.4	0.87	0.76	1.11	25.92	-6.15	31.98	0.84	0.86	0.88	46.57	37.56	52.08
All data	14.2	0.1	0.92	0.85	1.26	4.40	-10.10	25.43	0.91	0.92	0.95	43.35	35.73	39.27
All data	14.2	0.4	0.70	0.95	0.90	-1.47	-11.00	16.73	0.91	0.93	0.94	32.11	38.39	32.56
Stable	14.2	0.1	0.20	1.80	0.73	-17.81	12.77	12.13	0.18	0.81	0.59	8.99	18.12	12.70
Stable	14.2	0.4	0.28	1.98	0.46	-15.22	13.25	7.01	0.24	0.83	0.52	10.17	18.68	9.07
Unstable	14.2	0.1	0.82	0.82	1.28	36.98	-6.48	23.10	0.71	0.82	0.87	62.81	46.07	59.35
Unstable	14.2	0.4	0.60	0.91	0.92	27.00	-2.66	9.94	0.71	0.84	0.86	45.87	49.52	47.68
All data	18.0	0.1	0.88	0.36	0.95	8.22	-4.53	17.40	0.87	0.90	0.95	49.52	17.76	30.05
All data	18.0	0.4	0.91	0.65	0.65	4.80	-8.36	13.76	0.90	0.92	0.93	43.60	29.12	26.01
Stable	18.0	0.1	0.17	0.80	0.57	-17.45	6.00	9.85	0.13	0.79	0.56	10.35	8.50	10.77
Stable	18.0	0.4	0.23	1.39	0.35	-16.50	10.40	5.65	0.18	0.82	0.53	10.12	13.74	6.65
Unstable	18.0	0.1	0.73	0.34	1.02	52.34	-1.80	-1.80	0.60	0.75	0.88	71.35	23.69	43.41
Unstable	18.0	0.4	0.80	0.64	0.64	36.82	-7.97	17.30	0.71	0.81	0.81	63.70	37.95	38.67

Table 5.4 Linear regression of half-hourly H_{SR} (Eqs 5.1, 5.2, and 5.4) *vs* H_{EC} estimates for day of year 39 to 47 (2006) using time lags r = 0.5 and 1.0 s. The RMSE is relative to the 1:1 line. Average canopy height h = 10 m.

Data set	Height (m)	Time lag r (s)	Slope			Intercept (W m^{-2})			Coefficient of determination			RMSE (W m^{-2})		
			H_{SR}(5.1)	H_{SR}(5.2)	H_{SR}(5.4)	H_{SR}(5.1)	H_{SR}(5.2)	H_{SR}(5.4)	H_{SR}(5.1)	H_{SR}(5.2)	H_{SR}(5.4)	H_{SR}(5.1)	H_{SR}(5.2)	H_{SR}(5.4)
All data	11.2	0.5	0.75	0.40	1.00	-1.55	-1.42	23.37	0.84	0.88	0.87	39.01	15.36	46.07
All data	11.2	1.0	0.75	0.42	1.04	-5.83	-1.49	26.66	0.89	0.87	0.81	29.66	15.09	56.52
Stable	11.2	0.5	0.39	0.48	0.12	-27.69	0.97	1.27	0.30	0.72	0.39	28.07	5.82	3.85
Stable	11.2	1.0	0.29	0.55	0.14	-24.70	1.29	1.33	0.30	0.76	0.41	17.08	5.47	3.75
Unstable	11.2	0.5	0.64	0.41	1.01	22.76	-3.66	23.32	0.81	0.84	0.83	35.98	20.49	53.52
Unstable	11.2	1.0	0.67	0.43	1.01	11.77	-3.89	34.90	0.87	0.85	0.75	30.48	21.00	68.88
All data	11.2	0.5	0.73	0.39	0.94	-0.05	-0.86	26.63	0.87	0.88	0.88	29.03	14.91	41.95
All data	11.2	1.0	0.72	0.41	1.00	-3.03	-1.41	22.03	0.88	0.89	0.87	25.63	15.03	43.25
Stable	11.2	0.5	0.32	0.48	0.15	-26.47	1.01	1.86	0.18	0.66	0.35	17.66	6.46	5.27
Stable	11.2	1.0	0.28	0.56	0.16	-24.10	1.18	1.53	0.16	0.73	0.40	15.18	6.04	4.53
Unstable	11.2	0.5	0.65	0.40	0.93	17.36	-2.09	29.33	0.85	0.84	0.84	27.51	20.36	47.86
Unstable	11.2	1.0	0.62	0.42	0.99	13.31	-3.32	26.21	0.86	0.85	0.83	24.67	21.15	51.86
All data	18.0	0.5	0.83	0.20	0.30	0.86	-1.00	13.52	0.70	0.82	0.73	76.06	10.99	23.58
All data	18.0	1.0	0.88	0.25	0.40	-19.05	-0.96	19.49	0.71	0.85	0.34	75.01	11.45	67.84
Stable	18.0	0.5	0.28	0.34	0.05	-62.66	-0.05	0.58	0.02	0.42	0.34	67.08	7.44	2.72
Stable	18.0	1.0	0.11	0.41	0.14	-78.65	0.51	1.67	0.02	0.63	0.47	61.16	5.75	3.83
Unstable	18.0	0.5	0.70	0.20	0.28	32.04	1.26	16.48	0.56	0.77	0.64	74.16	12.97	25.75
Unstable	18.0	1.0	0.64	0.24	0.34	38.45	0.72	32.30	0.59	0.79	0.20	66.56	15.07	81.60

Table 5.5 Linear regression of half-hourly H_{SR} (Eqs 5.1, 5.2, and 5.4) *vs* H_{EC} estimates for day of year 234 to 243 (2006) using time lags r = 0.5 and 1.0 s. The RMSE is relative to the 1:1 line. The sensible heat flux density H_{SR} (Eq. 5.1) is corrected using the actual α presented in Table 5.2. Average canopy height h = 10 m.

Data set	Height (m)	Time lag r (s)	Slope			Intercept (W m^{-2})			Coefficient of determination			RMSE (W m^{-2})		
			H_{SR}(5.1)	H_{SR}(5.2)	H_{SR}(5.4)	H_{SR}(5.1)	H_{SR}(5.2)	H_{SR}(5.4)	H_{SR}(5.1)	H_{SR}(5.2)	H_{SR}(5.4)	H_{SR}(5.1)	H_{SR}(5.2)	H_{SR}(5.4)
All data	8.2	0.5	0.93	0.65	1.11	6.38	-2.94	27.02	0.94	0.94	0.84	27.11	18.13	63.57
All data	8.2	1.0	0.94	0.64	1.01	4.63	-2.88	22.12	0.95	0.94	0.84	24.37	17.77	55.78
Stable	8.2	0.5	0.31	0.82	0.12	-10.11	-2.96	-0.64	0.34	0.76	0.03	6.69	6.43	8.68
Stable	8.2	1.0	0.30	0.83	0.05	-9.73	-2.82	-2.02	0.33	0.75	0.01	6.51	6.62	9.15
Unstable	8.2	0.5	0.82	0.61	1.04	33.49	5.26	44.97	0.89	0.88	0.72	33.91	26.64	74.43
Unstable	8.2	1.0	0.87	0.60	0.97	23.48	5.81	32.88	0.91	0.88	0.75	31.68	25.89	66.04
All data	12.0	0.5	0.97	0.97	1.26	-0.14	-7.08	32.50	0.95	0.94	0.82	26.38	27.19	76.64
All data	12.0	1.0	0.94	0.94	1.10	2.91	-7.04	27.48	0.95	0.94	0.81	24.22	25.95	68.65
Stable	12.0	0.5	0.50	1.42	0.05	-12.24	-5.42	-2.10	0.37	0.76	0.01	9.64	11.25	9.51
Stable	12.0	1.0	0.44	1.41	0.04	-8.28	-4.98	-2.27	0.49	0.77	0.01	6.79	10.96	10.23
Unstable	12.0	0.5	0.87	0.90	1.18	23.61	8.23	53.39	0.89	0.87	0.69	35.17	38.18	91.07
Unstable	12.0	1.0	0.88	0.87	1.04	19.57	7.92	43.39	0.90	0.89	0.68	33.33	36.49	81.78
All data	15.0	0.5	0.95	1.20	1.39	1.50	-9.58	-7.24	0.93	0.91	0.81	28.99	45.41	84.18
All data	15.0	1.0	0.95	1.14	1.14	0.34	-10.37	25.90	0.95	0.94	0.82	26.32	31.55	62.25
Stable	15.0	0.5	0.52	1.48	0.03	-7.14	6.27	0.16	0.50	0.69	0.25	8.21	15.29	0.88
Stable	15.0	1.0	0.63	1.80	0.05	-4.72	-6.04	-2.65	0.58	0.74	0.05	8.06	15.13	10.44
Unstable	15.0	0.5	0.91	1.41	1.66	9.70	-59.47	-68.08	0.86	0.88	0.79	41.31	58.71	94.02
Unstable	15.0	1.0	0.95	1.07	1.10	2.44	5.62	37.79	0.88	0.89	0.70	40.08	43.57	82.28

All measurements were made in the roughness sublayer for the third experiment which was conducted in spring (2006). The measurement heights above the soil surface were z = 8.2, 12.0, and 15.0 m, and time lags of r = 0.5 and 1.0 s were used as shown in Table 5.5. The performance of Eq. (5.2) for estimating the sensible heat flux density under stable conditions is also superior to Eqs (5.1) and (5.4) for all measurement heights and both time lags as was the case for the other two experiments presented in Tables 5.3 and 5.4. For unstable conditions, Eq. (5.1) corrected using the actual α (Table 5.2) gave very good estimates of H_{SR} for all measurement heights and time lags. It should also be noted that Eq. (5.2) also performed very well under unstable conditions for z = 12.0 and 15.0 m. An improved performance of the SR is observed using the time lag r = 1.0 s in this study (Table 5.5) compared to the time lags of r = 0.1, 0.4, and 0.5 s (Tables 5.3 and 5.5), with slope and coefficient of determination close to 1 and lower RMSE values. This may be attributed to the use of an ideal time lag recommended by Chen *et al*. (1997a) for tall canopies (r = 1.0 s) that maximizes $(-S^3_{(r_m)}/r_m)^{1/3}$ (Fig. 5.3), which is crucial in the estimation of sensible heat flux density.

Sensible heat flux estimates obtained using Eq. (5.4) produced results with greater RMSE values for measurements made in the roughness sublayer. However, Eq. (5.1) yielded higher RMSE values in the inertial sublayer. Generally, Eq. (5.2) gave results with the least RMSE values for all the measurement heights, time lags, and stable and unstable conditions, although the sensible heat flux estimates under unstable conditions exhibited greater bias. Half-hourly estimates of H_{SR} (Eqs 5.1, 5.2, and 5.4) at a measurement height z = 15.0 m are plotted against H_{EC} values for a time lag r = 1.0 s, as shown in Fig. 5.3a, b, and c for unstable conditions. These comparisons show that H_{SR} estimates using the three equations are in good agreement with H_{EC} estimates under unstable atmospheric conditions. Sensible heat flux estimates involving Eq. (5.4) gave higher RMSE values as shown in Fig. 5.3c.

(a) (b)

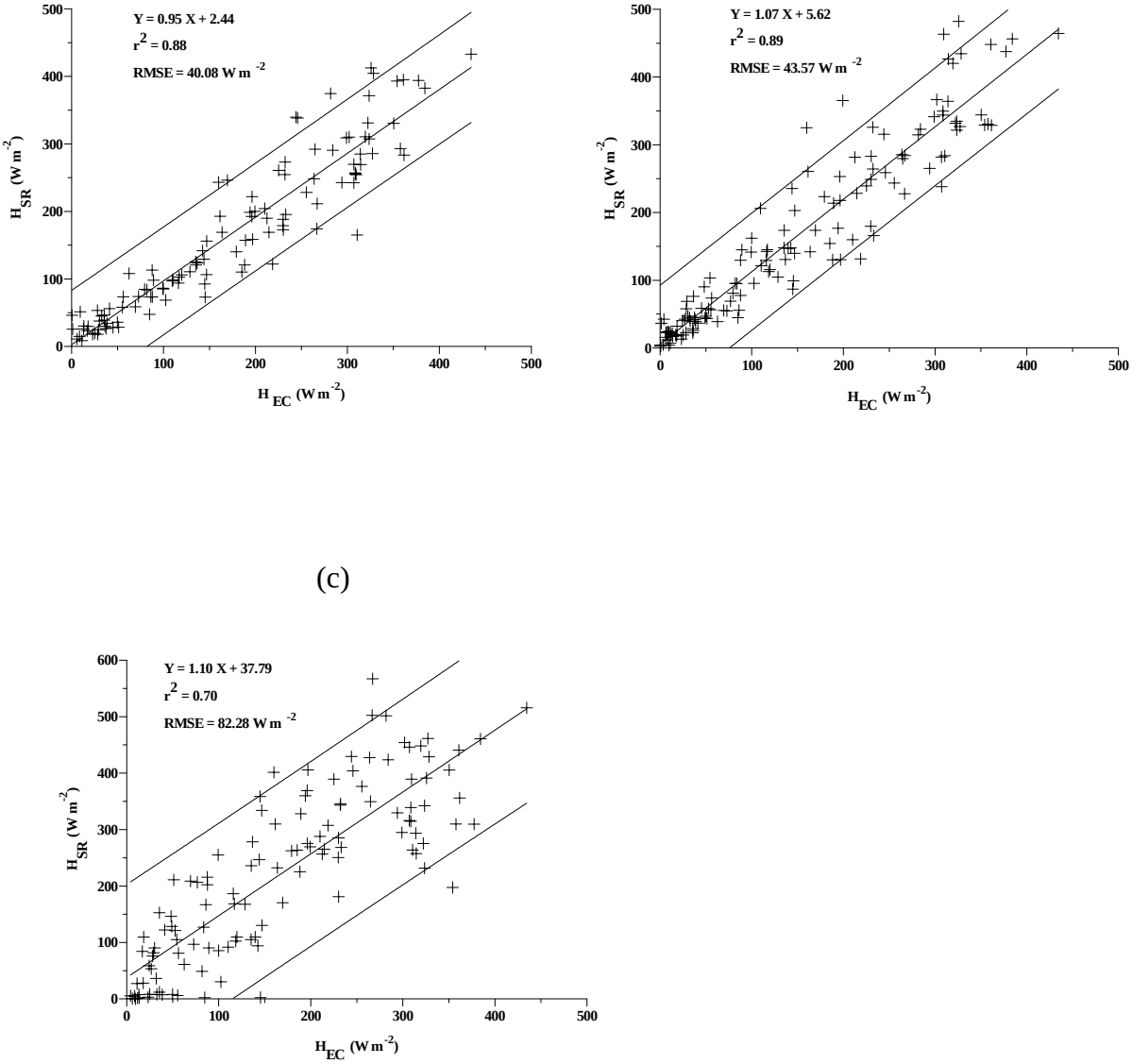

(c)

Fig. 5.3 Half-hourly surface renewal H_{SR} *vs* eddy covariance H_{EC} estimates of sensible heat flux density for unstable conditions using a time lag r of 1.0 s, for days of year 234 to 243 (2006): (a) H_{SR} at 15.0 m above the ground surface computed using Eq. (5.1) *vs* H_{EC} at 12.0 m; (b) H_{SR} at 15.0 m above the ground surface computed using Eq. (5.2) *vs* H_{EC} at 12.0 m; (c) H_{SR} at 15.0 m above the ground surface computed using Eq. (5.4) *vs* H_{EC} at 12.0 m.

5.4.2 Latent energy flux density

The latent energy flux density λE was estimated as a residual of the energy balance equation. The linear regression statistics of the latent energy flux density from surface renewal analysis λE_{SR} using r = 0.1, 0.4, 0.5, and 1.0 s for two measurement heights *vs* the latent energy flux density from the eddy covariance system λE_{EC} are presented in Table 5.6. The λE_{SR} estimates using the sensible heat flux equation H_{SR} (Eq. 5.1) gave very good estimates of λE_{EC} using all time lags compared to Eqs (5.2) and (5.4) as shown in Table 5.6. The latent energy flux computed as a residual of the energy balance equation using H_{SR} (Eq. 5.2) also gave good estimates of λE_{EC}. The surface renewal sensible heat flux H_{SR} (Eq. 5.4) produced λE_{SR} estimates with the highest RMSE values. In general, λE_{SR} estimates using the time lag r = 1.0 s gave excellent estimates of λE_{EC} compared to the other time lags.

The diurnal variations in λE_{EC} and λE_{SR} (using H_{SR}, Eq. 5.1 and time lag r = 0.4 s) for a typical clear day, day of year 267 (2005) and partly cloudy, day of year 268 (2005) are shown in Fig. 5.4a along with net irradiance and soil heat flux. Diurnal comparisons of the λE_{SR} obtained using H_{SR} (Eqs 5.1 and 5.2) and λE_{EC} estimates along with net irradiance are also plotted in Fig. 5.4b for two contrasting days using r = 1.0 s. Two x-axes are used to separate the curves for widely varying net irradiance conditions (day of year 238, 2006) and cloudless (day of year 240, 2006).

Table 5.6 Regression statistics of half-hourly λE_{SR} using H_{SR} (Eqs 5.1, 5.2, and 5.4) *vs* λE_{EC} estimates of latent energy flux density from 06h00 to 18h00, for day of year 263 to 272 (2005) and 234 to 243 (2006) using time lags r = 0.1, 0.4, 0.5, and 1.0 s.

z (m)	Time lag r (s)	Slope			Intercept (W m^{-2})			Coefficient of determination			RMSE (W m^{-2})		
		λE (5.1)	λE (5.2)	λE (5.4)	λE (5.1)	λE (5.2)	λE (5.4)	λE (5.1)	λE (5.2)	λE (5.4)	λE (5.1)	λE (5.2)	λE (5.4)
11.2	0.1	1.05	1.35	0.52	-3.39	2.41	26.41	0.83	0.92	0.52	51.58	41.90	50.57
11.2	0.4	1.00	1.26	0.72	-5.29	2.47	6.11	0.80	0.92	0.71	49.50	39.58	45.82
12.0	0.5	1.00	0.96	0.85	15.23	12.12	9.31	0.86	0.83	0.76	33.52	35.01	36.63
12.0	1.0	1.00	0.99	0.88	18.23	10.85	12.67	0.88	0.85	0.81	31.92	33.68	36.21

(a)

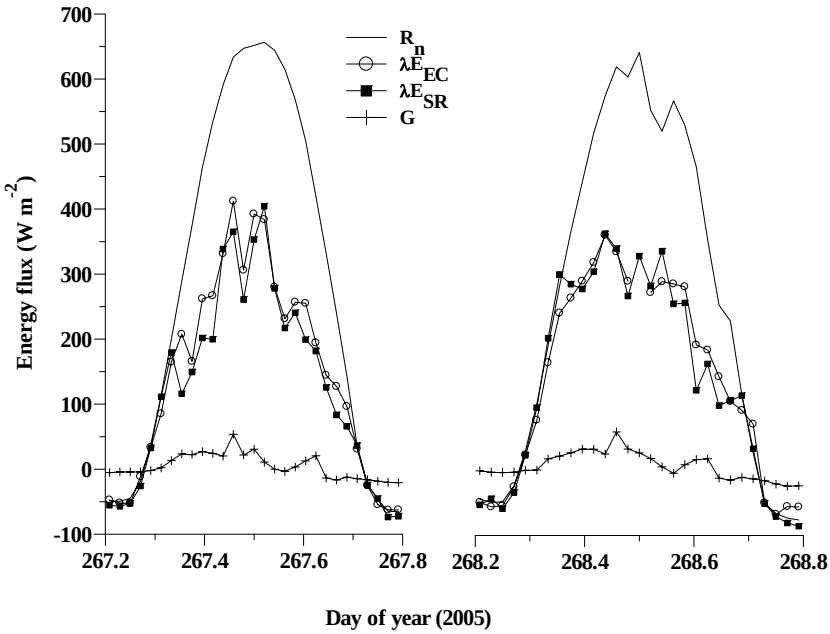

(b)

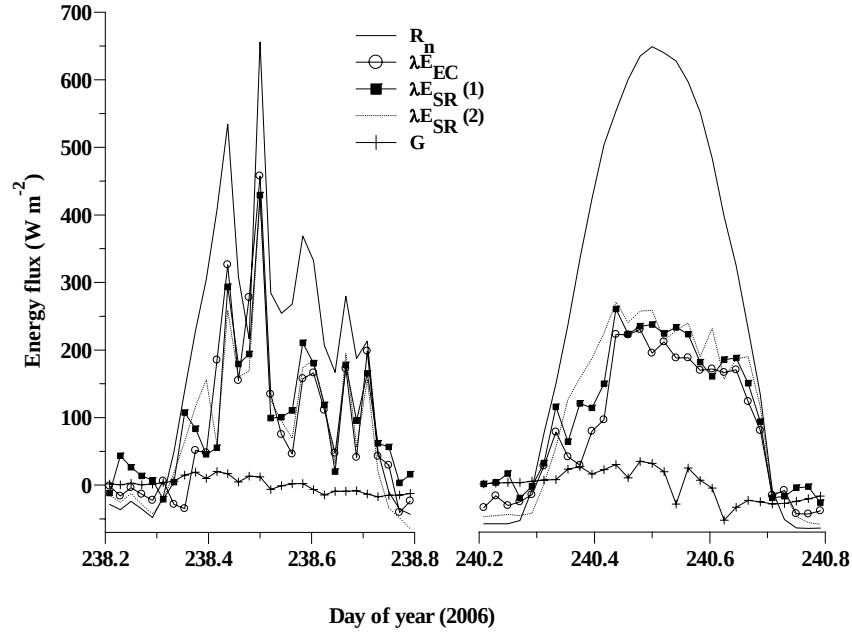

Fig. 5.4 Diurnal variations of half-hourly λE_{SR} and λE_{EC} estimates, net irradiance (R_n), and soil heat flux (G) from 06h00 to 18h00: (a) λE_{SR} at z = 11.2 m using time lag r = 0.4 s for clear and partly cloudy days (day of year 267 and 268, 2005 respectively); (b) λE_{SR} (obtained using H_{SR}, Eqs 5.1 and 5.2) at z = 12.0 m using time lag r = 1.0 s for a day with varying net irradiance and clear day (day of year 238 and 240, 2006 respectively).

The magnitude of λE_{EC} and λE_{SR} increased with the increase in net irradiance. The value of λE_{SR} varied from 30 W m^{-2} at 07h00 to 400 W m^{-2} at 12h00. The *SR* method appeared to give higher latent energy flux density in the early morning and late afternoon as shown in Fig. 5.4b. The agreement for day of year 240 (2006), almost cloudless day, is not as good compared to day of year 238 (2006). Generally, λE_{SR} and λE_{EC} showed good agreement and tracked the diurnal pattern in net irradiance.

5.5 Summary and conclusions

Three sets of experiments for estimating the sensible heat and latent energy fluxes over an Outeniqua Yellow wood stand are presented. For each experiment, three measurement heights above the canopy using eddy covariance and surface renewal methods are employed. The performance of three *SR* analysis approaches, the *SR* analysis using structure functions, the *SR* analysis using the micro-front time, and the empirical *SR* method based on similarity theory were evaluated for stable and unstable conditions using four time lags r = 0.1, 0.4, 0.5, and 1.0 s of the 10 Hz data.

Under stable conditions, the *SR* analysis using the micro-front time performed best in estimating the sensible heat flux density compared to the *SR* analysis using structure functions and the empirical *SR* method for all measurement heights and time lags. For unstable conditions, the *SR* analysis using structure functions corrected for α produced superior estimates of H_{SR} for all measurement heights and time lags. The performance of the *SR* analysis using the micro-front time was also good under unstable conditions for the measurements made in the roughness sublayer using time lags r = 0.5, and 1.0 s. Sensible heat flux estimates obtained using the empirical *SR* method produced results with greater RMSE values for measurements made in the roughness sublayer. Use of the time lag r = 1.0 s resulted in sensible heat flux density estimates that compared favourably with H_{EC} estimates than the time lags r = 0.1, 0.4, and 0.5 s. The surface renewal latent energy flux density estimates λE_{SR} using the sensible heat flux from the *SR* analysis based on structure functions gave very good estimates of λE_{EC} using all time lags compared to

the SR analysis using the micro-front time and the empirical SR method. The latent energy flux density estimates from the SR analysis using the micro-front time also gave good estimates of λE_{EC}.

The surface renewal sensible heat flux density using the SR analysis based on structure functions, performed best under unstable conditions, although it needs to be calibrated against eddy covariance sensible heat flux density estimates. The value of the weighting factor α varied from 0.58 to 0.61 in the roughness sublayer. Therefore the use of α = 0.60 can give good estimates of sensible heat and latent energy flux density using the SR analysis based on structure functions for measurements that are made in the roughness sublayer. The use of the SR analysis, based on structure functions for estimating sensible heat and latent energy flux density, hence has the advantage over the SR analysis using the micro-front time and the empirical SR method. For this method there is no requirement for additional measurements of wind speed, friction velocity and stability parameter.

Chapter 6: Long-term estimation of sensible heat and latent energy fluxes above a fetch-limited heterogeneous surface (*Jatropha curcas*) using surface renewal and eddy covariance methods

6.1 Introduction

Evaporative water loss, which is the total flux of water between the ground surface and the atmosphere, is one of the largest components of the hydrological cycle. Evaporation also appears as the latent energy flux term in the surface energy balance of different surfaces. Many atmospheric and hydrological processes are influenced by the partitioning of available energy flux into sensible heat and latent energy fluxes from a land surface (Humphreys *et al*., 2003). Recent micrometeorological studies (Anthoni *et al*., 1999; Grelle *et al*., 1999; Wilson and Baldocchi, 2000; Wever *et al*., 2002; Burba and Verma, 2005) indicate that, there is considerable seasonal and occasional interannual variability in surface energy balance components. Quantitative knowledge of long-term total evaporative loss is therefore basic to water resources management, agriculture, and atmospheric studies. As a result, there has been great interest to study the total evaporation (*ET*) for a variety of vegetative surfaces. Currently, different micrometeorological methods are used to investigate total evaporation and energy partitioning from a variety of surfaces.

In this study, the surface renewal (*SR*) and eddy covariance (*EC*) methods are used for a long-term term estimation of total evaporation above Jatropha (*Jatropha curcas*) trees. The *SR* method is a relatively low cost, attractive and simple method (Paw U *et al*., 1995; Snyder *et al*., 1996; Spano *et al*., 1997a, b, 2000; Paw U *et al*., 2005). The *SR* analysis for estimating sensible heat and latent energy flux from canopies involves high frequency air temperature measurements using fine-wire thermocouples. The *EC* method is a direct method, which for example uses high frequency measurements of air temperature, wind speed, and water vapour pressure fluctuations.

The Jatropha tree is a fast growing, drought resistant bio-fuel tree, and can be cultivated in low rainfall areas (PIER, 2007). *J. curcas* is well adapted to arid and

semi-arid conditions (ICRAF, 2003), but it also grows under sub-tropical humid climates. Although few studies suggest that *J. curcas* is unlikely to have a significant impact on water resources as it is deciduous and loses its leaves in the winter months and during periods of drought (Lele, 2007), there is currently very little information on the water use and hydrological impacts of *J. curcas*.

The main objective of this study is therefore to investigate the applicability of the SR method in estimating long-term sensible heat and latent energy fluxes over fetch-limited and heterogeneous surfaces such as, *J. curcas*. Seasonal estimates of total evaporation using the EC and SR methods are presented, spanning a period of almost two years.

6.2 Theory

6.2.1 Energy fluxes

Most of the micrometeorological methods used to estimate total evaporation are ultimately based on the energy balance equation, which accounts for all losses of heat and energy. The shortened energy balance equation is expressed as:

$$R_n = G + H + \lambda E \tag{6.1}$$

where R_n is the net irradiance, G the soil heat flux density, H the sensible heat flux density, and λE the latent energy flux density. The sensible heat flux can be estimated using different micrometeorological methods such as EC and SR methods. The latent energy flux density λE may be estimated as a residual of the shortened energy balance equation, using Eq. (6.1).

In SR analysis, it is assumed that turbulent coherent structures exchange scalars (heat and water vapour) between the surface and the atmosphere (Paw U *et al*., 2005). The full theory of the SR analysis is described in Paw U *et al*. (1995), Snyder *et al*. (1996), and Paw U *et al*. (2005). The SR analysis assumes that the sensible heat flux density H at measurement height above the soil surface z is determined as:

$$H_{SR} = \alpha z \rho c_p \frac{a}{\tau} \tag{6.2}$$

where α is a correction or weighting factor, ρ the air density, c_p the specific heat capacity of dry air at constant pressure, a the amplitude of air temperature ramps, and τ the total ramping period (inverse ramp frequency). The amplitude and inverse ramp frequency can be determined from the second, third, and fifth order of the structure function for air temperature (Van Atta, 1977). The structure function is defined as:

$$S^n(r) = \frac{1}{m-j} \sum_{i=1+j}^{m} (T_i - T_{i-j})^n \tag{6.3}$$

where n is the order of the structure function, m is the number of data points in the time interval measured at frequency f in (Hz), j is the time lag between data points corresponding to a time lag $r = j/f$, and T_i is the ith air temperature sample.

The EC method provides a direct measure of the vertical turbulent flux of a scalar entity of interest across the mean horizontal stream lines (Swinbank, 1951) providing fast response sensors (≈ 10 Hz) for the wind vector and scalar entity of interest (Meyers and Baldocchi, 2005). Friction velocity u_* is calculated as (Stull, 1983; Garratt, 1992):

$$u_* = [(\overline{u'w'})^2 + (\overline{v'w'})^2]^{1/4} \tag{6.4}$$

where u, v, and w are the three dimensional orthogonal wind speeds, and u', v', and w' are the fluctuations from the mean of u, v, and w respectively. The sensible heat flux (H_{EC}) is usually expressed as:

$$H_{EC} = \rho c_p \overline{w'T_s'} \tag{6.5}$$

where T_s' is the fluctuation from the mean sonic temperature T_s.

6.2.2 Footprint analysis

A footprint describes the relative contribution of upwind surface sources to the measured downwind turbulent fluxes. The estimation of the footprint of sensible heat and latent energy fluxes is therefore important in the field of micrometeorology, and

mainly depends on the measurement height, surface roughness, and atmospheric stability (Gash, 1986; Leclerc and Thurtell, 1990; Savage *et al*., 1997; Hsieh *et al*., 2000). The footprint function is mathematically defined by relating the measured flux $F(x, z_m - d)$ at a distance x from the source (at a measurement height z_m and for a surface with a zero displacement height d) to the spatial distribution of the surface flux (Horst and Weil, 1992):

$$F(x, z_m - d) = \int_{-\infty}^{x} S(x) f(x, z_m - d)\, dx \tag{6.6}$$

where $F(x, z_m - d)$ is the flux measured at height $z_m - d$, $S(x)$ the source strength at a distance x, f the footprint at a distance x (with distance x taken as the downwind fetch).

Hsieh *et al*. (2000) developed an analytical footprint model based on a combination of Lagrangian stochastic dispersion model results and dimensional analysis. The footprint function f for a length scale z_u in this study is defined as (Hsieh *et al*., 2000):

$$f(x, z_m - d) = \frac{1}{k^2 x^2} D z_u^P \left|L_o\right|^{1-P} \exp\left(\frac{-1}{k^2 x} D z_u^P \left|L_o\right|^{1-P}\right) \tag{6.7}$$

where k (= 0.4) is the von Karman's constant, x the downwind fetch distance, L_o the Obukhov length and D and P similarity constants, obtained by Hsieh *et al*. (2000) and expressed for different atmospheric stability conditions as:

D = 0.28 and P = 0.59, for unstable condition;

D = 0.97 and P = 1, for near neutral and neutral conditions;

D = 2.44 and P = 1.33, for stable conditions.

The length scale z_u expressed by Hsieh *et al*. (2000), and extended for a surface with a displacement height d and surface roughness length z_o (Savage *et al*., 2004), which is only valid for $z_m > d + z_o$, is defined as:

$$z_u = (z_m - d).\frac{z_m - d}{z_m - (d + z_o)}.\left[\ln\frac{z_m - d}{z_o} - 1 + \frac{z_o}{z_m - d}\right] \quad (6.8)$$

The cumulative fraction of the flux F to surface source flux S_o ratio, at distance x from the source and at an effective height of $z_m - d$ from the ground surface, can be estimated using (Hsieh *et al*., 2000):

$$\frac{F(x, z_m - d)}{S_o} = \exp\left(\frac{-1}{k^2 x} D z_u^P \left|L_o\right|^{1-P}\right) \quad (6.9)$$

and the peak location of the footprint, x_{peak} (m), can be calculated as:

$$x_{peak} = \frac{D z_u^P \left|L_o\right|^{1-P}}{2k^2} \quad (6.10)$$

The main advantage of the Hsieh *et al*. (2000) model is its ability to analytically relate atmospheric stability, measurement height, and surface roughness length to flux and footprint.

6.3 Materials and methods

Field measurements were carried out from November 2005 to July 2007 above a plot of *J. curcas* (Physic nut) trees (50 m × 60 m) as part of an agroforestry system at Ukulinga research farm (UKZN), Pietermaritzburg, South Africa (29.67^o S, 30.41^o E, altitude of 781 m). The site has a sub-tropical humid climate with summer rainfall. The Jatropha trees were planted in a 3 m × 3 m row and tree spacing. The Jatropha tree plot was surrounded by mixed Jatropha trees and Kikuyu grass (*Pennisetum clandestinum*) plots. The prevailing wind at the site was from S-E direction, and the fetch distance from the prevailing S-E winds was 40 m. A total of 392 days were used in the analysis.

Canopy height measurements were done every month. The canopy height varied from 0.8 to 2.0 m during the experimental period. Leaf area index (LAI) was measured using LAI-2000 Plant Canopy Analyzer (LI-COR, Lincoln, Nebraska,

USA). The LAI is expressed as the foliage area per unit 3 m × 3 m area. The LAI measured for winter was negligible because the Jatropha trees shed their leaves. The average LAI measured for spring (October, 2006) was 0.26 m^2 m^{-2} and for summer (December, 2006) was 0.50 m^2 m^{-2}.

Three unshielded type-E fine-wire thermocouples (75 μm diameter) were used to measure air temperature, placed at heights of 1.4, 1.8, 2.2 m above the ground surface for the *SR* method. Air temperature data were sampled at a frequency of 10 Hz and then lagged by 0.5 s and 1.0 s before forming the second, third and fifth air temperature structure function values as required by the Van Atta (1977) approach for the *SR* analysis (Eq. 6.3). Adjacent to the *SR* system, an RM Young three-dimensional ultrasonic anemometer (Model 81000, RM Young, Traverse city, Michigan, USA), was used as an *EC* system at a height of 2.2 m to measure sensible heat flux density and friction velocity (Chen *et al*, 1997b). All sensors were mounted on a lattice mast located around the middle of the plot, and were connected to a CR5000 datalogger (Campbell Scientific, Utah, USA). All eddy covariance data were also sampled at a frequency of 10 Hz and data processed online every 2 and 30-minutes in the datalogger and stored for further analysis.

For measuring the remaining components of the energy balance, a NR-Lite net radiometer (Model 240-110, Kipp & Zonen, Delft, The Netherlands) was used to measure net irradiance at 3.0 m above the soil surface. Two soil heat flux plates (model HFT-S, REBS, Seattle, USA) were used to measure soil heat flux at a depth of 80 mm and a system of parallel-thermocouples at depths of 20 and 60 mm were used to calculate the heat stored above the plates (Tanner, 1960). Volumetric soil water content in the first 60 mm of the soil surface was measured using a time domain reflectometer (CS616, Campbell Scientific). The sensors were connected to a CR23X datalogger and measurements were every 10 s and averages obtained every 10 minutes which were in turn used to calculate 30-minute averages for the latent energy flux calculations.

The gaps in the data in 2006 were mainly due to a shortage of instruments as the instruments were moved to other experimental sites, and power and other technical problems.

6.4 Results and discussion

6.4.1 Sensible heat flux density

Sensible heat flux was obtained using Eq. (6.2) for the surface renewal method and Eq. (6.5) for the eddy covariance method. The 30-minute averages of H_{SR} estimates for two time lags r = 0.5 and 1.0 s at 1.4, 1.8, and 2.2 m are calibrated against measured H_{EC} at 2.2 above the soil surface, to determine α. The weighting factor α (Table 6.1) is the slope of the linear fits through the origin of H_{EC} *vs* H_{SR} estimates. These comparisons are made to investigate the effect of measurement height, time lag, and canopy change due to tree growth on the H_{SR} estimates for unstable atmospheric conditions. As shown in Table 6.1, α varied with measurement height, time lag, and with the increase in canopy height. The time lag r = 1.0 s yielded better estimates of H_{SR} throughout the experimental period compared to r = 0.5 s. For z = 1.4 m, α was fairly stable and almost 1.0 from November 2005 to July 2006 when time lag, r = 1.0 s was used (Fig. 6.1a) but different from one for the other two measurement heights. There was a pronounced increase in the canopy height from October to December 2006, and α = 1 for z = 1.8 m (r = 1.0 s). The Jatropha trees grow fast during the summer months (December to February) with the canopy height increasing to 2.0 m. As a result, α altered with the increase in canopy height and was 1 for z = 2.2 m from December (2006) to July (2007), as shown in Fig. 6.1.

Table 6.1 The weighting factor α for unstable atmospheric conditions, using time lags r = 0.5 and 1.0 s at three measurement heights. The slope of the linear fits through the origin of H_{EC} *vs* H_{SR} estimates, is α.

Year	Day of year	Average canopy height (m)	Time lag r (s)	Average α value		
				z = 1.4 m	z = 1.8 m	z = 2.2 m
2005	321 - 365	0.8	0.5	0.97	0.86	0.84
		0.8	1.0	1.00	0.92	0.89
2006	1 - 180	1.1	0.5	0.96	0.88	0.83
		1.1	1.0	1.01	0.95	0.86
	280 - 335	1.5	0.5	1.10	0.94	0.87
		1.5	1.0	1.30	1.01	1.03
2007	1 - 200	2.0	0.5	1.20	0.96	0.90
		2.0	1.0	1.40	1.10	1.01

The H_{SR} estimates do not need calibration if α = 1. Therefore for this study the H_{SR} estimates at z = 1.4, 1.8, and 2.2 m when α = 1 were used. As shown in Fig. 6.1, very good agreement is observed between daily total H_{SR} estimates and H_{EC}.

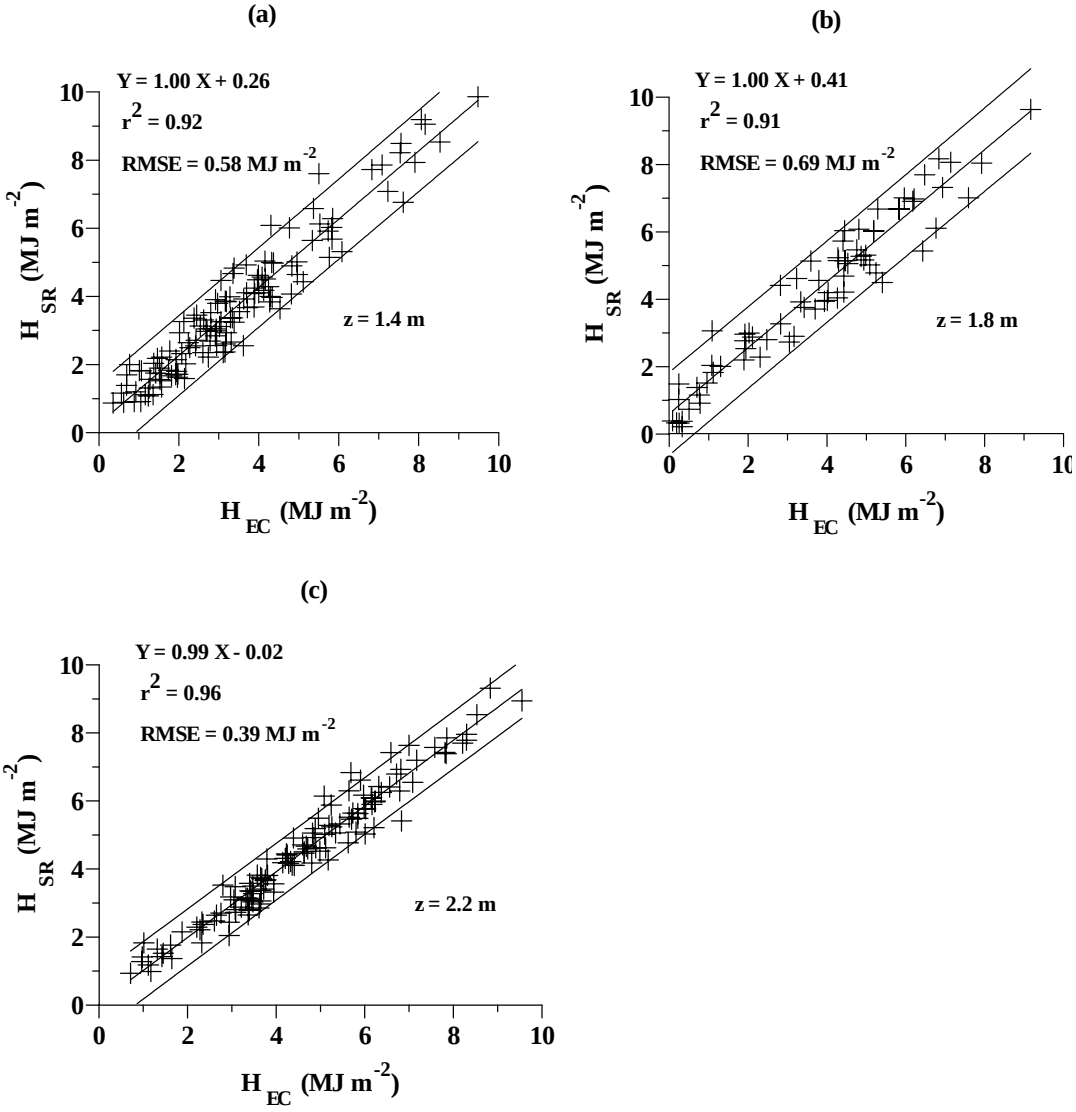

Fig. 6.1 Daily total H_{SR} (using α = 1) versus H_{EC} estimates of sensible heat flux (MJ m^{-2}) using time lag r of 1.0 s, under unstable atmospheric conditions: (a) H_{SR} at 1.4 m above the soil surface *vs* H_{EC} at 2.2 m from November 2005 to July 2006; (b) H_{SR} at 1.8 m above the soil surface *vs* H_{EC} at 2.2 m from October to December 2006; (c) H_{SR} at 2.2 m above the soil surface *vs* H_{EC} at 2.2 m from December 2006 to July 2007. The wide confidence bands represent 95 % confidence level for a single-predicted value.

Diurnal variations of the half-hourly H_{SR} estimates using time lag r = 1.0 s, H_{EC} estimates, and net irradiance are presented in Fig. 6.2 for four typical days in 2006 and two days in 2007. The sensible heat fluxes showed significant fluctuations with changes in net irradiance for the different seasons.

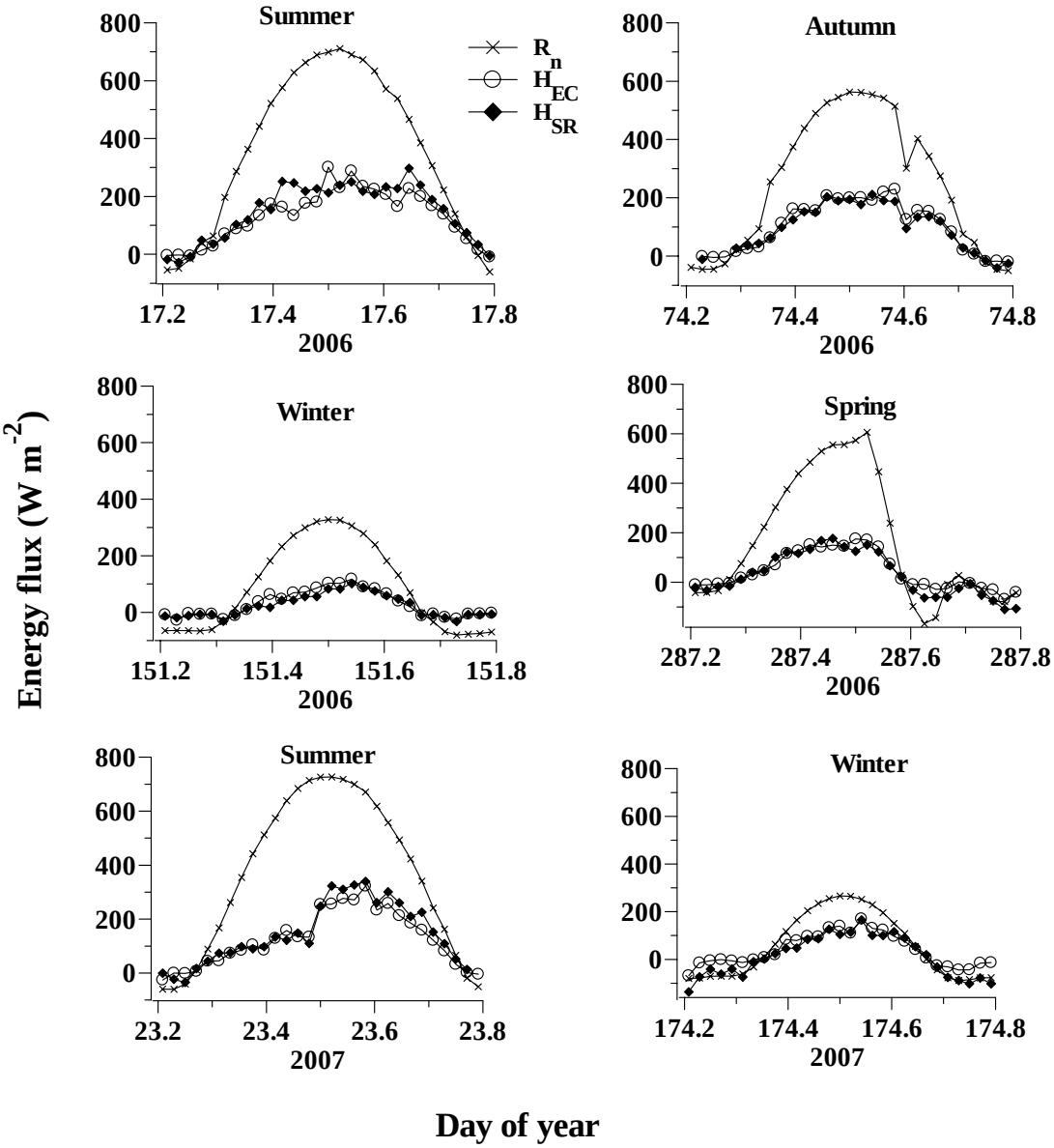

Fig. 6.2 Diurnal variations of the half-hourly H_{SR} and H_{EC} estimates and net irradiance, R_n, for different seasons in 2006 and 2007. The H_{SR} estimates were obtained using α = 1 for a time lag of 1.0 s.

In summer (mid-October to mid-February), the days are characterised by hot, sunny weather, often with afternoon thunderstorms. Sensible heat flux values ranged between -100 to 350 W m^{-2}, and net irradiance varied between -100 to 750 W m^{-2} (Fig. 6.2). In Autumn (mid-February to April), very little rain falls and it is warm but not too hot, becoming colder as the season progresses. The peak value of net irradiance decreased to 500 W m^{-2}, and the sensible heat fluxes decreased to around 200 W m^{-2}. Cold weather is experienced in winter (May to July), characterized by dry sunny days and cold nights with almost no rain. As shown in Fig. 6.2, the net irradiance was less than 300 W m^{-2}, and sensible heat flux values were less than 100 W m^{-2} for all the days in winter. Spring (August to mid-October) is characterized by warm days, becoming hotter as the season progresses. The net irradiance and sensible heat flux values increased to 600 W m^{-2} and 150 W m^{-2} respectively during the peak hours. There was no significant change in the seasonal sensible heat flux values between years 2006 and 2007.

6.4.2 Latent energy flux density

The latent energy flux density λE was estimated as a residual of the shortened energy balance equation (Eq. 6.1). The linear regression of the daily total latent energy flux density from surface renewal analysis λE_{SR} using r = 1.0 s *vs* the latent energy flux density from the eddy covariance system λE_{EC} is presented in Fig. 6.3. The λE_{SR} estimates using the SR analysis gave excellent estimates of λE_{EC}, with a slope of 1.00 and a coefficient of determination value of 0.96.

The magnitudes of the latent energy flux changed with the change in available energy flux and sensible heat flux from one season to the next. The latent energy flux values ranged between 350 and 450 W m^{-2} during the peak hours in summer. For winter, however the latent energy flux values were lower, less than 200 W m^{-2} for all the days.

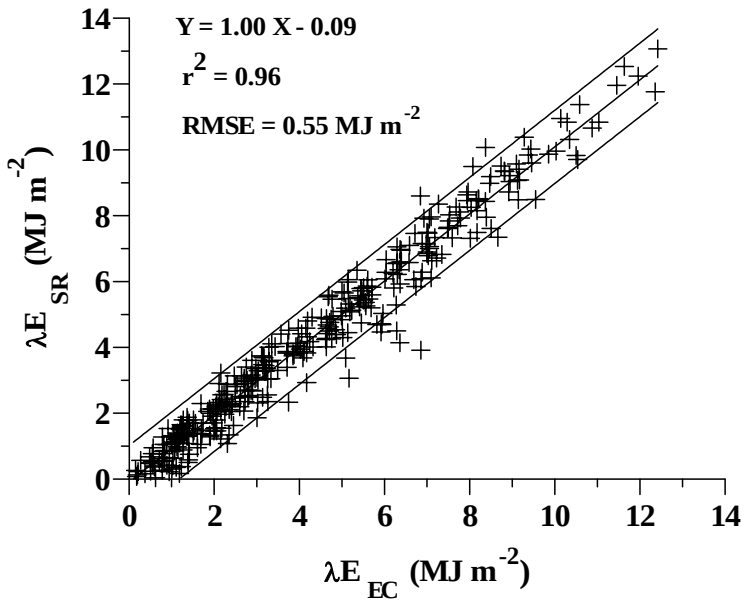

Fig. 6.3 Daily total λE_{SR} (using α = 1 and time lag r of 1.0 s) *vs* λE_{EC} estimates of latent energy flux (MJ m^{-2}), under unstable atmospheric conditions from November 2005 to July 2007.

6.4.3 Seasonal estimates of total evaporation

The daily variation in total evaporation ET estimates (mm) using the SR and EC methods, the available energy $A = R_n - G$, Bowen ratio values, rainfall, and volumetric soil water content are shown in Fig. 6.4, for day of year 321 (2005) to 365 (2006). The daily total evaporation estimates for day of year 12 to 191 (2007) are also presented in Fig. 6.5 along with the available energy flux, Bowen ratio values, rainfall, and volumetric soil water content.

Total evaporation estimates followed the trend of fluctuation of the available energy as shown in Figs 6.4 and 6.5. The available energy and ET estimates varied with time throughout the day and from day to day. Total evaporation and the available energy were low in the early morning and late afternoon for most of the days and peaked between 10h00 and 14h00. Total evaporation estimates increased with solar irradiance, especially during 10h00 and 14h00 periods.

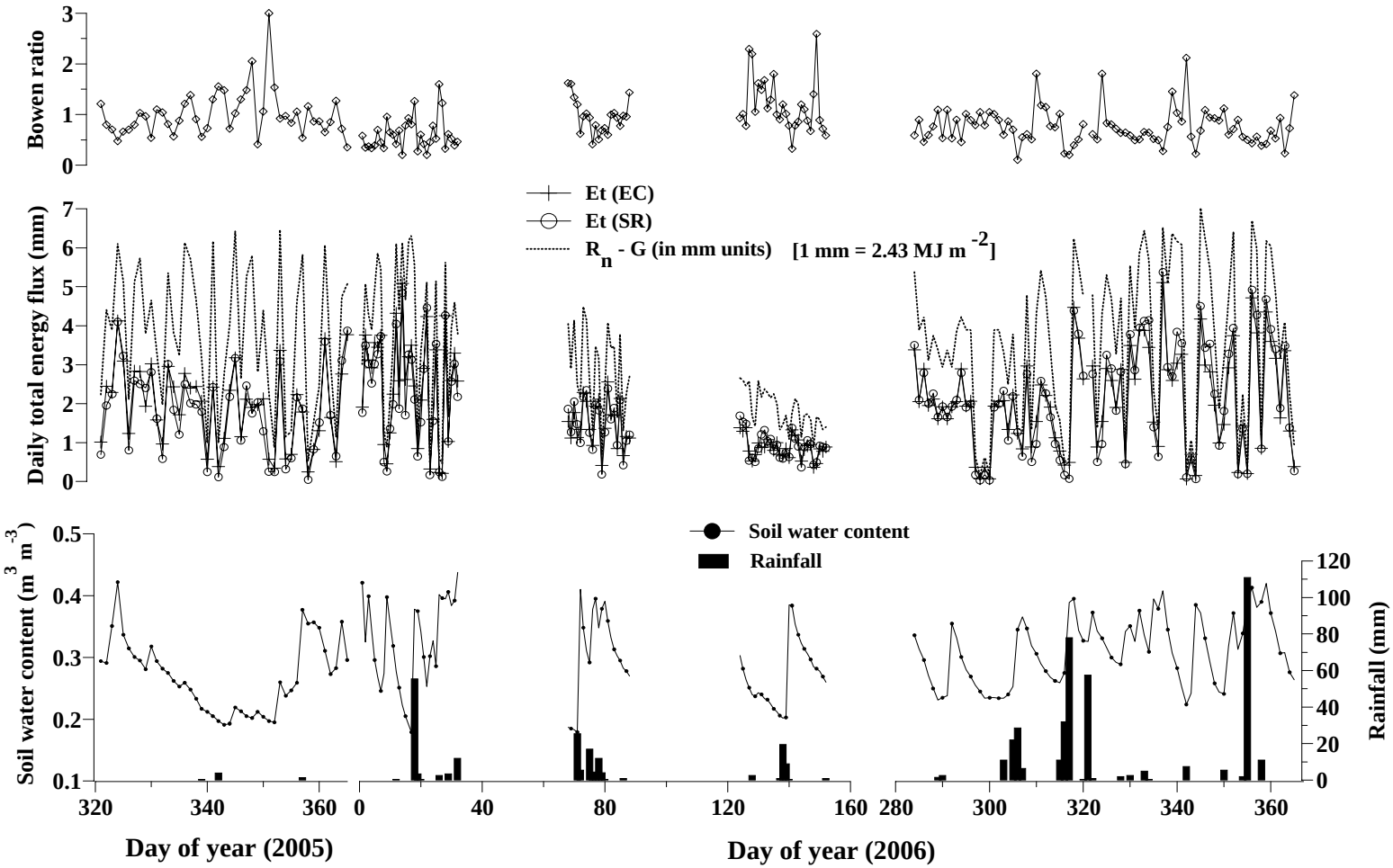

Fig. 6.4 Daily variation in ET estimates (mm) using the SR and EC methods, the available energy $A = R_n - G$ (mm), rainfall (mm), and volumetric soil water content ($m^3\ m^{-3}$) for day of year 321 (2005) to 365 (2006).

Most of the incoming energy was consumed in latent energy flux λE in summer (Figs 6.4 and 6.5), with daily average total ET estimates of 2.5 mm in December 2005. The daily average totals increased to 3.2 mm during December 2006 to February 2007, with the increase in canopy height and leaf area index. The maximum daily ET estimates exceeded 5 mm for few days in summer (Fig. 6.4), which is equivalent to a latent energy flux magnitude of 12.2 MJ m^{-2}. The Bowen ratio value, which is the ratio of the sensible heat to the latent energy flux, was mostly less than 1 in summer (Figs 6.4 and 6.5) due to the wet weather. In autumn, with the decrease in the available energy flux, the daily total ET estimates decreased to values less than 2.5 mm.

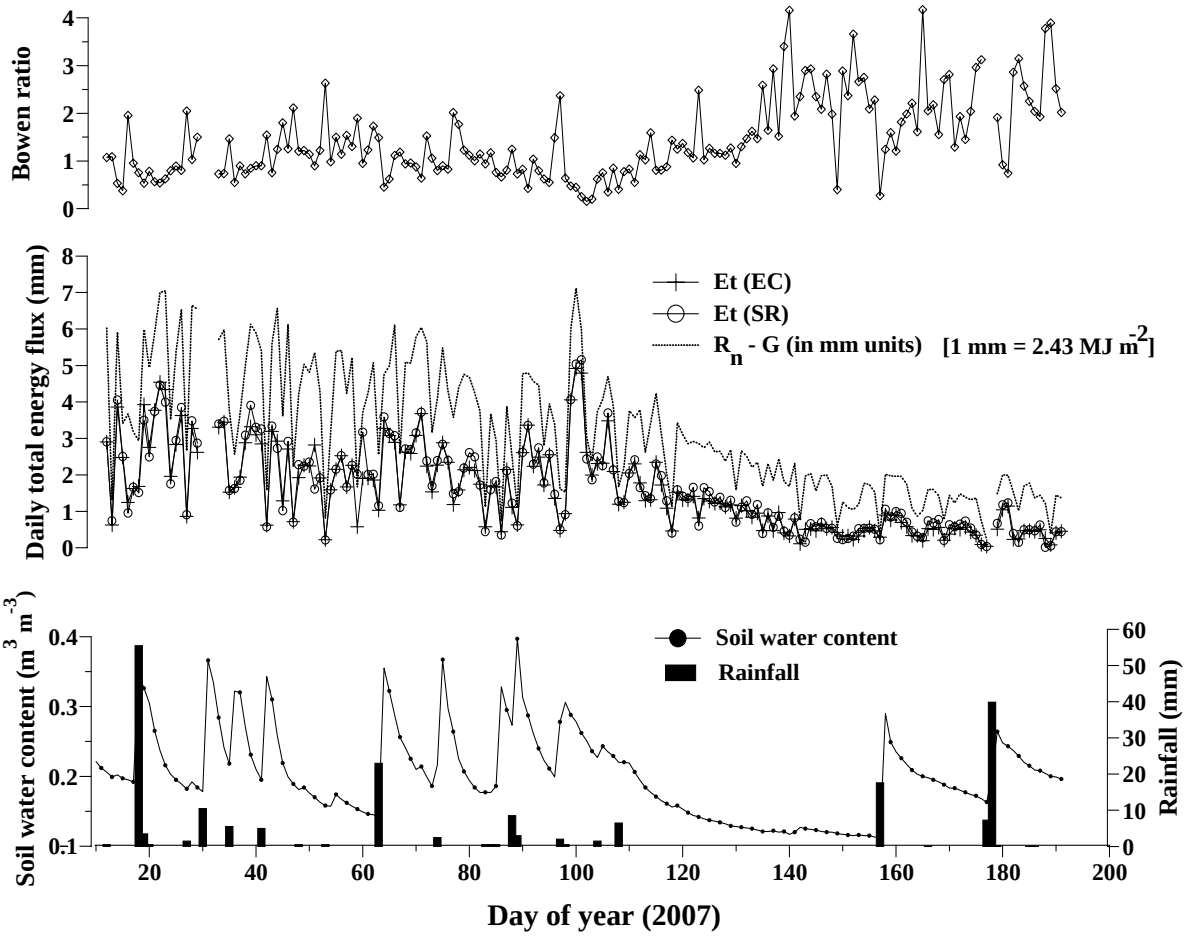

Fig. 6.5 Daily variation in ET estimates (mm) using the SR and EC methods, the available energy flux $A = R_n - G$ (mm), rainfall (mm), and volumetric soil water content (m^3 m^{-3}) for day of year 12 to 191 (2007).

The available energy flux and the daily ET estimates decreased in winter (May to July). The daily average total ET estimates were less than 1 mm. The Bowen ratio values were greater than 1.0 (Fig. 6.5) for all the days in winter, except for few days after rain events. The Jatropha trees shed their leaves in winter (LAI = 0). Therefore the ET estimates were mostly from the soil surface (soil evaporation).

The seasonal fluctuations in sensible heat, latent energy, and available energy fluxes were mainly due to the increases and decreases in the net irradiance and the soil heat flux. These variations were more prominent in summer (Figs 6.4 and 6.5), however these increases and decreases in the fluxes are less pronounced but still occur in the drier periods (winter) as shown in Fig. 6.6. The net irradiance was largest in summer and lowest in winter but varied also from day to day due to the effect of clouds on the incoming solar irradiance. The soil heat flux density has the smallest magnitude of all the energy balance components, and was also greatest in magnitude in summer (Fig. 6.6). The partitioning of the net irradiance into sensible heat and latent energy fluxes is dependent also on a range of other factors such as, the soil water content, atmospheric humidity, air temperature, wind speed, and the surface cover.

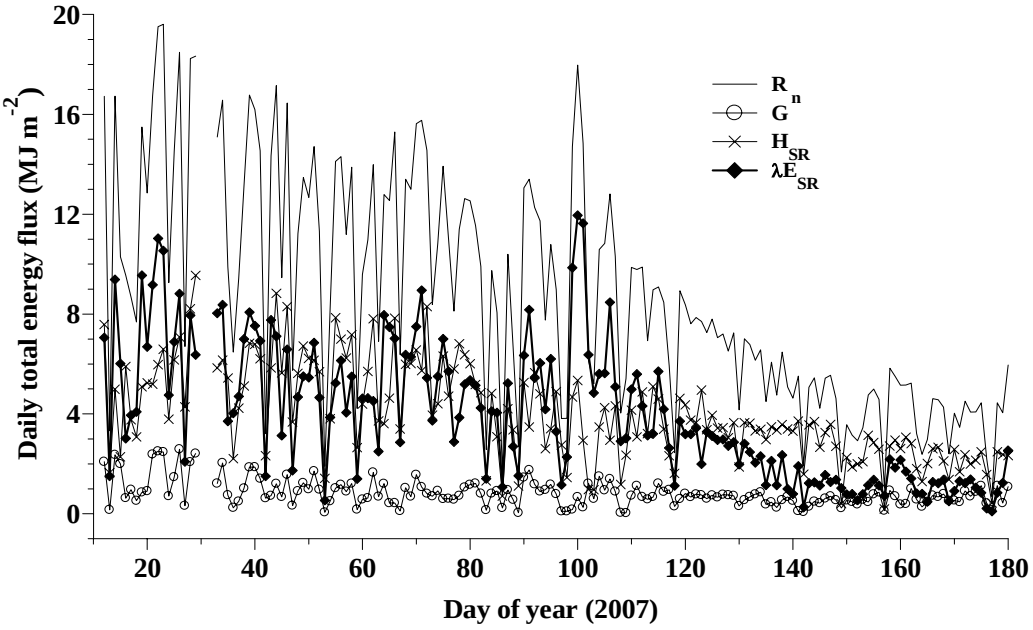

Fig. 6.6 Daily total fluxes of net irradiance R_n, soil heat flux G, sensible heat H_{SR}, and latent energy λE_{SR} for day of year 10 to 180 (2007).

6.4.4 Footprint of measurements

A footprint analysis was undertaken to observe the relative contribution of upwind surface sources to the measured downwind sensible heat and latent energy fluxes, because measurements were made in a plot with limited fetch. The footprint model developed by Hsieh *et al*. (2000), corrected and modified for a surface with a displacement height d and surface roughness length z_o (Savage *et al*., 2004) was used to estimate relative contributions from areas at various upwind distances x. The footprint calculations included footprint function f (Eq. 6.7), the cumulative fraction of the flux F to surface source flux S_o ratio (Eq. 6.9), and the peak location of the footprint x_{peak} (Eq. 6.10).

The footprint magnitude and the peak location of the footprint calculated using Obukhov length L_o values from the EC system at 2.20 m for unstable atmospheric conditions are shown in Fig. 6.7 for day of year 256 (L_o = -6.91) and 300 (L_o = -4.87), 2006 and day of year 120 (L_o = -9.64) and 180 (L_o = -1.95), 2007. These footprint plots show that the peak location of the footprint x_{peak} varied from day to day depending on the atmospheric stability. The cumulative fraction of the measured flux F to surface source flux S_o ratio (Eq. 6.9), and the peak location of the footprint are presented in Fig. 6.8 for the same four days used in Fig. 6.7 for unstable conditions. The ratio of the measured flux F to surface source flux S_o is greater than 90 % for day of year 256 (2006), 120 and 180 (2007) for a fetch distance x of 40 m for the site. As shown in Fig. 6.8, for day of year 300 (2006) the ratio is 85 %. Based on this analysis, more than 90 % of the measured flux was coming from the upwind fetch distance of 40 m. These footprint plots are calculated for unstable conditions during the peak hours of the measured fluxes. Therefore, the trend of the peak location of the footprint and the cumulative fraction of the measured flux F to surface source flux S_o ratio could be different for neutral and stable conditions. The footprint analysis presented in Figs 6.7 and 6.8 were made for unstable conditions using L_o values at 12h00. However, atmospheric stability may vary within a day from time to time, from unstable to near neutral and to stable conditions.

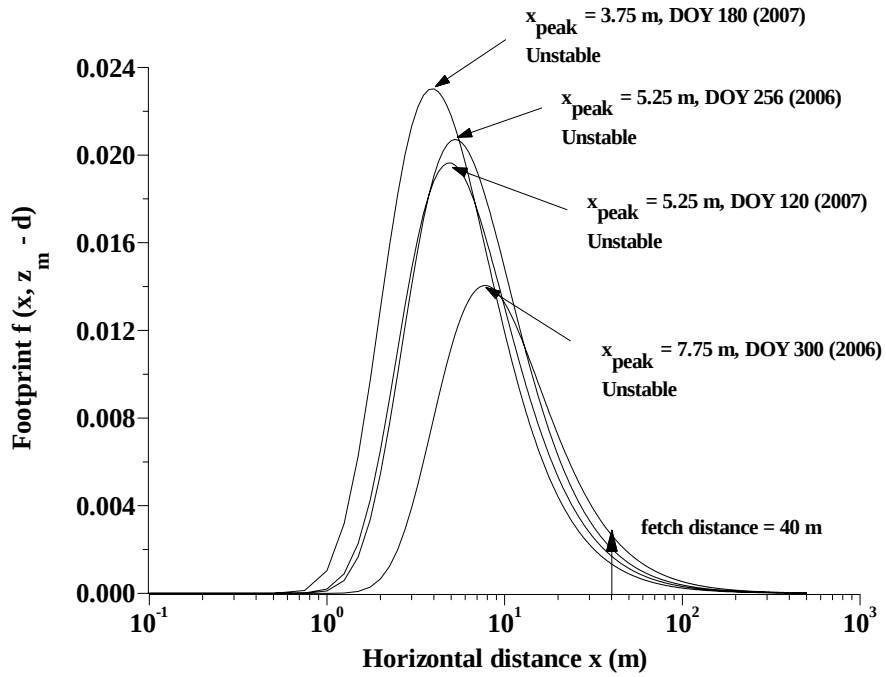

Fig. 6.7 The estimated footprint and the peak location of the footprint at midday for four selected days in 2006 and 2007, based on the *EC* measurements at 2.20 m from the ground surface and horizontal distance x (m) from the measurement position.

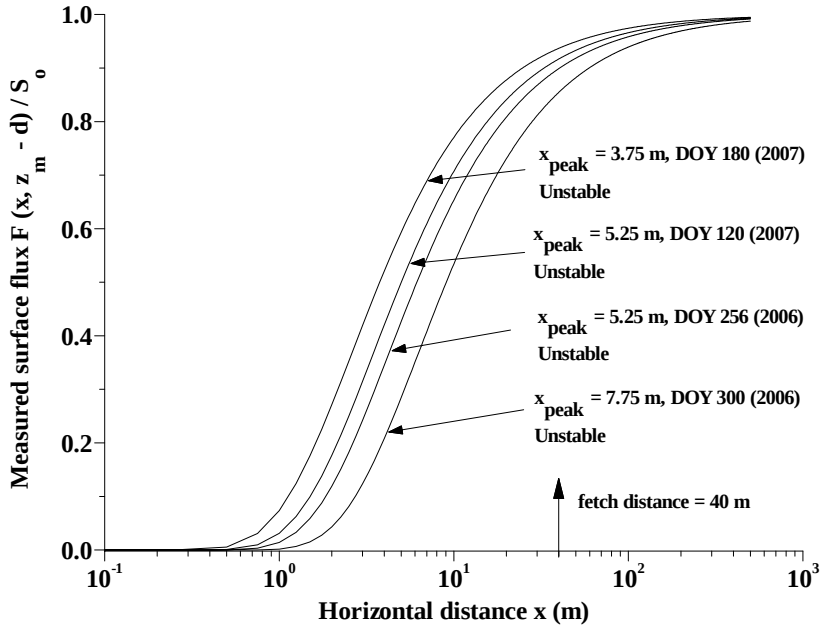

Fig. 6.8 The cumulative fraction of the measured flux F to surface source flux S_o ratio and the peak location of the footprint at midday for four selected days in 2006 and 2007.

Since the measured sensible heat and latent energy fluxes are based on the partitioning of the net irradiance, the weighted footprints as a function of the net irradiance, wind speed U (m s^{-1}), and L_o from 08h00 to 16h00 are presented in Tables 6.2 and 6.3 for a cloudy and a clear day. The cumulative fraction of the measured flux F to surface source flux S_o ratio weighted as a function of the net irradiance was 0.81 (Table 6.2) for a cloudy day (day of year 54, 2007) and 0.90 (Table 6.3), for a clear day, day of year 60 (2007). This footprint analysis shows that 81 % of the measured flux was coming from the upwind fetch distance of 40 m for a cloudy day, and 90 % for a clear day.

Table 6.2 The fraction of the measured cumulative flux F to surface source flux S_o ratio weighted as a function of the net irradiance R_n, wind speed U (m s^{-1}), and L_o, for a cloudy day (day of year 54, 2007).

Time	U (m s^{-1})	L_o	F / S_o	R_n (W m^{-2})	[(F / S_o) R_n] (W m^{-2})
800	0.76	-17.57	0.854	22.7	19.4
900	0.83	-79.13	0.734	112.5	82.6
1000	0.97	-23.87	0.833	137.0	114.2
1100	1.21	-38.48	0.798	167.7	133.8
1200	1.69	-31.56	0.844	453.7	382.7
1300	2.07	-46.29	0.817	393.7	321.7
1400	1.96	-54.84	0.783	384.8	301.2
1500	2.54	-67.43	0.803	369.2	296.4
1600	2.48	-116.86	0.804	274.6	220.9
			0.81		

Table 6.3 The fraction of the measured cumulative flux F to surface source flux S_o ratio weighted as a function of the net irradiance R_n, wind speed U (m s^{-1}), and L_o for a clear day (day of year 60, 2007).

Time	U (m s^{-1})	L_o	F / S_o	R_n (W m^{-2})	[(F / S_o) R_n] (W m^{-2})
800	0.67	-0.90	0.968	129.7	125.5
900	0.91	-0.59	0.984	303.6	298.8
1000	0.94	-0.66	0.973	452.1	439.7
1100	1.33	-6.49	0.935	562.3	525.7
1200	1.75	-11.61	0.914	619.7	566.7
1300	2.03	-24.09	0.877	625.9	549.1
1400	2.41	-42.36	0.831	583.8	485.4
1500	2.82	-69.06	0.811	487.2	395.1
1600	2.86	-80.08	0.782	348.8	272.6
			0.90		

The high ratio of the measured flux F to surface source flux S_o values - generally close to 80 % for this fetch-limited site, using the Hsieh *et al*. (2000) footprint model, is surprising. A recommendation for future research is that the footprint calculations should be confirmed using other footprint models for this site.

6.5 Summary and conclusions

The surface renewal SR and eddy covariance EC methods were used to estimate long-term term sensible heat and latent energy flux (total evaporation) above heterogeneous surface, *J. curcas* (Physic nut) at Ukulinga research farm, Pietermaritzburg, South Africa. Seasonal estimates of total evaporation using the EC and SR methods were investigated, spanning a period of almost two years.

This study demonstrates that it is possible to estimate long-term sensible heat and latent energy fluxes using the SR and EC methods over heterogeneous canopies. The SR method needs to be calibrated using a standard method such as the EC method, to account for the weighting factor α which changes with measurement height, canopy height and structure, the time lag used, and depends on thermocouple size. Continuous measurements of canopy height and leaf area index measurements are needed, especially for long-term studies over fast growing trees to determine α. For this study, the sensible heat flux from the SR method was estimated using two time lags r = 0.5 and 1.0 s at sensor placement height of 1.4, 1.8, and 2.2 m. The time lag r = 1.0 s provided better estimates of H_{SR} compared to r = 0.5 s. The weighting factor, α was approximately 1 for sensor placement heights between 0.2 and 0.6 m above the Jatropha tree canopy. The daily sensible heat and latent energy flux estimates using the SR analysis (using time lag r = 1.0 s) gave excellent estimates of daily EC sensible heat and latent energy fluxes, with slopes of 1.00 and coefficient of determination values greater than 0.90.

Total evaporation ET estimates tracked the trend of fluctuation of the available energy flux. The available energy flux and ET varied with time throughout the day and from day to day. Total evaporation estimates peaked in summer (with an average daily amount of greater than 3 mm). In summer, ET estimates were mainly

dictated by the available energy flux, often varying from one day to the next due to the influence of clouds. In winter, the daily ET estimates from the Jatropha trees were very low, with an average daily amount of less than 1 mm.

A footprint analysis was done to investigate the relative contribution of upwind surface sources to the measured downwind sensible heat and latent energy fluxes, as the measurements were made in a plot with limited fetch. The estimated footprint, peak location of the footprint, and the cumulative fraction of the measured flux to surface source flux ratio were calculated. The footprint analysis for unstable conditions during the peak hours of the measured fluxes showed that more than 90 % of the measured flux was coming from the upwind fetch distance of 40 m. However, atmospheric stability varies from time to time within a day; therefore a footprint analysis was also done from 08h00 to 16h00 for a clear and a cloudy day. The results showed that 81 % of the measured flux was coming from the upwind fetch distance of 40 m for a cloudy day, and 90 % for a clear day.

Ideally, for this site, given the measurement heights and the limited fetch, it would have been advantageous to perform the measurements at 20 Hz and not at the 10 Hz frequency used. However, given that only a single CR5000 datalogger was available to accommodate the number of *SR* thermocouples at the various heights and the 3D sonic anemometer, this was not possible.

Chapter 7: Open water evaporation for a small shallow dam in winter using surface renewal and eddy covariance methods

7.1 Introduction

Evaporation from open water surfaces and from land surfaces covered with vegetation is one of the main components of the hydrologic cycle. Estimates of the amount and rate of evaporation from open water surfaces are required in water resources management for a variety of purposes, such as the design of storage reservoirs, catchment water balance studies, municipal and industrial water supply, irrigation of agricultural lands, and management of wet lands (Brutsaert, 1982; Marsh and Bigras, 1988; Finch, 2001). However, studies of open water evaporation from fresh water systems were biased towards reservoir and larger lakes and relatively few investigations have been conducted for dams and ponds (Rosenberry *et al*., 2007).

Different methods have been used in the past to estimate open water evaporation, such as the water balance method, mass transport approach, potential evaporation approach (Penman, 1948), floating pans, FAO-56 reference Penman-Monteith method, Priestley-Taylor method, models based on meteorological data, Bowen ratio energy budget (*BREB*) method, and eddy covariance (*EC*) method (Rosenberg *et al*., 1983). A model based on the concept of an equilibrium temperature for the determination energy budget for a well-mixed body of water, which takes into account the heat stored in the water body was introduced by Edinger *et al*. (1968) and further developed by Keijman (1974) and de Bruin (1982). Rosenberry *et al*. (2007) have compared the *BREB* method with 14 different evaporation methods for a small mountain lake. Craig (2006) used the Penman-Monteith method and accurate water depth measurements made using a pressure sensitive transducer to estimate evaporation and seepage losses of agricultural water storages. Comparisons of short-term measurements of shallow lake evaporation using the *EC* and energy budget methods are presented by Stannard and Rosenberry (1991) and Assouline and Mahrer (1993). The accuracy and reliability of different methods for estimating open water evaporation is discussed in detail by Craig and Hancock (2004).

Surface renewal (*SR*) analysis is a relatively low cost, and simple method for estimating sensible heat, latent energy flux, and other scalars (Paw U *et al*., 1995; Snyder *et al*., 1996; Spano *et al*., 1997a, b, 2000; Paw U *et al*., 2005; Castellvi *et al*., 2006). The *SR* method has the advantage over other micrometeorological methods since it requires only measurement of the scalar of interest at one point. The *SR* analysis for estimating sensible heat flux from canopies involves high frequency air temperature measurements (typically 2 to 10 Hz) using fine-wire thermocouples. The *SR* method has been used for estimating sensible heat and latent energy flux above different surfaces such as bare soil, short canopies and tall vegetation. Zapata and Martinez-Cob (2001) have used the *SR* method to measure latent energy flux from an endorreic salty lagoon, an aquatic environment characterized by short, sparse vegetation with high proportions of bare soil. However, we are unaware of previously reported studies in the scientific literature for estimating open water evaporation using the *SR* method.

This study presents the use of the *SR* method for estimating sensible heat flux and open water evaporation from a shallow reservoir. The *SR* method has not been tested over open water surfaces. The aim of this study is therefore to calibrate the sensible heat flux obtained with the *SR* method against measurements obtained using the *EC* method and to evaluate the performance of the *SR* method for estimating sensible heat and latent energy fluxes above open water surface.

7.2 Theory

In *SR* analysis, it is assumed that turbulent coherent structures exchange scalars (air temperature and water vapour pressure) between the surface and the atmosphere (Paw U *et al*., 1995; Snyder *et al*., 1996; Paw U *et al*., 2005; Castellvi *et al*., 2006). High frequency air temperature fluctuations exhibit organized coherent structures as shown in Fig. 7.1 which look like ramp events (Bergström and Högström, 1989; Gao *et al*., 1989; Shaw *et al*., 1989). The *SR* analysis assumes that the sensible heat flux density H at measurement height z is determined as:

$$H_{SR} = \alpha z \rho c_p \frac{a}{\tau} \tag{7.1}$$

where α is a correction or weighting factor, ρ the air density, c_p the specific heat capacity of dry air at constant pressure, a the amplitude, and τ the total ramping period (inverse ramp frequency) of air temperature ramps. The amplitude and inverse ramp frequency can be determined from the second, third, and fifth order of the structure function for air temperature (Van Atta, 1977). The structure function is defined as: $S^n(r) = \frac{1}{m-j} \sum_{i=1+j}^{m} (T_i - T_{i-j})^n$, where m is the number of data points in the time interval measured at frequency (f) in Hz, n is the order of the structure function, j is the time lag between data points corresponding to a time lag $r = j/f$ and T_i is the ith temperature sample.

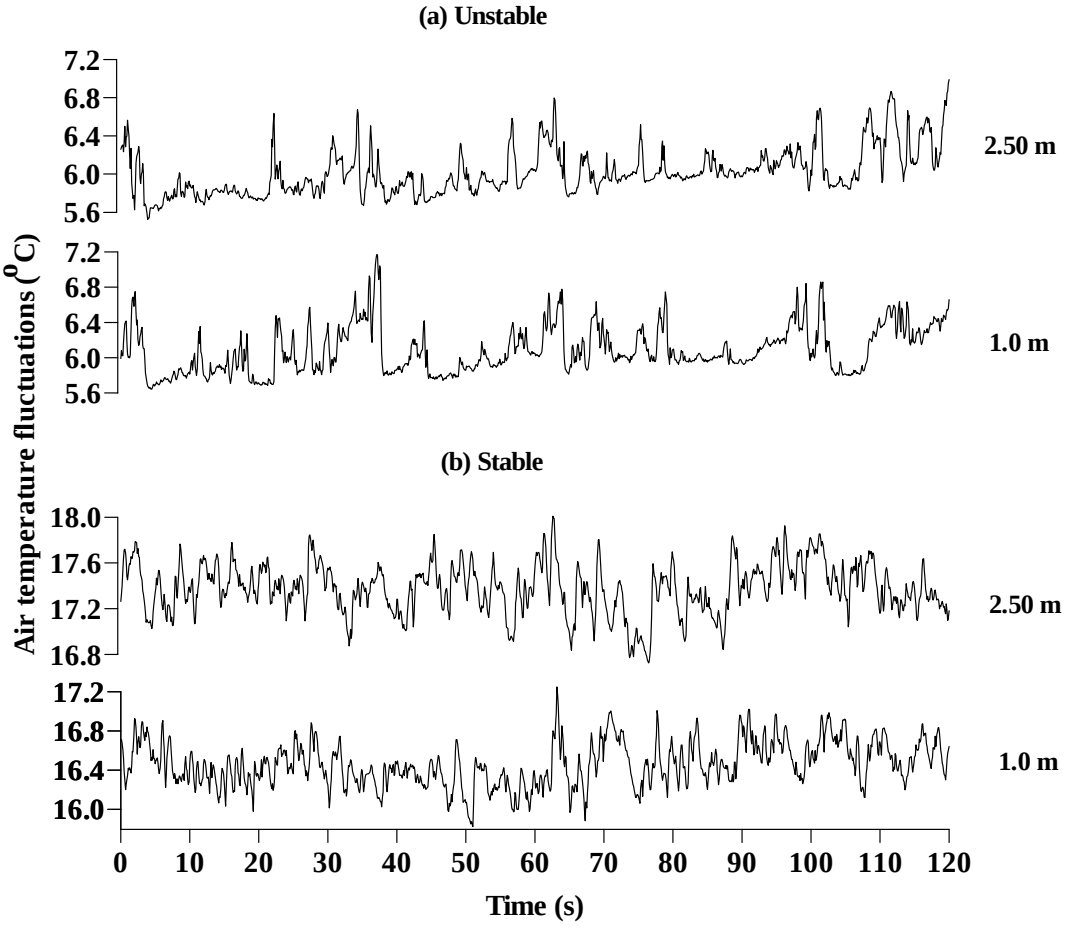

Fig. 7.1 Air temperature ramps observed in a sample of 120 s of 10 Hz air temperature traces. The measurements were taken at 1.0 and 2.50 m above open water surface in Midmar dam, South Africa for day of year 194 (2007): (a) for unstable conditions (08h00); (b) for stable conditions (16h00).

Chen *et al*. (1997a, b) developed a *SR* analysis model based on finite micro-front time during the formation of air temperature ramps, that estimates H from fluctuations of high frequency air temperature measurements using a cubic temperature structure function, and an additional measurement of friction velocity. According to the model, H is estimated in the inertial sublayer as:

$$H_{SR} = -\alpha\beta^{2/3}\gamma\rho c_p \left[\frac{S^3_{(r_m)}}{r_m}\right]^{1/3} u_*^{2/3} \frac{z}{(z-d)^{2/3}}, \tag{7.2}$$

where $\alpha\beta^{2/3}\gamma$ is an empirical combined coefficient (a roughly constant value of 0.4 for bare soil, mulch, and forest), $S^3_{(r_m)}$ is the third order of the structure function for air temperature, r_m is the time lag that maximizes $(S^3_{(r)}/r)^{1/3}$, u_* the friction velocity, and d is the zero-plane displacement height. The zero-plane displacement height is approximately $2/3$ of the canopy height (h). For this study (water), h is zero and consequently d is assumed to be zero. Chen *et al*. (1997b) have obtained values for the coefficients α, β, and γ for bare soil, straw mulch, and forest. The values for the coefficients β and γ obtained by Chen *et al*. (1997b) for bare soil are used for this study over water, since the canopy height h and d are zero in both cases.

The variable αz in Eq. (7.1) is the volume of air per unit ground area exchanged on average for each ramp in the sample period for a height z (Paw U *et al*., 1995). Castellvi *et al*. (2002) interpreted αz as the mean eddy size responsible for the renewal process. Castellvi (2004), based on a one-dimensional diffusion equation, derived the following relationship for estimating the parameter α when measuring well above the canopy in the inertial sublayer:

$$\alpha = \left[\frac{k}{\pi}\frac{(z-d)}{z^2}\frac{\tau u_*}{\phi_h(\zeta)}\right]^{1/2}, \qquad (z-d) > z^* \tag{7.3}$$

where k is von Karman constant ($k \approx 0.35$), ζ a stability parameter defined as $(z-d)/L_o$, with L_o the Obukhov length, and $\phi_h(\zeta)$ the stability function for sensible

heat transfer valid for the inertial sublayer, and z^* the roughness sublayer depth, which is assumed to be zero for this study since the canopy height is zero.

Castellvi (2004), by combining Eqs (7.1), (7.3), and the Obukhov length (L_o), proposed the following empirical expression for estimating sensible heat flux density in the inertial sublayer:

$$H_{SR} = \rho c_p \left(\frac{g}{T}\right)^{1/5} \frac{[k(z-d)]^{4/5}}{\pi^{3/5}} \left[-\gamma^3 \frac{S^3_{(r_m)}}{r_m}\right]^{3/5} \frac{1}{a^{3/5}} \left[\frac{1}{-\zeta \phi^3_h(\zeta)}\right]^{1/5} \tag{7.4}$$

where g is the acceleration due to gravity, T the mean absolute air temperature, $S^3_{(r_m)}$ the third order of the structure function for air temperature, r_m the time lag that maximizes $(S^3_{(r)}/r)^{1/3}$, and γ is empirical parameter which varies by less than 25 % from unity for different surfaces (Chen *et al*., 1997b). For a variety of short canopies, Castellvi (2004) found very good estimates of sensible heat flux density at different heights above the canopy, using $\gamma = 1.1$ in Eq. (7.4) compared to eddy covariance measurements.

The simplified energy balance equation may be used to estimate the latent energy flux λE using the surface renewal and eddy covariance methods from measured net irradiance R_n, the sensible heat flux density H, and the heat stored in water G as:

$$\lambda E = R_n - H - G \tag{7.5}$$

The heat stored in water G can be determined from measurements of profile water temperature (Brutsaert, 1982) as:

$$G = \rho_w c_w \Delta z \frac{\overline{\Delta T_w}}{\Delta t} \tag{7.6}$$

where ρ_w is the density of water, c_w the specific heat capacity of water, Δz the depth of water, $\overline{\Delta T_w}$ the average water temperature difference from one time period to another, and Δt the change in time.

7.3 Materials and methods

Field work was carried out at Midmar Dam, near Howick, in the midlands of KwaZulu-Natal, South Africa (29 ^{o}30' S, 30 ^{o}10' E, altitude 985 m) from day of year 186 to 201 (5 to 20 July, 2007). The reservoir is a relatively small dam, with a reservoir surface area of 1793.15 ha and net capacity of 235.42 million m^3 (DWAF, 2007). The site has a summer rainy season and is characterized by warm and wet days with air temperatures exceeding 30 ^{o}C in summer. In winter, the days are dry and frequently cold with temperatures less than 20 ^{o}C and decreasing to less than 0 ^{o}C during the night. The mean annual rainfall is 992 mm (popular literature), with November, December and January being the wettest months. Prevailing winds are from the southeast, east and south corresponding to water to land wind flows.

For the surface renewal (*SR*), four unshielded type-E fine-wire thermocouples (75-μm diameter) were used to measure air temperature, placed at heights of 1.0, 1.3, 1.9, and 2.5 m above the reservoir water surface. Thermocouple measurements were made differentially and temperature data were sampled at a frequency of 10 Hz. Time lags of 0.40 s and 0.80 s were used for the *SR* analysis before forming the second, third and fifth air temperature structure function values as required by the Van Atta (1977) approach. The data were then averaged and stored every two minutes in the datalogger. Structure functions using the time lags and the analysis technique from Van Atta (1977) were used to determine the amplitude (a) and the inverse ramp frequency τ characterizing temperature fluctuations as presented by Snyder *et al*. (1996) in Eq. (7.1). The coefficients β (Eq. 7.2) and γ (Eqs 7.2 and 7.4) were set to 0.398 and 1.104 respectively, values obtained by Chen *et al*. (1997b) for their experiment over bare soil. The value of $S^3_{(r)}/r$ in Eqs (7.2) and (7.4) was determined from the high frequency air temperature data in the CR3000 datalogger (Campbell Scientific, Utah, USA). The parameter α in Eqs (7.1) and (7.2) for each height was

obtained from the slope of linear regression forced through the origin of measured H using the eddy covariance versus the right-hand side of Eqs (7.1) and (7.2) using α = 1 for all half-hourly measurement periods.

An RM Young three-dimensional ultrasonic anemometer (Model 81000, RM Young, Traverse city, Michigan, USA), was installed to measure sensible heat flux density and friction velocity at 2.50 m above the water surface. All sensors were mounted on a scaffold which was installed inside the reservoir, 75 m from the shore line, and were connected to a CR3000 datalogger. All eddy covariance data were also sampled at a frequency of 10 Hz and data were processed online in the datalogger and stored for further analysis. Friction velocity u_* was calculated as: $[(\overline{u'w'})^2 + (\overline{v'w'})^2]^{1/4}$ (Stull, 1983; Garratt, 1992), where u, v, and w are the three dimensional orthogonal wind speeds, and u', v', and w' are the fluctuations from the mean of u, v, and w respectively. Eddy covariance sensible heat flux H_{EC} was estimated as: $H_{EC} = \rho c_p \overline{w'T_s'}$, where T_s' is the fluctuation from the mean sonic temperature.

Net irradiance was measured using a NR-Lite net radiometer (Model 240-110, Kipp & Zonen, Delft, The Netherlands) at 2.40 m above the water surface. Water temperature T_w was measured using seven type-E thermocouples attached to a hollow aluminium pole at different depths with the one end attached to a polystyrene float to measure the surface temperature of the water. A sink load was connected to the other end of the bar to ensure a vertical position of the bar.

The sensors were all connected to a CR23X datalogger and measurements were every 1.0 s and averages obtained every 2 minutes which were in turn used to calculate 30-minute averages for the latent energy flux calculations. The water temperature measurement depth was adjusted with the decrease in reservoir water depth due to evaporation and stream flow reduction. At the beginning of the experiment, the reservoir water depth was 0.75 m and the T_w measurement depths were 0.0 (surface of the water), 20, 40, 80, 160, 320, and 640 mm from the surface. The water depth decreased to 0.54 m on day of year 192 (2007) and the T_w

measurement depths were adjusted to 0.0, 20, 40, 80, 160, 260, 520 mm. Towards the end of the experiment, on day of year 199 (2007) the water depth had decreased by 0.14 m, and T_w measurements were taken at 0.0, 20, 40, 80, 140, 240, 380 mm from the water surface.

7.4 Results and discussion

7.4.1 Sensible heat flux density

The half-hourly H_{EC} values were plotted against *SR* sensible heat flux estimates H_{SR} computed using Eq. (7.1) for time lags r = 0.4 and 0.8 s, at four measurement heights: z_1 = 1.0 m, z_2 = 1.30 m, and z_3 = 1.90 m, z_4 = 2.50 m above the water surface to determine the weighting or calibration factor α by forcing the linear regression through the origin (Table 7.1).

The combined empirical coefficient $\alpha\beta^{2/3}\gamma$ (Eq. 7.2), a roughly constant value of 0.4 (for bare soil, mulch, and forest) resulted in H_{SR} being overestimated compared to the measured H_{EC}. The value 0.4 for the combined coefficient does not hold true for open water surface. Therefore, the parameter α in Eq. (7.2) for each height and time lag was determined from the slope of linear regression forced through the origin of measured H_{EC} values versus the right-hand side of H_{SR} (Eq. 7.2) using β = 0.398 and γ = 1.104 , values obtained by Chen *et al*. (1997b) for bare soil. The weighting factor α was also calculated using Eq. (7.3) for each half-hourly data and averaged to determine the mean α values. As shown in Table 7.1, the α values obtained using Eq. (7.1) varied with measurement height and the time lag used. The α values decreased with the increase in measurement height. The α values for Eq. (7.2) are different for the time lags r = 0.4 and 0.8 s, but the values did not vary with the increase in measurement height.

Table 7.1 Linear regression statistics of half-hourly H_{EC} (y) *vs* H_{SR} (x) (Eqs 7.1 and 7.2) estimates and mean α values obtained using Eq. (7.3) for time lags r = 0.4 and 0.8 s for n = 690 data points.

z (m)	Time lag	α		Coefficient of determination		α (Eq. 7.3)
	r (s)	Eq. (7.1)	Eq. (7.2)	Eq. (7.1)	Eq. (7.2)	(mean)
1.0	0.4	0.176	0.173	0.40	0.44	0.255
1.0	0.8	0.261	0.189	0.46	0.47	0.335
1.3	0.4	0.159	0.171	0.38	0.44	0.254
1.3	0.8	0.233	0.188	0.45	0.48	0.311
1.9	0.4	0.129	0.176	0.41	0.50	0.237
1.9	0.8	0.181	0.184	0.47	0.51	0.349
2.5	0.4	0.107	0.178	0.41	0.53	0.207
2.5	0.8	0.156	0.189	0.48	0.57	0.265

Average α values of 0.175 for r = 0.4 s and 0.188 for r = 0.8 s were obtained using Eq. (7.2). The mean α values calculated using Eq. (7.3) are greater than those obtained using Eqs (7.1) and (7.2). Generally, the α values for r = 0.8 s are greater than the values for r = 0.4 s. There are no previously determined α values for open water surface in the scientific literature reported against which the α values of Table 7.1 could be compared. Of note though is that for a bare soil surface, α = 0.69 (time lag r = 0.1) for measurement taken at 0.03 m above the surface (Chen *et al.*, 1997b).

The *SR* sensible heat flux H_{SR} was estimated using Eqs (7.1), (7.2), and (7.4) and was compared with H_{EC} values to see the performance of each equation. The diurnal variation of H_{EC} and H_{SR} averaged for the two time lags and calibrated using α values (Table 7.1) for three days in winter is shown in Fig. 7.2. The sensible heat flux values were extremely small (-40 to 40 W m^{-2}), and less than 30 W m^{-2} for most of the days. Sensible heat flux values obtained from shallow water bodies in warm environments measured using *EC* method were small, generally between -50 to 50 W m^{-2} (Stannard and Rosenberry, 1991; Assouline and Mahrer, 1993). The *SR* sensible heat flux estimated using Eqs (7.1) and (7.2) compared well with H_{EC} for all measurement heights. The *SR* method (Eq. 7.4) also performed well for the measurements taken at 1.0 and 1.30 m but overestimated compared to the *EC* method for the two highest measurement heights at 1.90 and 2.50 m (Fig. 7.2).

The sensible heat flux values peaked between 09h00 and 10h00 as shown in Fig. 7.2. Sensible heat flux was positive in the morning and negative in the afternoon. In the morning, the water temperature was greater (2 to 3 ^{o}C) than the air temperature; hence heat energy was transferred from the water to the air resulting in positive H_{EC} and H_{SR} values. In the afternoon, the water temperature was less than the air temperature resulting in downward heat energy transfer and negative H_{EC} and H_{SR}. In general, the SR method performed well in estimating H.

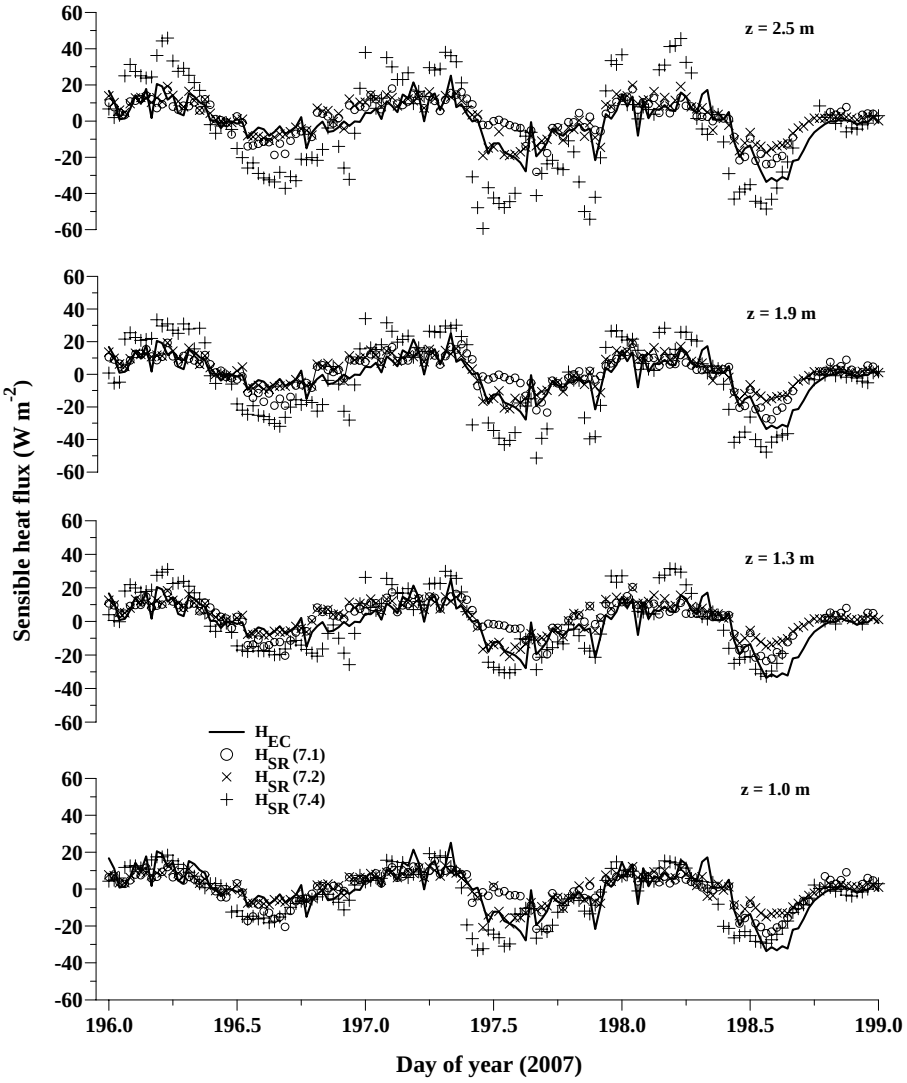

Fig. 7.2 Diurnal variations of half-hourly measured H_{EC} and estimated H_{SR} using Eqs (7.1), (7.2), and (7.4) at 1.0, 1.3, 1.9, and 2.5 m above the water surface for day of year 196 to 198 (2007). The H_{SR} estimates are the average of the two time lags r = 0.4 and 0.8 s.

7.4.2 Heat stored in water

Heat stored in water G was calculated from the two minute changes in mean water temperature using Eq. (7.6). The heat storage term was fluctuating from negative to positive in each 2-minute period, due to turbulent waves of varying temperature travelling past the thermocouples. The storage term is therefore smoothed by calculating hourly running means of G for each 2-minute data (Burba *et al.*, 1999) and then averaged to 30-minute for the latent energy flux calculations. The diurnal variations of the half-hourly stored heat G, net irradiance R_n, the mean water temperature T_w, and air temperature T_a are shown in Fig. 7.3.

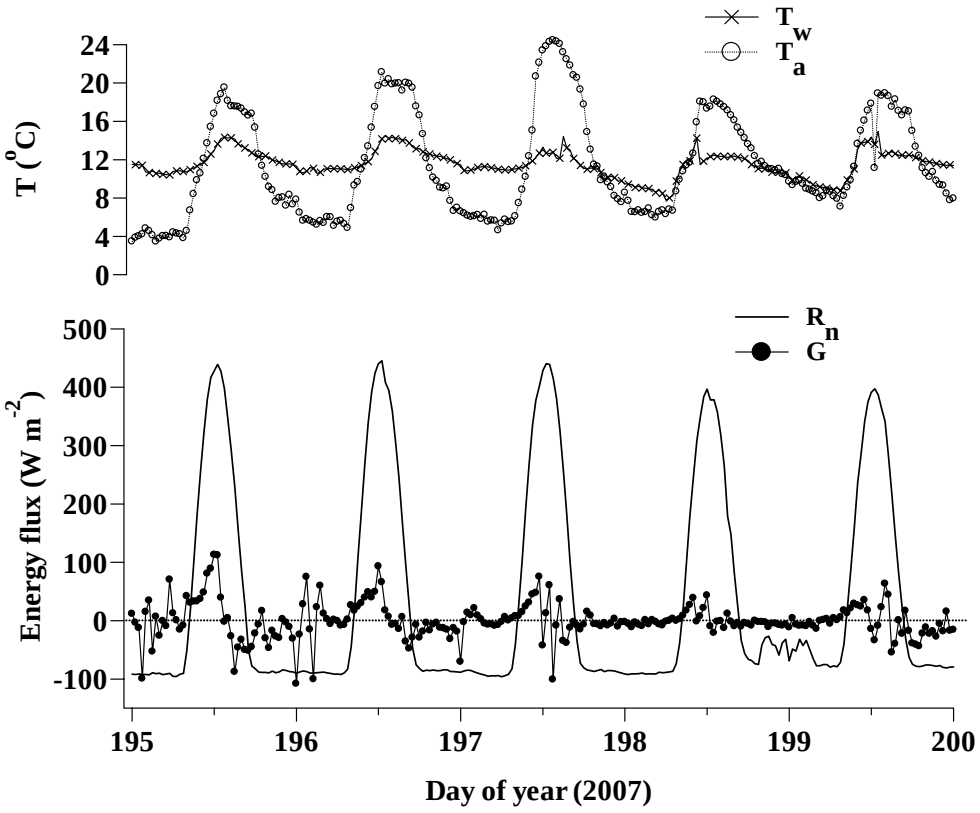

Fig. 7.3 Diurnal variations of half-hourly stored heat G, measured net irradiance R_n, the mean water temperature T_w, and air temperature T_a for day of year 195 to 199 (2007).

The heat stored followed the trend of fluctuations of R_n and peaked at the same time as the peak in R_n. The water temperatures were low (8 to 14 ^{o}C) and followed the pattern of the net irradiance. The magnitude of G ranged from -100 to 100 W m^{-2} for most of the days with extremes of -200 to 200 W m^{-2} for day of year 188, 189, and 193 (2007). The stored heat was much larger in magnitude compared to the sensible heat flux and a significant proportion of R_n. Therefore, G plays an important role in the energy balance and evaporation estimation of shallow water bodies.

7.4.3 Latent energy flux density

The latent energy flux density λE was estimated, using Eq. (7.5), as a residual of the shortened energy balance equation. The linear regression analysis of the average latent energy flux from the SR analysis λE_{SR} of r = 0.4 and 0.8 s at 1.0, 1.30, 1.90, and 2.50 m *vs* the latent energy flux density from the eddy covariance system λE_{EC} at 2.50 m above the water surface are presented in Table 7.2. The λE_{SR} estimates using the sensible heat flux equations (Eqs 7.1, 7.2, and 7.4) gave very good estimates of λE_{EC} as shown in Table 7.2.

Table 7.2 Regression statistics of half-hourly λE_{SR} (average of two time lags r = 0.4 and 0.8 s) using H_{SR} (Eqs 7.1, 7.2, and 7.4) *vs* λE_{EC} estimates of latent energy flux density.

z (m)	Slope			Intercept (W m^{-2})			Coefficient of determination			RMSE (W m^{-2})		
	λE (7.1)	λE (7.2)	λE (7.4)	λE (7.1)	λE (7.2)	λE (7.4)	λE (7.1)	λE (7.2)	λE (7.4)	λE (7.1)	λE (7.2)	λE (7.4)
1.00	0.99	0.99	1.03	0.83	-0.35	-0.61	0.99	0.99	0.99	10.61	10.33	15.95
1.30	0.99	0.99	1.03	0.22	-1.16	-2.21	0.99	0.99	0.99	11.11	10.51	11.65
1.90	0.99	0.99	1.05	0.72	-0.82	-1.88	0.99	0.99	0.98	11.03	9.9	21.29
2.50	0.99	0.99	1.06	1.31	-4.00	-4.17	0.99	0.99	0.98	10.99	9.14	16.28

The latent energy flux computed using H_{SR} (Eq. 7.1) gave excellent estimates of λE_{EC} compared to Eqs (7.2) and (7.4). The surface renewal sensible heat flux H_{SR} (Eq. 7.4) produced λE_{SR} estimates with the largest RMSE values for all measurement heights. The λE_{SR} estimates at 1.0 m were slightly better than λE_{SR} at 1.30, 1.90, and 2.50 m compared to λE_{EC}.

The magnitudes of the half-hourly λE_{EC} and λE_{SR} values ranged from 20 to 450 W m^{-2} during the day, and 0 to 100 W m^{-2} during the night. The magnitude of λE_{SR} increased from 30 W m^{-2} at 09h00 to 200 W m^{-2} at 11h00. The latent energy fluxes, λE_{EC} and λE_{SR}, peaked between 13h00 and 14h00. The magnitudes of the half-hourly λE_{EC} and λE_{SR} were almost the same in magnitude as the available energy $R_n - G$, because of the small magnitudes of the sensible heat fluxes (Fig. 7.4).

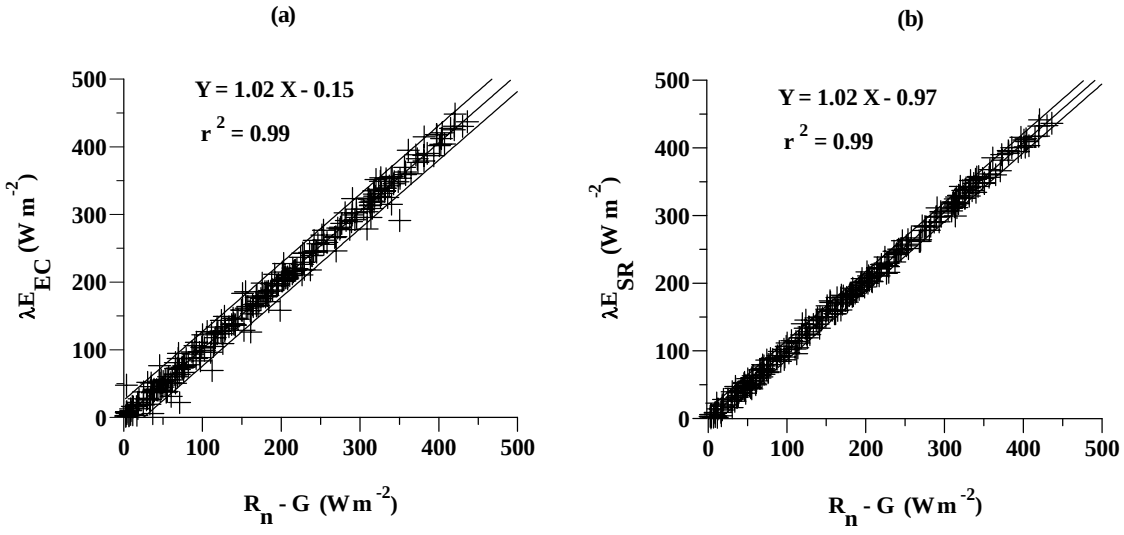

Fig. 7.4 A linear regression of half-hourly latent energy flux λE *vs* the available energy flux $R_n - G$: (a) λE_{EC} at 2.50 m above the water surface *vs* $R_n - G$; (b) λE_{SR} using H_{SR} (Eq. 7.1) at 1.0 m above the water surface *vs* $R_n - G$.

The daily total evaporation (mm), λE_{EC} and λE_{SR} at 1.0 m, for the entire measurement period is shown in Fig. 7.5. The daily total evaporation ranged between 2.0 and 3.5 mm. The daily average evaporation for the whole measurement period was 2.70 mm. Previously reported values of the daily evaporation rates from open water surface range between 2 and 5 mm in winter (de Bruin, 1982), and 5 to 10 mm in summer (Burba *et al*., 1999; Gianniou and Antonopoulos, 2007).

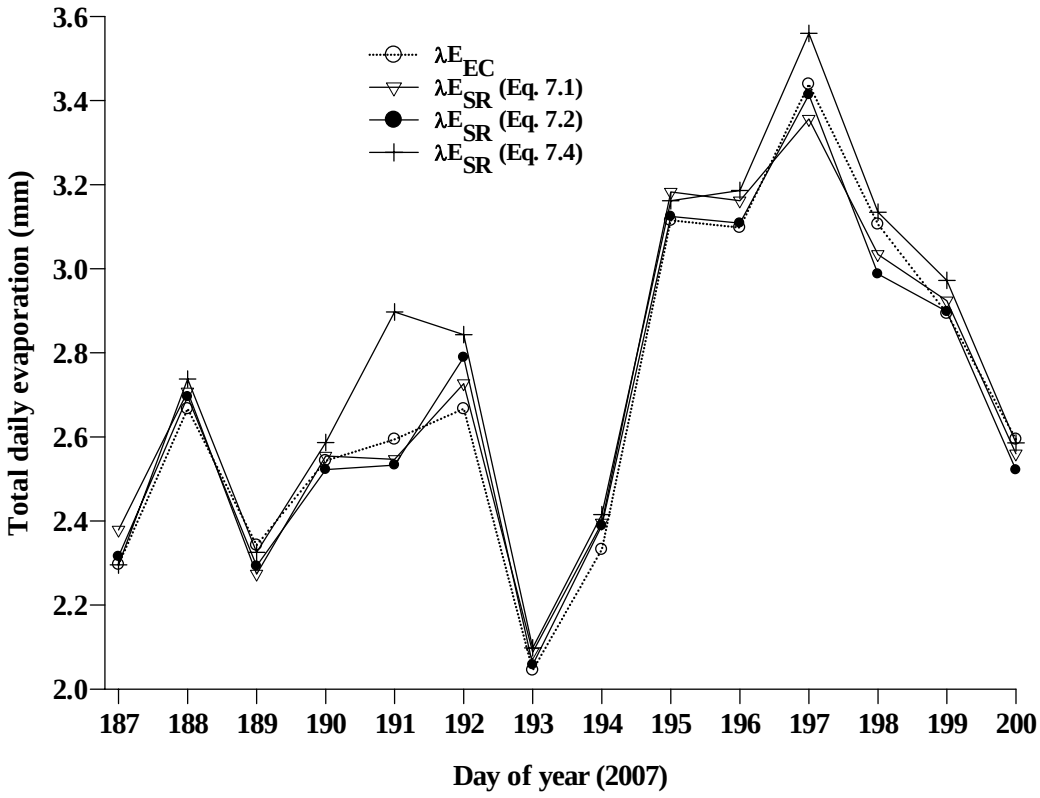

Fig. 7.5 Total daily evaporation estimates (mm) using *EC* and *SR* methods for day of year 187 to 200 (2007). The λE_{SR} is estimated using the sensible heat flux, Eqs (7.1), (7.2), and (7.4) at 1.0 m above the water surface.

7.5 Summary and conclusions

Sensible heat and latent energy fluxes were estimated using the eddy covariance EC and surface renewal SR methods in winter 2007, over an open water surface in Midmar Dam, midlands of KwaZulu-Natal, South Africa. The performance of the SR analysis in estimating the sensible heat flux density is evaluated using two time lags r = 0.4 and 0.8 s at 1.0, 1.30, 1.90, 2.50 m above the water surface. The calibration (weighting factor), α for each height and time lag was determined from the slope of linear regression forced through the origin of measured H_{EC} values versus H_{SR}. Average α values of 0.175 for r = 0.4 s and 0.188 for r = 0.8 s were obtained for open water surface from this study.

The sensible heat flux values were small (-40 to 40 W m^{-2}) for all days during the measurement period. The stored heat in water was much larger in magnitude (-200 to 200 W m^{-2}) compared to the sensible heat flux. Therefore, the stored heat in water, G, plays an important role in the energy balance and evaporation estimation of shallow water bodies. The SR and EC latent energy fluxes were almost the same in magnitude as the available energy flux, due to the small values of the sensible heat fluxes. The daily total evaporation ranged between 2.0 and 3.5 mm. The daily total evaporation estimates for the entire measurement period using the EC and SR methods averaged 2.70 mm.

The surface renewal method offers a simple, low cost, and accurate estimate of sensible heat and latent energy fluxes over an open water surfaces once the weighting factor α is determined. Alternatively, the SR method can be used to estimate sensible heat flux which is exempt from calibration with additional measurement of wind speed for estimating friction velocity iteratively.

Chapter 8: General conclusions and recommendations for future research

8.1 Conclusions

The main aim of this research is to estimate sensible heat flux density over a range of representative surfaces using the surface renewal (*SR*) method and make comparison with measurements obtained using the eddy covariance (*EC*) method. The *SR* method for estimating sensible heat flux and the shortened energy balance equation allows the latent energy flux to be estimated as a residual term, using additional measurement of net irradiance and soil heat flux density. For this calculation, advection fluxes, canopy stored heat, and the energy fluxes associated with photosynthesis and respiration are ignored. Surface renewal analysis for estimating sensible heat flux from canopies involves high frequency air temperature measurements using fine-wire thermocouples. Other methods used for comparison purposes are the Bowen ratio (*BR*), flux variance (*FV*), and surface layer scintillometry (*SLS*) methods. The *FV* method is also based on high frequency air temperature measurements.

There are three *SR* analysis approaches: an ideal *SR* analysis model based on structure function analysis; *SR* analysis model with a finite micro-front period; and empirical *SR* analysis model based on similarity theory. The ideal *SR* analysis model based on structure function analysis must be calibrated against another standard method, such as the *EC* method to determine the correction or weighting factor α, to account for unequal heating or cooling of air parcels below the air temperature sensor height. The weighting factor α, depends on measurement height above the soil surface z, canopy structure and on thermocouple size. Therefore, the weighting factor α should be known for a specific canopy. For this study, the *SR* method was used over a range of representative surfaces, such as grassland, Triffid weed (*Chromolaena odorata*), Outeniqua Yellow wood forest (*Podocarpus Falcatus*), *Jatropha curcas*, and open water surface, and α is determined for each surface. The other two *SR* analysis methods, are exempt from calibration, but they need the extra measurement of wind speed to estimate the friction velocity iteratively.

To meet the specific objectives of this research, high frequency air temperature data were collected at four measurement heights over an open and mixed grassland, to estimate sensible heat flux density using the *SR* analysis for time lags r = 0.25 s and r = 0.50 s, during unstable atmospheric conditions at four measurement heights: z_1 = 0.5 m, z_2 = 0.8 m, z_3 = 1.0 m, and z_4 = 1.5 m above grass canopy surface. The ideal *SR* analysis model based on structure function analysis technique from Van Atta (1977) was used to estimate sensible heat flux H_{SR}. The correction factor α was close to 1.0 at 0.5 m above the canopy and decreased for the other three measurement heights. The measurements show very good agreement between the surface renewal sensible heat flux density H_{SR} estimates at 0.5 m above the canopy and the eddy covariance sensible heat flux density H_{EC} estimates. Good agreement for the other three heights (0.8, 1.0, 1.5 m) between H_{SR} and H_{EC} is also obtained with a coefficient of determination greater than 0.8, but there was bias with the slopes different from 1. The H_{SR} measurements at 0.5 m above the canopy also showed good agreement compared to the sensible heat flux density obtained using the Bowen ratio H_{BR} and surface layer scintillometer H_{SLS} estimates. The H_{SR} estimates at 0.5 m above the grass canopy provided accurate estimates of latent energy flux density λE_{SR} when used with measured net irradiance and soil heat flux density.

The performance of the three *SR* analysis approaches were evaluated for unstable conditions using four time lags r = 0.1, 0.4, 0.5, and 1.0 s over alien invasive plant, Triffid weed (*C. odorata*) at 2.30, 2.85, and 3.60 m above the soil surface. The *SR* sensible heat flux H_{SR} computed using r = 0.1 and 0.4 s provided poor estimates of sensible heat flux with bias. The *SR* sensible heat flux closest to the canopy top, at 2.30 m above the soil surface underestimated the *EC* sensible heat flux estimates. The best results were obtained using the empirical *SR* method with regression slopes of 0.89 and root mean square error (RMSE) values less than 30 W m^{-2} at 2.85 and 3.60 m using time lag r = 1.0 s.

The empirical SR analysis based on similarity theory is also compared with two MOST based methods, FV and SLS methods in the roughness sublayer over *C. odorata*. Generally, MOST effectively predicts mean and turbulent statistics in the inertial sublayer where fluxes are approximately constant. For this experiment, all measurements were made in the roughness sublayer where the applicability of MOST fails. However, turbulent fluxes can be normalized for the roughness sublayer. Sensible heat and latent energy flux estimates obtained using the empirical SR method were compared with the FV and SLS estimates in the roughness sublayer under unstable conditions and free convection limit. The FV and SLS measurements normalized for the roughness sublayer performed well in estimating the sensible heat and latent energy fluxes at 2.85 and 3.60 m above the soil surface. The free convection limit of the empirical SR analysis also performed very well in estimating the sensible heat flux. The use of the free convection limit of the empirical SR method under slightly unstable conditions has an advantage, since it only requires the high frequency air temperature data. Generally, the results show that there is good agreement between the SR sensible heat and latent energy fluxes using a time lag, r = 1.0 s and the EC, FV and SLS measurements.

To test the performance of the SR analysis over tall canopies, three sets of experiments were carried out for estimating sensible heat and latent energy flux over 10-m high Outeniqua Yellow wood stand at three measurement heights above the canopy using the SR and EC methods. The performance of the three SR analysis approaches in estimating the sensible heat flux density is also evaluated for stable and unstable atmospheric conditions using four time lags r = 0.1, 0.4, 0.5, and 1.0 s. The weighting factor α was determined by plotting H_{SR} against H_{EC} estimates. An average value of 0.60 is obtained for α over Outeniqua Yellow wood forest for measurements made in the roughness sublayer. Under stable conditions, the SR analysis model with finite micro-front period produced better estimates of H_{SR}. For unstable conditions, the SR analysis model based on structure function analysis corrected for α produced superior estimates of H_{SR}, using a time lag r = 1.0 s. The SR latent energy flux estimates λE_{SR} based on structure function analysis gave very

good estimates of λE_{EC}. In general, the agreement between the *SR* sensible heat and latent energy flux estimates and *EC* estimates are good.

The *SR* and *EC* methods were used to estimate sensible heat and latent energy flux over *J. curcas* (Physic nut) trees planted in rows. The objective was to test the *SR* method over a heterogeneous surface and to investigate the applicability of the *SR* analysis for a long-term sensible heat and total evaporation estimation. The results show that it is possible to estimate long-term sensible heat and latent energy fluxes using the *SR* and *EC* methods over heterogeneous canopies. Continuous measurements of canopy height and leaf area index measurements are needed, especially for long-term studies over fast growing trees to determine the weighting factor α, for the *SR* method. The weighting factor, α was approximately 1 for heights between 0.2 and 0.6 m above the Jatropha tree canopy. The daily sensible heat and latent energy flux estimates using the *SR* analysis gave excellent estimates of daily *EC* sensible heat and latent energy fluxes. Seasonal estimates of total evaporation using the *EC* and *SR* methods were investigated, spanning a period of almost two years. Total evaporation (*ET*) estimates tracked the trend of fluctuation of the available energy. The available energy and *ET* varied with time throughout the day and from day to day. Total evaporation estimates were at peak in summer (with an average daily amount of greater than 3 mm). In summer, *ET* estimates were mainly dictated by the available energy flux, often varying from one day to the next due to the influence of clouds. In winter, the daily *ET* estimates from the Jatropha trees were very low, with an average daily amount of less than 1 mm.

A footprint analysis was made to investigate the relative contribution of upwind surface sources to the measured downwind sensible heat and latent energy fluxes, as the measurements were made in a plot with limited fetch. The estimated footprint, peak location of the footprint, and the cumulative fraction of the measured flux to surface source flux ratio were calculated. The results showed that 81 % of the measured flux was coming from the upwind fetch distance of 40 m for a cloudy day, and 90 % for a clear day. The high ratio of the measured flux F to surface source flux S_o values - generally close to 80 % for the fetch-limited *J. curcas* site, is

surprising. Therefore, an important recommendation for future research is that these footprint calculations should be confirmed using other footprint models for this site.

The use of the *SR* method for estimating sensible heat flux and open water evaporation from a shallow dam was also investigated. The *SR* method, to the author's knowledge, has not been tested over open water surfaces. The aim of this study is therefore to calibrate the sensible heat flux obtained using the *SR* method against measurements obtained using the *EC* method. The calibration factor, α for each height and time lag was determined from the slope of linear regression forced through the origin of measured H_{EC} values *vs* H_{SR}. Average α values of 0.175 for time lag, r = 0.4 s and 0.188 for r = 0.8 s were obtained for open water surface from this study. The sensible heat flux values were extremely small for all days during the measurement period. The stored heat in water was much larger in magnitude compared to the sensible heat flux values. Therefore, the stored heat in water plays an important role in the energy balance and evaporation estimation of shallow water bodies. The *SR* and *EC* latent energy fluxes were almost the same in magnitude as the available energy flux, due to the small values of the sensible heat fluxes. The daily total evaporation ranged between 2.0 and 3.5 mm.

The study has confirmed that the *SR* method can be used for routine estimation of sensible heat and latent energy fluxes with a reliable accuracy, over a variety of surfaces: short canopies, tall canopies, heterogeneous surface, and open water surface. The *SR* method offers a relatively simple, low cost, and accurate estimate of sensible heat and, together with net irradiance and soil heat flux, the latent energy flux, if the weighting factor α is determined. The weighting factor α, once determined, is unlikely to change with weather conditions unless there are significant changes in the vegetation canopy structure. If there is a change in canopy structure, recalibration of the *SR* method is needed. However, this can be done easily since measurements can be replicated inexpensively. Alternatively, the *SR* method can be used to estimate sensible heat flux which is exempt from calibration using the other two *SR* analysis approaches, with the additional measurement of wind speed for estimating friction velocity iteratively. Short time lags ($r \leq 0.5$ s) are recommended for short canopies while for tall canopies longer time lags ($r > 0.5$ s) should give

good estimates of sensible heat and latent energy fluxes. The advantages of the *SR* method over other micrometeorological methods are the relatively low cost, easy installation and maintenance, relatively low cost for replicate measurements, and the *SR* method is less dependent on fetch since it is based on the theory of short-term heat transfer between a surface and air parcels passing through the surface.

8.2 Recommendations for future research

The search for methods for estimating sensible heat and latent energy flux (evaporation) using simple, inexpensive, and portable methods, has been the subject of interest in the past few decades. The *SR* method has the advantage over other micrometeorological methods since it requires only measurement of the scalar of interest at one point. Therefore, the *SR* method can offer a relatively simple, low-cost, and accurate estimate of sensible heat flux. The *SR* method has been mostly used for estimating sensible heat flux over different surfaces, and the latent energy flux is obtained as a residual of the energy balance equation. Most of the studies have focused on the determination of the weighting factor α, and analysing the performance of the *SR* sensible heat flux.

The *SR* analysis can be applied to other scalars such as water vapour, carbon dioxide, and other gases. However, there has been little research on the application of the *SR* analysis to estimate the flux of other scalars. Therefore, further studies should focus on the use of the *SR* method to estimate fluxes of water vapour, carbon dioxide, and other scalars. Also, the *SR* method applied here does not allow real-time estimation of sensible heat flux and further research on this aspect would be valuable.

References

Albertson, J.D., Parlange, M.B., Katul, G., Chu, C.R., Striker, H., Tyler, S., 1995. Sensible heat flux estimates using variance methods. Water Resour. Res. 31(4), 969-974.

Allen, R.G., Pruitt, W.O., Wright, J.L., Howell, T.A., Ventura, F., Snyder, R., Itenfisu, D., Steduto, P., Berengena, J., Yrisarry, J.B., Smith, M., Pereira, L.S., Raes, D., Perrier, A., Alves, I., Walter, I., Elliott, R., 2006. A recommendation on standardized surface resistance for hourly calculation of reference ET_o by the FAO56 Penman-Monteith method. Agric. Water Mange. 81, 1-22.

Anandakumar, K., 1999. Sensible heat flux over a wheat canopy: optical scintillometer measurements and surface renewal analysis estimations. Agric. For. Meteorol. 96, 145-156.

Andreas, E.L., 2000. Obtaining surface momentum and sensible heat fluxes from crosswind scintillometer. J. Atmos. Oceanic Technol. 17, 3-16.

Angus, D.E., Watts, P.J., 1984. Evapotranspiration- how good is the Bowen ratio method? Agric. Water Mange. 8, 133-150.

Anthoni, P.M., Law, B.E., Unsworth, M.H., 1999. Carbon and water vapour exchange of an open-canopied ponderosa pine ecosystem. Agric. For. Meteorol. 95, 151-168.

Arya, S.P., 2001. Introduction to Micrometeorology. Second edition. Academic Press. London, UK. 420 pp.

Asktorab, H.W.O., Pruitt, K.T., Paw U, K.T., George, W.V., 1989. Energy balance determinations close to the soil surface using a micro-Bowen ratio system. Agric. For. Meteorol. 46, 259-274.

Assouline, S., Mahrer, Y., 1993. Evaporation from lake Kinneret. 1. Eddy correlation system measurements and energy budget estimates. Water Resour. Res. 29 (4), 901-910.

Bergström, H., Högström, U., 1989. Turbulent exchange above a pine forest: II. Organized structures. Boundary-Layer Meteorol. 49, 231-263.

Bowen, I.S., 1926. The ratio of heat losses by conduction and by evaporation from any water surface. Phys. Rev. 27, 779-787.

Brutsaert, W.H., 1982. Evaporation Into the Atmosphere. Theory, History, and Applications. D. Reidel Publishing Co, Dordrecht, Holland. 299 pp.

Burba, G.G., Verma, S.B., 2005. Seasonal and interannual variability in evapotranspiration of native tallgrass praire and cultivated wheat ecosystems. Agric. For. Meteorol. 135, 190-201.

Burba, G.G., Verma, S.B., Kim, J., 1999. Energy fluxes of an open water area in a mid-latitude prairie wetland. Boundary-Layer Meteorol. 91, 495-504.

Businger, J.A., Wyngaard, J.C., Izumi, I., Bradley, E.F., 1971. Flux profile relationships in the atmospheric surface layer. J. Atmos. Sci. 28, 181-189.

Calder, I., Dye, P., 2000. Hydrological impacts of invasive alien plants. In: Best management practices for preventing and controlling invasive alien species. The South Africa: United States of America Bi-National Commision. The Working for Water Programme. Symposium Proceedings, pp. 160-179.

Campbell, G.S., Diak, G.R., 2005. Net and thermal radiation estimation and measurement. In: Hatfield, J.L., Baker, J.M. (Eds), Micrometeorology in Agricultural Systems. Agronomy Monograph no. 47. pp. 59-92.

Castellvi, F., 2004. Combining surface renewal analysis and similarity theory: a new approach for estimating sensible heat flux. Water Resour. Res. 40, W05201, 1-20.

Castellvi, F., Martinez-Cob, A., 2005. Estimating sensible heat flux using surface renewal analysis and flux variance method: A case study over olive trees at Sastago (NE of Spain). Water Resour. Res. 41, W09422, 1-10.

Castellvi, F., Martinez-Cob, A., Perez-Coveta, O., 2006. Estimating sensible and latent heat fluxes over rice using surface renewal. Agric. For. Meteorol. 139, 164-169.

Castellvi, F., Perez, P.J., Ibanez, M., 2002. A method based on high frequency temperature measurements to estimate sensible heat flux avoiding the height dependence. Water Resour. Res. 38 (6), WR000486-20, 1-10.

Cava, D., Contini, D., Donateo, A., Martano, P., 2007. Analysis of short-term closure of the surface energy balance above short vegetation. Agric. For. Meteorol. In Press.

Cellier, P., Brunet, Y., 1992. Flux-gradient relationships above tall plant canopies. Agric. For. Meteorol. 58, 93-117.

Cellier, P., Olioso, A., 1993. A simple system for automated long-term Bowen ratio measurement. Agric. For. Meteorol. 66, 81-92.

Chen, W., Novak, M.D., Black, T.A., Lee, X., 1997a. Coherent eddies and temperature structure functions for three contrasting surfaces. Part I: Ramp model with finite micro front time. Boundary-Layer Meteorol. 84, 99-123.

Chen, W., Novak, M.D., Black, T.A., Lee, X., 1997b. Coherent eddies and temperature structure functions for three contrasting surfaces. Part II: Renewal model for sensible heat flux. Boundary-Layer Meteorol. 84, 125-147.

Clemence, B., Miller, J., Siddons, G., 1987. A summary of climatic conditions in Natal. Agrometeorology Report, Cedara Research Instituite, Department of Agriculture, Natal Region. 126 pp.

Craig, I.P., 2006. Comparison of precise water depth measurements on agricultural storages with open water evaporation estimates. Agric. Water Mange. 85, 193-200.

Craig, I.P., Hancock, N., 2004. Methods for assessing dam evaporation- an introductory paper paper. In: IAA Conference, Adelaide, May, Australia.

de Bruin, H.A.R., 1982. Temperature and energy balance of a water reservoir determined from standard weather data of a land station. J. Hydrol. 59, 261-274.

de Bruin, H.A.R., Kohsiek, W., Van Den Hurk, B.J.J.M., 1993. A verification of some methods to determine the fluxes of momentum, sensible heat and water vapour using standard deviation and structure parameter of scalar meteorological quantities. Boundary-Layer Meteorol. 63, 231-257.

de Bruin, H.A.R., Meijninger, W.M.L., 2002. Displaced-beam small aperture scintillometer test. Part I: the WINTEX data-set. Boundary-Layer Meteorol. 105, 129-148.

de Bruin, H.A.R., van den Hurk B.J.J.M., Kohsiek W., 1995. The scintillation method tested over dry vine yard area. Boundary-Layer Meteorol. 76, 25-40.

Deardorf, J.W., 1978. Observed characterstics of the outer layer. AMS course on the planetary boundary layer. Boulder, Colorado (unpublished manuscript).

Drexler, J.Z., Snyder, R.L., Spano, D., Paw U, K.T., 2004. A review of models and micrometeorological methods used to estimate wetland evapotranspiration. Hydrol. Process. 18, 2071-2101.

Duce, P., Spano D., Snyder, R.L., 1998. Effect of different fine-wire thermocouple design on high frequency temperature measurement. In: AMS 23rd Conf. on Agricultural and Forest Meteorology. Albuquerque, NM, Nov. 2-6, pp. 146-147.

Duce, P., Spano D., Snyder, R.L., Paw U, K.T., 1997. Surface renewal estimates of evapotranspiration. Short canopies. Acta Hort. 449, 57-62.

DWAF, 2007. Information on South African dams. Hydrological services, Department of Water Affairs and Forestry. Available at (http://www.dwaf.gov.za/hydrology/dwafapp2_wma/). Accessed, October 29, 2007.

Dye, P.J., Olbricht, B.W., 1993. Estimating transpiration from six year old Eucalyptus grandis trees: development of a canopy conductance model and comparison with independent sap flux measurements. Plant, Cell Environ. 16, 45-53.

Edinger, J.E., Duttweiler, D.W., Geyer, J.C., 1968. The response of water temperature to meteorological conditions. Water Resour. Res. 4, 1137-1143.

Finch, J.W., 2001. A comparison between measured and modelled open water evaporation from a reservoir in south-east Englad. Hydrol. Process. 15, 2771-2778.

Finnigan, J.J., 2004. The footprint concept in complex terrain. Agric. For. Meteorol. 127, 117-129.

Finnigan, J.J., Clements, R., Malhi, Y., Leuning, R., Cleugh, H.A., 2003. A re-evaluation of long term flux measurement techniques: 1. Averaging and coordinate rotation. Boundary-Layer Meteorol. 107, 1-48.

Fritschen, L.J., Fritschen, C.L., 2005. Bowen ratio energy balance method. In: Hatfield, J.L., Baker, J.M. (Eds), Micrometeorology in Agricultural Systems Agronomy Monograph no. 47. pp. 397-405.

Fritschen, L.J., Simpson, J.R., 1989. Surface energy balance and radiation systems: general description and improvements. J. Applied Meteorol. 28, 680-689.

Fuchs, M., Tanner, C.B., 1970. Error analysis of Bowen ratio measured by differential psychrometry. Agric. Meteorol. 7, 329-334.

Gao, W., Shaw, R.H., Paw U, K.T., 1989. Observation of organized structure in turbulent flow within and above a forest canopy. Boundary-Layer Meteorol. 47, 349-377.

Garratt, J.R., 1980. Surface influences upon vertical profiles in the atmospheric near-surface layer. Quart. J. Roy. Meteorol. Soc. 106, 803-819.

Garratt, J.R., 1992. The Atmospheric Boundary Layer. Cambridge University Press, Cambridge. 316 pp.

Gash, J.H.C., 1986. A note on estimating the effect of a limited fetch on micrometeorological evaporation measurements. Boundary-Layer Meteorol. 35, 409-413.

Gianniou, S.K., Antonopoulos, V.S., 2007. Evaporation and energy budget in lake Vegoritis, Greece. J. Hydrol. 345, 212-223.

Green, A.E., Astill, M.S., McAneney, K.J., Nieveen, J.P., 2001. Path-averaged fluxes determined from infrared and microwave scintillometers. Agric. For. Meteorol. 109, 233-247.

Green, A.E., Green, S.R., Astill, M.S., Caspari, H.W., 2000. Estimating latent heat flux from a vineyard using scintillometry. TAO, 11(2), 525-542.

Green, A.E., McAneney, K.J., Astill, M.S., 1994. Surface layer scintillation measurements of daytime heat and momentum fluxes. Boundary-Layer Meteorol. 68, 357-373.

Grelle, A., Lindroth, A., Molder, M., 1999. Seasonal variation of boreal forest surface conductance and evaporation. Agric. For. Meteorol. 98-99, 563-578.

Grobler, J.H., 1984. Natal Parks, Game and Fish Preservation Board. In: Greyling, T., Huntley, B.J., editor. Pretoria: Foundation for Research Development.

Hartogensis, O.K., de Bruin, H.A.R., van de Weil, B.J.H., 2002. Displaced-beam small aperture test. Part II: Cases-99 stable boundary-layer experiment. Boundary-Layer Meteorol. 105, 149-176.

Heilman, J.L., Brittin, C.L., Neale, C.M.U., 1989. Fetch requirements for Bowen ratio measurements of latent and sensible heat fluxes. Agric. For. Meteorol. 44, 261-273.

Higbie, R., 1935. The rate of absorption of a pure gas into a still liquid during short periods of exposure. Trans. Amer. Inst. Chem. Eng. 31, 365-388.

Hill, R.J., 1992. Review of optical scintillation methods of measuring the refractive-index spectrum, inner scale and surface fluxes. Waves Random Media 2, 179-201.

Hill, R.J., 1997. Algoithms for obtaining atmospheric surface-layer fluxes from scintillation measurements. J. Atmos. Oceanic Tech. 14, 456-467.

Hill, R.J., Cliford, S.F., 1978. Modified spectrum of atmospheric temperature fluctuations and its application to optical propagation. J. Optical Soc. Amer. 68, 1201-1211.

Hill, R.J., Ochs, J.R., Wilson, J.J., 1992. Measuring surface layer fluxes of heat and momentum using optical scintillation. Boundary-Layer Meteorol. 58, 391-408.

Horst, T.W., Weil, J.C., 1992. Footprint estimation for scalar flux measurements in the atmospheric surface-layer. Boundary-Layer Meteorol. 59, 279-296.

Hsieh, C., Katul, G., 1996. Estimation of momentum and heat fluxes using dissipation and flux variance methods in the unstable surface layer. Water Resour. Res. 32(8), 2453-2462.

Hsieh, C., Katul, G., Chi, T., 2000. An approximate analytical model for footprint estimation of scalar fluxes in thermally stratified atmospheric flows. Adv. Water Resour. 23, 765-772.

Humphreys, E.R., Black, T.A., Ethier, G.J., Drewitt, G.B., Spittlehouse, D.L., Jork, E.-M., Nesic, Z., Livingston, N.J., 2003. Annual and seasonal variability of sensible and latent heat fluxes above a coastal Douglas-fir forest, British Colombia, Canada. Agric. For. Meteorol. 115, 109-125.

ICRAF, 2003. *Jatropha curcas*. Agroforestree Database. Available at (Http://www.worldagroforestrycentre.org/Sites/TreeDBS/AFT/SpeciesInfo.cfm?SpID=1013). Accessed, September 5, 2005.

Kaimal, J.C., Finnigan, J.J., 1994. Atmospheric Boundary Layer Flows, Their Structure and Measurement. Oxford University Press, New York. 289 pp.

Katul, G., Goltz, M., Hsieh, C., Cheng, Y., Mowry, F., Sigmon, J., 1995. Estimation of surface heat and momentum fluxes using the flux variance method above uniform and non-uniform terrain. Boundary-Layer Meteorol. 74, 237-260.

Katul, G., Hsieh, C., Oren, R., Ellsworth, D., Philips, N., 1996. Latent and sensible heat flux predictions from a uniform pine forest using surface renewal and flux variance methods. Boundary-Layer Meteorol. 80, 249-282.

Keijman, J.Q., 1974. The estimation of the energy balance of a lake from simple weather data. Boundary-Layer Meteorol. 7, 399-407.

Kohsiek, W., Meijninger, W.M.L., Moene, A.F., Heusinkveld, B.G., Hartogensis, O.K., Hillen,W.C.A.M., de Bruin, H.A.R., 2002. An extra large aperture scintillometer for long range applications. Boundary-Layer Meteorol. 105, 119-127.

Kolmogorov, A.N., 1941. The local structure of turbulence in compressible turbulence for very large Reynolds number. Akad. Nauk. SSSR 30, 301-305.

Kustas, W.P., Blanford, J.H., Stannard, D.I., Douglas, C.S.T., Nichols, W.D., Weltz, M.A., 1994. Local energy flux estimates for unstable conditions using variance data in semiarid rangelands. Water Resour. Res. 30, 1351-1361.

Leclerc, M.Y., Thurtell, G.W., 1990. Footprint prediction of scalar fluxes using a Markovian analysis. Boundary-Layer Meteorol. 52, 247-258.

Lee, X., Black, T.A., 1993. Atmospheric turbulence within and above a Douglas-Fir stand. Part I: Statistical properties of the velocity field. Boundary-Layer Meteorol. 64, 149-174.

Lele, S.V., 2007. The cultivation of *Jatropha curcas* (Ratan Jyot). Available at (http://www.svlele.com/jatropha_plant.htm). Accessed, November 5, 2007.

Lloyd, C.R., Culf, A.D., Dolman, A.J., Gash, J.H.C., 1991. Estimates of heat flux from observations of temperature observations. Boundary-Layer Meteorol. 57, 311-322.

Mahrt, L., 2000. Surface heterogeneity and vertical structure of the boundary layer. Boundary-Layer Meteorol. 96, 33-62.

Marsh, P., Bigras, S.C., 1988. Evaporation from Mackenzie delta lakes, N.W.T., Canada. Arctic and Alpine Research 20(2), 220-229.

Massman, W.J., 2000. A simple method for estimating frequency response corrections for eddy covariance systems. Agric. For. Meteorol. 104, 185-198.

Massman, W.J., Lee, X., 2002. Eddy covariance flux corrections and uncertainties in long-term studies of carbon and energy exchanges. Agric. For. Meteorol. 113, 121-144.

McAneney, K.J., Green, A.E., Astill, M.S., 1995. Large-aperture scintillometry: the homogeneous case. Agric. For. Meteorol. 76, 149-162.

Medtherm Corp., 2007. Fine wire thermocouple probes for measuring transient gas temperature. Available at (http://www.dr-kubelik.de/infomaterial/TCFW%20Brochure%20B112.pdf). Accessed, December 7, 2007.

Meijninger, W.M.L., de Bruin, H.A.R., 2000. The sensible heat fluxes over irrigated areas in western Turkey determined with a large aperture scintillometer. J. Hydrol. 229, 42-49.

Meijninger, W.M.L., Hartogensis, O.K., Kohsiek, W., Hoedjes, J.C.B, Zuurbier, R.M., de Bruin, H.A.R., 2002. Determination of area-averaged water vapour fluxes with large aperture and radio wave scintillometers over heterogeneous surface – Flevoland field experiment. Boundary-Layer Meteorol. 105, 63-83.

Meyers, T.P., Baldocchi, D.D., 2005. Current micrometeorological flux methodologies with applications in agriculture. In: Hatfield, J.L., Baker, J.M. (Eds), Micrometeorology in Agricultural Systems Agronomy Monograph no. 47. pp. 381-396.

Monin, A.S., Obukhov, A.M., 1954. Basic laws of turbulent mixing in the atmosphere near the ground. Trudy. Akad. Nauk. SSSR 24 (151), 163-187.

Monteith, J.L., Unsworth, M.H., 1990. Principles of Environmental Physics. Second edition. Edward Arnold. London. 291pp.

Nie, D., Kanemasu, E.T., Fritschen, L.J., Weaver, H.L., Smith, E.A., Verma, S.B., Field, R.T., Kustas, W.P., Stewart, J.B., 1992. An intercomparison of surface energy-flux measurement systems used during FIFE 1987. J. Geophys. Res. 97, 18715-18724.

Oncley, S.P., Foken, T., Vogt, R., Kohsiek, W., deBruin, H.A.R., Bernhofer, C., Christen, A., van Gorsel, E., Grantz, D., Feigenwinter, C., Lehner, I., Liebethal, C., Liu, H., Mauder, M., Pitacco, A., Ribeiro, L., Weidinger., T., 2007. The energy balance experiment EBEX-2000. Part I: overview and energy balance. Boundary-Layer Meteorol. 123, 1-28.

Padro, J., 1993. An investigation of flux variance methods and universal functions applied to three land-use types in unstable conditions. Boundary-Layer Meteorol. 66, 413-425.

Panofsky, H.A., Dutton, J.A., 1984. Atmospheric Turbulence: Models and Methods for Engineering Applications. John Wiley & Sons. New York. 397 pp.

Pasquill, F., 1972. Some aspects of boundary layer description. Quart. J. Roy. Meteorol. Soc. 98, 469-494.

Paw U, K.T., Brunnet, Y., 1991. A surface renewal measure of sensible heat flux density. In: Preprints, 20th Conference on Agricultural and Forest Meteorology, 10-13 September, Salt Lake City, UT. American Meteorological Society, Boston, MA, pp. 52-53.

Paw U, K.T., Brunnet, Y., Collineau, S., Shaw, R.H., Maitani, T., Qui, J., Hipps, L., 1992. On coherent structure in turbulence within and above agricultural plant canopies. Agric. For. Meteorol. 61, 55-68.

Paw U, K.T., Qui, J., Su, H.B., Watanabe, T., Brunnet, Y., 1995. Surface renewal analysis: a new method to obtain scalar fluxes. Agric. For. Meteorol. 74, 119-137.

Paw U, K.T., Snyder, R.L., Spano, D., Su, H.B., 2005. Surface renewal estimates of scalar exchange. In: Hatfield, J.L., Baker, J.M. (Eds), Micrometeorology in Agricultural Systems Agronomy Monograph no. 47. pp. 455-483.

Penman, H.L., 1948. Natural evaporation from open water, bare soil and grass. Proc. Royal Soc. London A193, No. 1032, 120-145.

PIER, 2007. Institute of Pacific Islands Forestry, Pacific Island Ecosystems at Risk (PIER). Available at (http://www.hear.org/pier/species/jatropha_curcas.htm). Accessed, November 5, 2007.

Preston-Whyte, R.A., Tyson, P.D., 1988. The Atmosphere and Weather of Southern Africa. Oxford University Press**:** Cape Town. 374pp.

Prueger, J.H., Hatfield, J.L., Aase, J.K., Pikul, J.L., 1997. Bowen-ratio comparisons with lysimetric evapotranspiration. Agron. J. 89, 730-736.

Prueger, J.H., Kustas, W.P., Hipps, L.E., Hatfield, J.L., 2004. Aerodynamic parameters and sensible heat flux estimates for a semi-arid ecosystem. J. Arid Environ. 57, 87-100.

Qui, J., Paw U, K.T., Shaw, R.H., 1995. Pseudo-wavelet analysis of turbulence patterns in three vegetation layers. Boundary-Layer Meteorol. 72, 177-204.

Raupach, M.R., Finnigan, J.J., Brunet, Y., 1989. Coherent eddies in vegetation canopies. In: Proc. 4th Australasian Conf. on Heat and Mass Transfer, Christchurch, New Zealand, May 9-12. Bergell House, New York. pp 75-90.

Raupach, M.R., Finnigan, J.J., Brunet, Y., 1996. Coherent eddies in vegetation canopies: The mixing-layer analogy. Boundary-Layer Meteorol. 78, 351-382.

Rosenberg, N.J., Blad, B.L., Verma, S.B., 1983. Microclimate: The Biological Environment. Second edition. John Wiley & Sons, New York. 495 pp.

Rosenberry, D.O, Winter, T.C., Buso, D.C., Likens, G.E., 2007. Comparison of 15 evaporation methods applied to a small mountain lake in the northern USA. J. Hydrol. 340, 149-156.

Sauer, T.J., Horton, R., 2005. Soil heat flux. In: Hatfield, J.L., Baker, J.M. (Eds), Micrometeorology in Agricultural Systems Agronomy Monograph no. 47. pp. 131-154.

Savage, M.J., 2007. Sensible heat estimation using a high frequency temperature-based method Above Various Canopies. 13th South African National Chapter of the International Association for Hydrological Sciences (SANCIAHS) Symposium. Cape Town, Republic of South Africa.

Savage, M.J., Everson, C.S., Metelerkamp, B.R., 1997. Evaporation measurement above vegetated surfaces using micrometeorological techniques. Water Research Commision Report No. 349/1/97, p248, ISBN 1-86845 363 4.

Savage, M.J., Everson, C.S., Odhiambo, G.O., Mengistu, M.G., Jarmain, C., 2004. Theory and practice of evapotranspiration measurement, with special focus on SLS as an operational tool for the estimation of spatially-averaged evaporation. Water Research Commision Report No. 1335/1/04, p204, ISBN 1-77005-247-X.

Savage, M.J., Everson, C.S., Odhiambo, G.O., Mengistu, M.G., Jarmain, C., 2005. Theory and practice of evapotranspiration measurement, with special focus on SLS as an operational tool for the estimation of spatially-averaged evaporation. 12th South African National Chapter of the International Association for Hydrological Sciences (SANCIAHS) Symposium. Midrand, Republic of South Africa.

Savage, M.J., McInnes, K.J., Heilman, J.L., 1995. Placement height of eddy correlation sensors above short turfgrass surface. Agric. For. Meteorol. 74, 195-204.

Schmid, H.P., 2002. Footprint modelling for vegetation atmosphere exchange studies: a review and perspective. Agric. For. Meteorol. 113, 159-183.

Scintec, 2006. Surface Layer Scintillometer SLS20, SLS20-A, SLS40, SLS40-A. User's Manual. Scintec, Atmosphärenmessetechnik, Tübingen, Germany.

Sellers, P.J., Mintz, Y., Sud, Y.C., Dalcher, A., 1986. A simple biosphere model (SiB) for use within general circulation models. J. Atmos. Sci. 43, 505-531.

Shaw, R.H., Paw U, K.T., Gao, W., 1989. Detection of temperature ramps and flow structures at deciduous forest site. Agric. For. Meteorol. 47, 123-138.

Sinclair, T.R., Allen, L.H., Lemon, E.R., 1975. An analysis of errors in the calculation of energy flux densities above vegetation by a Bowen ratio profile method. Boundary-Layer Meteorol. 8, 129-139.

Snyder, R.L., Spano, D., Duce, P., Paw U, K.T., 1997. Surface renewal estimates of evapotranspiration. Theory. Acta Hort. 449, 49-55.

Snyder, R.L., Spano, D., Paw U, K.T., 1996. Surface renewal analysis for sensible heat and latent heat flux density. Boundary-Layer Meteorol. 77, 249-266.

Spano, D., Duce, P., Snyder, R.L., Paw U, K.T., 1997a. Surface renewal estimates of evapotranspiration: tall canopies. Acta Hort. 449, 63-68.

Spano, D., Snyder, R.L., Duce, P., Paw U, K.T., 1997b. Surface renewal analysis for sensible heat flux density using structure functions. Agric. For. Meteorol. 86, 259-271.

Spano, D., Snyder, R.L., Duce, P., Paw U, K.T., 2000. Estimating sensible and latent heat flux densities from grape vine canopies using surface renewal. Agric. For. Meteorol. 104, 171-183.

Stannard, D.I., Rosenberry, D.O., 1991. A comparison of short-term measurements of lake evaporation using eddy correlation and energy budget methods. J. Hydrol. 122, 15-22.

Stull, R.B., 1984. Transilient turbulence theory: 1. The concept of eddy-mixing across finite distances. J. Atmos. Sci. 41, 3351-3367.

Stull, R.B., 1988. An Introduction to Boundary Layer Meteorology. Kluwer Academic Publishers, Dordrecht, 666 pp.

Sugita, M., Kawakubo, N., 2003. Surface and mixed-layer variance methods to estimate regional sensible heat flux at the surface. Boundary-Layer Meteorol. 106, 117-145.

Swinbank, W.C., 1951. Measurement of vertical transfer of heat and water vapour by eddies in the lower atmosphere. J. Meteorol. 8, 135-145.

Tanner, C.B., 1960. Energy balance approach to evapotranspiration from crops. Soil Sci. Proc. Amer. 24, 1-9.

Thiermann, V., 1992. A displaced-beam scintillometer for line-averaged measurements of surface layer turbulence. Tenth Symposium on turbulence and diffusion. American Meteorological Society. Portland, Oregon, USA.

Thiermann, V., Grassl, H., 1992. The measurement of turbulent surface-layer fluxes by use of bichromatic scintillation. Boundary-Layer Meteorol. 58, 367-389.

Thom, A.S., 1975. Momentum, mass and heat exchange in plant communities. In: Monteith, J.L. (Eds), Vegetation and the Atmosphere. Principles. Academic Press. London, UK. Vol. 1. pp 57-109.

Tillman, J.E., 1972. The indirect determination of stability, heat and momentum fluxes in the atmospheric boundary layer from simple scalar variable during dry unstable conditions. J. Appl. Meteorol. 11, 783-792.

Twine, T.E., Kustas, W.P., Norman, J.M., Cook, D.R., Houser, P.R., Meyers, T.P., Prueger, J.H., Starks, P.J., Wesley, M.L., 2000. Correcting eddy-covariance flux underestimates over a grassland. Agric. For. Meteorol. 103, 279–300.

Van Atta, C.W., 1977. Effect of coherent structures on structure functions of temperature in the atmospheric boundary layer. Arch. Mech. 29, 161-171.

Versveld, D.B., Le Maitre, D.C., Chapman, R.A., 1998. Alien invading plants and water resources in South Africa: A Preliminary Assessment. WRC Report No. TT99/98, Water Research Commission, Pretoria, South Africa.

Wang, T.I., Ochs, G.R., Clifford, S.F., 1978. A saturation-resistant optical scintillometer to measure C_n^2. J. Opt. Soc. Amer. 68, 334-338.

Watts, C.J., Chehbouni, A., Rodriguez, J-C., Kerr, Y.H., Hartogensis, O.K., de Bruin, H.A.R., 2000. Comparison of sensible heat flux estimates using AVHRR with scintillometer measurements over semi-arid grass land in northwest Mexico. Agric. For. Meteorol. 105, 81-89.

Weaver, H.L., 1990. Temperature and humidity flux-variance relations determined by one-dimensional eddy correlation. Boundary-Layer Meteorol. 53, 77-91.

Weber, R.O., 1999. Remarks on the definition and estimation of friction velocity. Boundary-Layer Meteorol. 93, 197-209.

Wesely, M., 1988. Use of variance techniques to measure dry air-surface exchange rates. Boundary-Layer Meteorol. 44, 13-31.

Wesson, K.H., Katul, G., Lai, C.-T., 2001. Sensible heat flux estimation by flux variance and half-order time derivative methods. Water Resour. Res. 37(9), 2333-2343.

Wever, L.A., Flanagan, L.B., Carlson, P.J., 2002. Seasonal and interannual variation in evepotranspiration, energy balance and surface conductance in a northern temperate grassland. Agric. For. Meteorol. 112, 31-49.

Whateley, A., Porter, R.N., 1983. The woody vegetation communities of the Hluhluwe-Corridor-Umfolozi Game Reserve Complex. Bothalia. 14, 745-758.

Wieringa, J., 1993. Representative roughness parameters for homogeneous terrain. Boundary-Layer Meteorol. 63, 323-363.

Wilson, K., Goldstein, A., Falge, E., Aubinet, M., Baldocchi, D.D., Berbigier, P., Bernhofer, C., Ceulemans, R., Dolman, H., Field, C., Grelle, A., Ibrom, A., Law, B.E., Kowalski, A., Meyers, T.P., Moncrieff, J., Monson, R., Oechel, W., Tenhunen, J., Valentini, R., Verma, S., 2002. Energy balance closure at FLUXNET sites. Agric. For. Meteorol. 113, 223–243.

Wilson, K.B., Baldocchi, D.D., 2000. Seasonal and interannual variability of energy fluxes over a broadleaved temperate deciduous forest in North America. Agric. For. Meteorol. 100, 1-18.

Wyngaard, J.C., Cote, O.R., Izumi, Y., 1971. Local free convection, similarity and the budgets of shear stress and heat flux. J. Atmos. Sci. 28, 1171-1182.

Zapata, N., Martinez-Cob, A., 2001. Estimation of sensible and latent heat flux from natural sparse vegetation surface using surface renewal. J. Hydrol. 254, 215-228.